

# **Experimental investigation and modeling of tire tread block friction on ice**

Von der Fakultät für Maschinenbau  
der Gottfried Wilhelm Leibniz Universität Hannover  
zur Erlangung des akademischen Grades  
Doktor-Ingenieur  
genehmigte

**Dissertation**

von  
**Dipl.-Ing. Stefan Ripka**  
geboren am 21. April 1980 in Hannover

**2012**

Vorsitzender: Prof. Dr.-Ing. Berend Denkena  
1. Referent: Prof. Dr.-Ing. Jörg Wallaschek  
2. Referent: Prof. Dr.-Ing. Gerhard Poll

Tag der Promotion: 21. Dezember 2012

## Preamble

Die vorliegende Arbeit entstand im Rahmen meiner Tätigkeit als wissenschaftlicher Mitarbeiter am Institut für Dynamik und Schwingungen der Gottfried Wilhelm Leibniz Universität Hannover. Die Arbeit basiert auf verschiedenen Ergebnissen der Forschungskooperation mit der Continental Reifen Deutschland GmbH. Das Ziel dieser Kooperation war der Aufbau von Verständnis zu den Reibmechanismen von gleitenden Reifenprofilklötzen auf Schnee und Eis.

Dank gilt Herrn Prof. Dr.-Ing. Jörg Wallaschek für das entgegengebrachte Vertrauen und natürlich für die vielen Freiheiten, die ich am Institut genießen durfte. Mein Dank gilt ebenfalls Herrn Prof. Dr.-Ing. Gerhard Poll und Herrn Prof. Dr.-Ing. Berend Denkena für die Übernahme des Koreferats bzw. den Vorsitz der Prüfungskommission.

Vielen Dank an Dr.-Ing. Burkhard Wies von der Continental Reifen Deutschland GmbH der sich von meinen Forschungsergebnissen immer wieder begeistern ließ und Herrn Dipl.-Ing. Klaus Wiese für die tolle Zusammenarbeit im Rahmen der Forschungskooperation. Klaus, ich habe diese Zeit sehr genossen. Ebenfalls bedanken möchte ich mich bei dem Projektteam, welches mir auf Conti-Seite mit Rat und Tat zur Seite stand sowie Herrn Dr. Reinhard Mundl für die anregenden Diskussionen und die kritische Begutachtung meiner Messungen.

Weiterer Dank gilt den vielen Studierenden, die im Rahmen vieler verschiedener Arbeiten entscheidend zum Gelingen dieser Arbeit beigetragen haben. Besonderer Dank gilt meinem langjährigen Hiwi Bartholomäus Kleina auf den ich mich stets verlassen konnte.

Ein herzlicher Dank gebührt meinen Institutskollegen der "Gummigruppe" Herrn Dipl.-Ing. Hagen Lind, Herrn Dipl.-Ing. Tim Linke, Herrn Dipl.-Ing. Sasa Mihajlovic, Herrn Dipl.-Ing. Martin Zimmermann und Herrn Dr.-Ing. Matthias Wangenheim für das tolle Arbeitsklima und die anregenden Diskussionen. Stellvertretend für alle Werkstattmitarbeiter gilt mein Dank Herrn Jürgen Anton für die problemlose Zusammenarbeit, auch wenn einige Bauteile besser gestern als heute fertig sein mussten.

Besonderer Dank gilt meiner Familie, insbesondere meinen Eltern Michael und Birgit Ripka, die meine Entscheidungen immer unterstützt und mich in meinem Tun und Handeln bestärkt haben. Ein besonders herzlicher Dank gilt auch meiner Frau Claudia für ihre Zuneigung, ihre Geduld und ihre Unterstützung besonders während der vielen Wochenenden, die ich am Schreibtisch verbracht habe. Ohne Euch wäre dies hier nicht möglich gewesen.

Stefan Ripka

Hannover, im Dezember 2012

# Contents

|   |            |
|---|------------|
| <b>List of Symbols</b>  | <b>VII</b> |
| <b>Kurzfassung</b>  | <b>IX</b>  |
| <b>Abstract</b>   | <b>X</b>   |
| <b>1 Introduction</b>   | <b>1</b>   |
| 1.1 Motivation . . . . .  | 2          |
| 1.2 Outline of the present thesis . . . . .   | 4          |
| <b>2 State of the art</b>   | <b>5</b>   |
| 2.1 Weather formation on earth and phase transitions of water . . . . .                                   | 5          |
| 2.2 Ice as a contact partner in tire friction . . . . .   | 9          |
| 2.2.1 Formation of ice . . . . .  | 10         |
| 2.2.2 The ice surface: Water layer and surface melting . . . . .  | 11         |
| 2.2.3 Properties of ice and their measurement . . . . .   | 12         |
| 2.3 Properties of rubber . . . . .  | 14         |
| 2.4 Mechanisms of rubber friction . . . . .   | 15         |
| 2.5 Tire and tire tread block testing . . . . .   | 17         |
| 2.5.1 Tire test methods . . . . .   | 18         |
| 2.5.1.1 Vehicle tests . . . . .   | 18         |
| 2.5.1.2 Tire lab tests . . . . .  | 19         |
| 2.5.2 Tire tread block test rigs . . . . .  | 20         |
| 2.6 Frictional investigation of tires and tire tread blocks . . . . .                                     | 21         |
| 2.6.1 Performance characteristics of tires on ice . . . . .   | 22         |
| 2.6.2 Mechanisms of sliding on ice investigated by F.P. BOWDEN and T.P. HUGHES . . . . .                  | 24         |
| 2.6.3 Investigation of the kinetic friction on ice by D.C.B. EVANS, J.F. NYE and K.J. CHEESEMAN . . . . . | 25         |
| 2.6.4 Friction measurements of S. VENKATESH . . . . .   | 26         |
| 2.6.5 Investigation of rubber-ice friction by A.D. ROBERTS and co-authors . . . . .                       | 27         |
| 2.6.6 Friction measurements and modeling by P. OKSANEN and J. KEIONEN . . . . .                           | 29         |
| 2.6.7 Arctic Friction Research Study ARTTU . . . . .  | 30         |
| 2.6.8 Friction measurements and simulation of L. BÄURLE . . . . .   | 31         |
| 2.6.9 Investigation of rubber-ice friction of SCHRAMM et al. . . . .                                      | 32         |

---

|          |  |           |
|----------|--|-----------|
| 2.6.10   | The analytical thermodynamical approach to calculate rubber-ice friction by WIESE et al. . . . .                         | 33        |
| 2.6.11   | The analytical thermodynamical approach to calculate rubber-ice friction by SKOUVAKLIS et al. . . . .                    | 33        |
| 2.6.12   | Additional publications of other researchers . . . . .   | 33        |
| <b>3</b> | <b>Analysis of the state of the art and research objective</b>   | <b>36</b> |
| 3.1      | Analysis of the state of the art . . . . .   | 36        |
| 3.2      | Research objective of this thesis . . . . .  | 37        |
| <b>4</b> | <b>Experimental investigation of friction mechanisms of rubber on ice</b>  | <b>40</b> |
| 4.1      | Investigation of adhesion . . . . .  | 40        |
| 4.2      | The High Speed Linear Test Rig "HiLiTe": Design features, execution, evaluation and validation of measurements . . . . . | 42        |
| 4.2.1    | Design features of HiLiTe . . . . .  | 42        |
| 4.2.2    | Ice surface preparation . . . . .  | 44        |
| 4.2.3    | Execution of measurements . . . . .  | 45        |
| 4.2.4    | Evaluation of measurements . . . . .   | 46        |
| 4.2.5    | Validation of HiLiTe measurements with outdoor tire test results . . . . .   | 48        |
| 4.2.5.1  | Validation of rubber compound measurements . . . . .   | 48        |
| 4.2.5.2  | Validation of rubber geometry measurements . . . . .   | 49        |
| 4.3      | Friction measurements of tire tread blocks on ice . . . . .  | 52        |
| 4.3.1    | Variation of sliding velocity and normal pressure . . . . .  | 52        |
| 4.3.2    | Variation of the ambient temperature . . . . .   | 53        |
| 4.3.3    | Variation of the humidity . . . . .  | 54        |
| 4.3.4    | Influence of tread block geometry and inclination angle . . . . .  | 57        |
| 4.3.5    | Influence of different ice properties on the friction process . . . . .  | 58        |
| 4.3.5.1  | Influence of ice impurities on the friction process . . . . .  | 59        |
| 4.3.5.2  | Influence of the ice grain size on the friction coefficient . . . . .  | 60        |
| 4.3.6    | Determination of the contact area of sliding tire tread blocks on ice . . . . .  | 61        |
| 4.4      | Post-processing of measurements on ice . . . . .   | 63        |
| 4.5      | Results and discussion . . . . .   | 66        |
| 4.5.1    | The rubber-ice friction model . . . . .  | 66        |
| 4.5.2    | Impact of the ice properties on the friction process . . . . .   | 73        |
| 4.5.3    | The friction coefficient as a function of the square root of the sliding velocity . . . . .                              | 75        |
| 4.6      | Conclusions and consequences for tire development . . . . .  | 76        |
| <b>5</b> | <b>Development of a simulation model for siped tire tread blocks</b>   | <b>77</b> |
| 5.1      | Rigid body model . . . . .   | 78        |
| 5.1.1    | Single degree of freedom model . . . . .   | 78        |
| 5.1.2    | Multi degree of freedom model . . . . .  | 80        |
| 5.1.2.1  | Model set-up . . . . .   | 80        |

---

|          |   |            |
|----------|---|------------|
| 5.1.2.2  | Validation of the siped tread block model . . . . .   | 82         |
| 5.1.2.3  | Investigation of instationary sliding motion . . . . .  | 83         |
| 5.2      | Approximation of a siped tire tread block with the beam model of EULER<br>and BERNOULLI . . . . . | 86         |
| 5.3      | TIMOSHENKO beam model . . . . .   | 88         |
| 5.3.1    | TIMOSHENKO beam model setup . . . . .   | 89         |
| 5.3.2    | Validation of the TIMOSHENKO beam model . . . . .   | 93         |
| 5.4      | Parameter identification for the tread block models . . . . .                                     | 96         |
| <b>6</b> | <b>Conclusion and Outlook</b>   | <b>97</b>  |
|          | <b>Bibliography</b>   | <b>101</b> |

## List of Symbols

The list of symbols gives a general overview of the used symbols. It shows the general notation. In the case of deviations the special meaning is mentioned in the text. A detailed description of the tire tread block geometry can be found in Chapter 1.

### Latin Notation

|                  |   |
|------------------|---|
| $A$              | Area [ $\text{mm}^2$ ]  |
| $E$              | Youngs modulus [ $\frac{\text{N}}{\text{mm}^2}$ ]                   |
| $F$              | Force [N]   |
| $G$              | Shear modulus [ $\frac{\text{N}}{\text{mm}^2}$ ]                    |
| $J^A$            | Moment of inertia for point $A$ [ $\text{kgm}^2$ ]                  |
| $K$              | Level of salinity of water [%]                                      |
| $P$              | Power [W]   |
| $W$              | Energy loss [J]   |
| $L$              | Tread block length [mm]   |
| $T$              | Temperature [ $^{\circ}\text{C}$ ]                                  |
| $c$              | Spring constant [ $\frac{\text{N}}{\text{m}}$ ]                     |
| $c_{\varphi}$    | Rotational spring constant [Nm]                                     |
| $d$              | Sipe depth [mm]   |
| $d_{\varphi}$    | Rotational damping constant [Nms]                                   |
| $e$              | Euler's number  |
| $f$              | Sipe length [mm]  |
| $h$              | Height of the water layer [ $\mu\text{m}$ ]                         |
| $\ell$           | Tread block element length [mm]                                     |
| $m$              | Tread block element mass [kg]                                       |
| $p$              | Normal load [bar]   |
| $rF$             | Relative humidity [%]   |
| $t$              | Time [s]  |
| $v$              | Sliding velocity [ $\frac{\text{m}}{\text{s}}$ ]                    |
| $v_0$            | Absolute sliding velocity [ $\frac{\text{m}}{\text{s}}$ ]           |
| $v_{\text{rel}}$ | Relative sliding velocity [ $\frac{\text{m}}{\text{s}}$ ]           |
| $w$              | Tread block width [mm]  |
| $x, y, z$        | Coordinate system, direction of the corresponding coordinate system |

## Greek Notation

|           |  |
|-----------|--|
| $\eta$    | Viscosity of the water layer [ $\frac{\text{kg}}{\text{ms}}$ ] |
| $\lambda$ | Thermal conductivity [ $\frac{\text{W}}{\text{mK}}$ ]          |
| $\mu$     | Friction coefficient [–]                                       |
| $\rho$    | Density [ $\frac{\text{kg}}{\text{m}^3}$ ]                     |
| $\tau$    | Time constant for rubber deformation [–]                       |
| $\varphi$ | Angle of tread block element deformation [ $^\circ$ ]          |

## Indices

|                        |   |
|------------------------|---|
| $( )_A$                | Parameter for acrylic glas  |
| $( )_F$                | Friction, referring to the direction of friction, e.g. Friction Force $F_F$ |
| $( )_I$                | Parameter for ice   |
| $( )_L$                | Parameter for air   |
| $( )_N$                | Normal, referring to the normal direction, e.g. Normal Force $F_N$          |
| $( )_W$                | Parameter for water   |
| $( )_y$                | Parameter in y-direction of the coordinate system                           |
| $( )_{\text{dry}}$     | Parameter of dry state  |
| $( )_{\text{ice}}$     | Parameter related to ice  |
| $( )_{\text{in}}$      | Parameter measured in the lab, indoor                                       |
| $( )_{\text{max}}$     | Maximum value of a parameter  |
| $( )_{\text{viscous}}$ | Parameter of viscous state  |
| $( )_{\text{wet}}$     | Parameter of wet state  |



## Kurzfassung

Aufgrund des steigenden Bedürfnisses nach mehr Sicherheit auf den Straßen gewinnen Winterreifen immer mehr an Bedeutung. Der Kundenwunsch nach ständig verbesserten Eigenschaften der Winterreifen erfordert ein hohes Maß an Entwicklungsarbeit der Reifenhersteller. Ein tiefes Verständnis der dominierenden Gummi-Eis Reibmechanismen hilft, schnell und kostengünstig bestimmte Reifeneigenschaften gezielt weiter zu entwickeln. Dieses Verständnis kann einerseits durch verschiedene Grundsatzversuche im Labor, andererseits auch durch Simulationen erlangt werden.

Im Rahmen dieser Arbeit wird ein Modell eines gleitenden Reifenprofilklotzes auf einer Eisfahrbahn entwickelt. Dazu werden verschiedene Reibversuche auf einem Hochgeschwindigkeitslinearprüfstand durchgeführt, um die dominierenden Reibmechanismen selbst und die Einflüsse auf selbige zu identifizieren. Mit Hilfe der Methode der Totalreflektion wird die Kontaktfläche von gleitenden Reifenprofilklötzen auf Eis visualisiert. Die beobachteten Phänomene werden beschrieben und die ursächlichen Mechanismen erläutert. Die Modellvorstellung wird mit Hilfe verschiedener Messungen in einem weiten Parameterbereich validiert. Die durchgeführten Versuche werden kritisch betrachtet und existierende Herausforderungen werden herausgestellt. Abschließend werden Möglichkeiten aufgezeigt, das Reibpotential zwischen Reifenprofilklotz und Eis zu erhöhen. Weiterhin werden verschiedene Möglichkeiten vorgestellt, einen gleitenden Reifenprofilklotz mit Hilfe analytischer Ansätze zu simulieren. Erste Grundlagen wie z.B. die Implementierung eines Reibgesetzes und der Kontakt zur Fahrbahn werden mit Hilfe eines Einmassenschwingers erläutert. Um die Genauigkeit des Modells zu erhöhen werden die Eigenschaften eines Zweimassenschwingers betrachtet, sowie die Balkentheorien von EULER-BERNOULLI und TIMOSHENKO auf ihre Tauglichkeit zur Abbildung der vorab definierten Anforderungen untersucht. Grundlegende Simulationen werden durchgeführt und die Modelle werden mit verschiedenen Messungen validiert.

**Schlagwörter:** Reifenprofilklotz, Reibung, Eis, Experiment, Simulation

## Abstract

Winter tires gain more and more attention due to safety reasons. The customers need on more traffic safety results in an increasing effort of the tire industry to improve the winter tire characteristics. With the help of a deep understanding of the dominating rubber-ice friction mechanisms new tires can be engineered cost-effectively. The understanding of the relevant friction mechanisms can be gained from basic tests on the one hand but also from simulations on the other hand.

This thesis deals with the investigation of sliding tire tread blocks on ice. With the help of a high speed linear test rig the rubber-ice friction is investigated in depth. With the help of the total initial reflection the contact area of sliding tire tread blocks on ice is visualized. The observed phenomena are described and the influences are explained. Based on these investigations a detailed model of the sliding tire tread block is derived. It is validated with measurements carried out in a wide parameter range. The experiments are considered critically and existing challenges are pointed out. Methods for optimizing the tire tread block ice friction are presented. In a second step different analytical models are presented which are all capable to simulate sliding tire tread blocks. Basic methods like the tread block road interaction and the implementation of a friction law in the model are introduced with a single mass oscillator. Additionally, a two mass oscillator is used to increase the model accuracy. The suitability of EULER-BERNOULLI and TIMOSHENKO beam theory for modeling a sliding tire tread block is analyzed also. Basic simulations are done and the models are validated with different measurements.

**Key words:** Tire tread block, Friction, Ice, Contact area, Experiment, Simulation

# 1 Introduction

Every day we "meet" friction and have to get along with it. Everybody knows the problem of low friction when walking on ice: In the ideal case we stumble, but it can also happen that we slip. However, friction also helps us. A screw can connect two planks due to friction. It also gives us the opportunity to listen to music. A violin or a cello keeps silent if the fiddlestick does not initiate oscillations on the chord because of friction. Also, our locomotion is based on friction. Railways move because its power is transmitted to the rail by friction, and car and truck tires transmit the engine power by rubbing on the ground (cp. [70]). Even though there is a large variety of technical areas where rubber friction is of crucial importance for the function of machines or machine components, like e.g. in tires, sealings and wiper blades, science can only explain the basics yet. There is still a lot of work to do for a detailed understanding of the rubber friction phenomena.

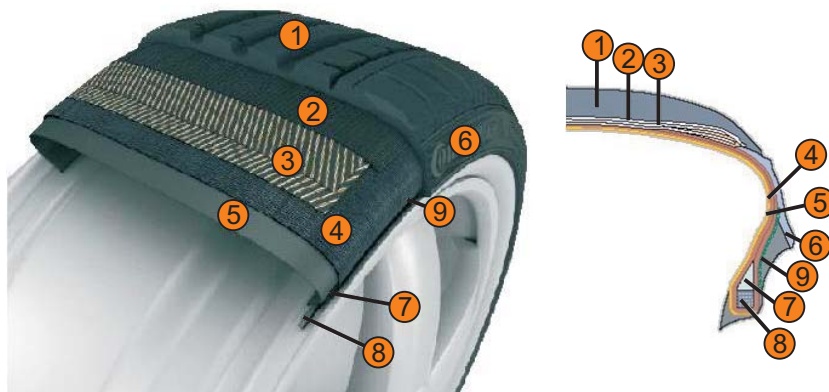


**Figure 1.1:** Cut through a tire: ① Tread pattern, ② Cap ply, ③ Steel cord, ④ Carcass, ⑤ Inner liner, ⑥ Side wall, ⑦ Apex, ⑧ Bead bundle, ⑨ Bead reinforcement (Pictures from CONTINENTAL)

The following pages are used to emphasize the importance of winter tires and to give an outline of the present thesis. First of all basic tire and tire tread block vocabulary is introduced by considering a sliced tire (Fig. 1.1). Tread pattern, cap ply, side wall, inner liner and apex are made of rubber. Other materials like steel and textile parts can also be found. They are normally rubber coated like steel cords, carcass and bead bundle. Depending on the function up to ten different rubber compounds are used to manufacture a tire. This rubber and non rubber material mix makes the tire behaviour very complex. Obviously summer and winter tires differ in their designs (Fig. 1.2). A basic difference is the tire tread

pattern which is described in more detail now. The summer tire tread pattern consists of straight grooves (void) and massive tread blocks (Fig. 1.2 a). The winter tire in contrast has a more complex structure of grooves and in addition a siped structure of the tread blocks (Fig. 1.2 b). The void of the tread block consists of the single sipes and each remaining part of the tread block is called tread block element (Fig. 1.2 b). Another difference between summer and winter tires is the material. Normally, the rubber compound hardness differs depending on the ambient temperature.

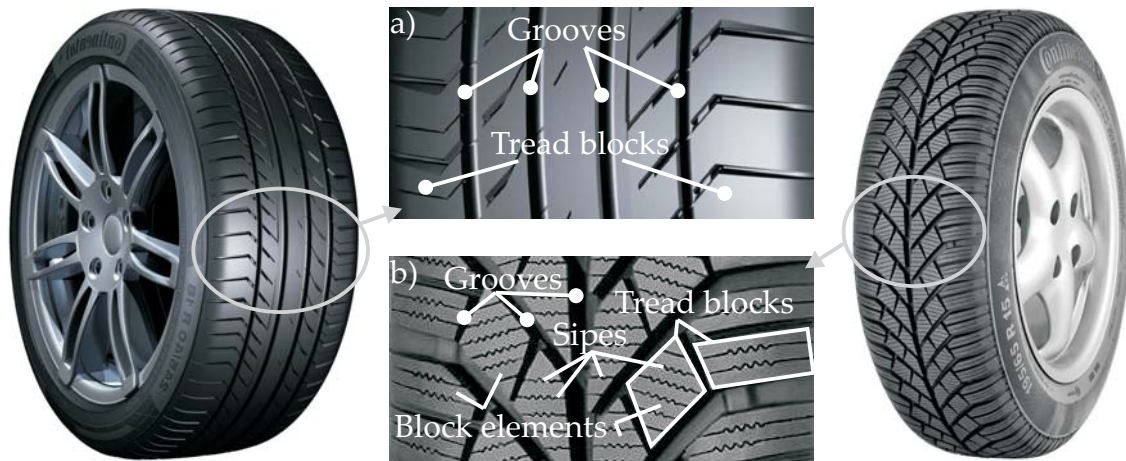


**Figure 1.2:** Summer tire (left) vs. winter tire (right): Nomenclature of a) Summer tire tread pattern, b) Winter tire tread pattern (Tire pictures from CONTINENTAL)

## 1.1 Motivation

The friction potential of the road surface and therefore traction of the tires decreases significantly under snowy and icy road conditions. So the stopping distance of a summer tire on a dry road is very short. In contrast snowy and icy road conditions result in a much longer stopping distance (Fig. 1.3). Compared to a summer tire the winter tire has a much shorter stopping distance on snowy and icy road and thus clearly increases the traffic safety in wintery conditions.

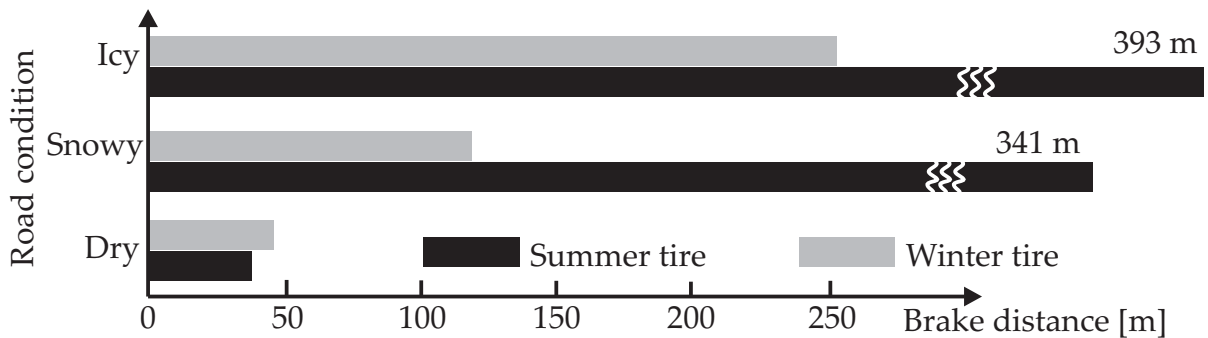


**Figure 1.3:** Comparison of winter and summer tires: Brake distances from a velocity of  $v = 100 \frac{\text{km}}{\text{h}}$  to  $v = 0 \frac{\text{km}}{\text{h}}$  at different road conditions (According to [61])

Since the fourth of December 2010, German law rules that if the road is icy, snowy or slippery a tire marked with "M+S" ("Mud + Snow") has to be used [1]. In Europe, especially in Germany, there are approximately 120 days with dry roads and approx. 180 rainy days. The period of snowy and icy roads lasts only about 65 days per year [121] but it holds a very special risk: Snowy and icy roads can be very slippery. The friction coefficient is very low under certain conditions. TOPP et al. ([121], based on [71]) estimated the relative accident probability for road surfaces with low friction potential (Fig. 1.4). Keeping this fact in mind, the use of winter tires is recommended because they are adjusted to the winterly conditions. As a consequence the tire industry continuously tries to further improve the performance of winter tires. Tire characteristics like braking and vehicle handling are in the focus of research and development and in most tire manufacturing companies the safety aspect is dominating the development of winter tires.

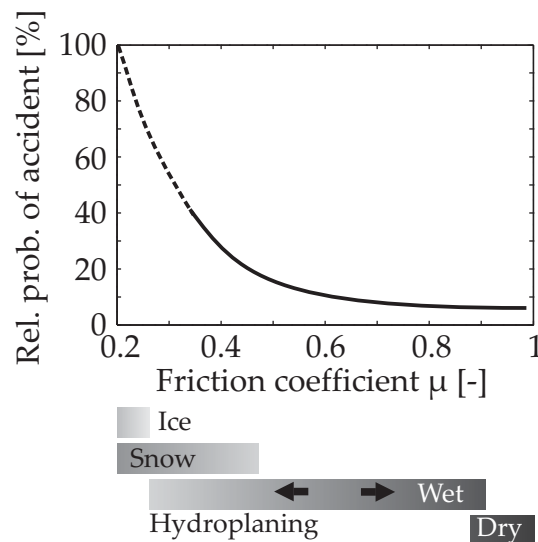


**Figure 1.4:** Relative probability of accident depending on friction level (According to [121])

The evaluation of winter tires is very complex and cost intensive because the vehicle tests can be done under certain conditions only. Up to now they have to be carried out to judge the performance improvement of newly designed winter tires. The execution of these tests is limited to a few months of the year as well as to selected areas in the world due to the requirements to the climate. Hence, it can happen that the development of a new winter tire takes several years, because multiple development loops have to be done. Methodologies which allow to improve the efficiency of the winter tire development and reduce the time-to-market have become more and more important for this reason. If tire evaluation could be done all year round, a large benefit would be the result. There are two possible routes to reach such a target. One is to improve the reliability of simulating the tire performance or the influence of single parts. The other one is using an all year available lab where the performance of parts of the tire or of the whole tire can be tested under controlled conditions. Both simulation and test can reduce the development time and also the development costs. However, understanding relevant friction mechanisms is

of importance for both approaches and the study of relevant friction mechanisms of winter tires on snow and ice can be of great significance for the whole tire industry.

## 1.2 Outline of the present thesis

After explaining the motivation "Why should winter tire research be done?!" the following lines outline the structure of the present thesis.

Chapter 2 provides a review of the state of the art of the research already done. The literature review helps to define the research gap which is reduced with this thesis (cp. Chapter 3). Starting with weather formation on earth and the phase transitions of water the properties of ice are introduced. This part starts with the formation, goes on with the surface properties and ends up with the characterization of ice. A view on its influence on the friction process is also given. The next two subsections of Chapter 2 give a brief introduction on rubber material and rubber friction mechanisms in general. It is followed by a section on tire and tire tread block testing. Here, different test methods and test rigs are presented. Finally, the focus is directed to tire and tire tread block friction mechanisms.

As already mentioned, in Chapter 3 the presented "State-of-the-art" is analyzed. This critical reflection gives the basis to formulate open questions and the aims of this thesis.

Chapter 4 is the main part of this thesis. It presents the results of experimental investigations of the tire tread block-ice friction mechanisms which are used to introduce a rubber-ice friction model. The chapter starts with the analysis of adhesion effects with the aim to clarify if this effect is important for rubber-ice contact. Afterwards the high speed linear test rig "HiLiTe" is introduced. It is used to study different factors of rubber-ice friction like sliding velocity, normal load, temperature, humidity, tread block geometry and ice salinity as well as ice grain size. The observations are described in detail. Based on the analysis of the HiLiTe measurements and the "State-of-the-art" (cp. Chapter 2) a tire tread block-ice friction model is derived. The final section of Chapter 4 is dedicated to the validation of the rubber-ice friction model. Observed friction phenomena as well as the influence of various physical parameters on the rubber-ice friction are explained with the help of the rubber-ice friction model. The chapter closes with a conclusion and a discussion of the consequences of these results for future tire development.

Besides the friction measurements, this work contains different approaches for the simulation of a siped tire tread block (Chapter 5). Different analytical models are presented which are all capable of simulating a sliding siped tire tread block. The models are compared with each other and advantages and disadvantages are elaborated. The models are validated and in a second step, selected scenarios are simulated.

The thesis ends with the conclusion (Chapter 6) of the presented work. Additionally, an outlook is given which outlines possible future work in the field of tire tread block-ice friction research.

## 2 State of the art

The following chapter gives an overview of the researches already done. It starts with the weather formation and the phase transitions of water. This knowledge is necessary for a detailed understanding of the complex rubber-ice friction mechanisms. Afterwards, the basics of ice formation are introduced. Information on the ice surface and its physical properties are given, and the influences on rubber friction are outlined. Subsequently, basic rubber material properties and rubber friction mechanisms are explained in general. This section is followed by a general overview of tire test methods. First of all, some outdoor test equipment and lab test rigs are presented. Several results of tire performance tests are shown. They show different trends in the tire performance and the influence of the tire tread block geometry on the friction coefficient is discussed. Finally, friction theories and measurement results are reviewed.

### 2.1 Weather formation on earth and phase transitions of water

Water is the basic ingredient to form snow and ice. Basic information about the weather formation is given now to understand the mechanisms of ice formation and transformation. Furthermore, the interaction between water and the surrounding air is considered and explained according to the basic vocabulary regarding water. For detailed information on weather generation and meteorology in general see [2], [45].

The word "weather" describes the atmospheric conditions on earth. The weather can be hot or cold, wet or dry, calm or stormy, clear or cloudy. The earth is surrounded by different air layers which all have special properties. The nearest layer to the earth is the troposphere with a height from eight (at the North and South Pole) up to sixteen kilometers at the equator. It is followed by the stratosphere, mesosphere, thermosphere and exosphere. However, most weather phenomena occur in the troposphere because water vapour can be found there. Thereby, it has to be kept in mind that the water there is not soaked up like in a sponge but it is mixed up with the surrounding nitrogen, oxygen and inert gas particles. The water vapour in the air plays an important role for different weather phenomena. This is the reason why commonly used definitions of humidity are introduced at this point. Different variables are available to characterize the water content of the air. The first one

is the absolute humidity  $AH$ . The absolute humidity declares the mass of water  $m_W$  per cubic meter of total moist air  $V$

$$AH = \frac{m_W}{V}. \quad (2.1)$$

The unit of the absolute humidity is  $\frac{\text{kg}}{\text{m}^3}$ . The second variable is the maximum humidity  $MH$ . It indicates the maximum possible content of dissolved water within one cubic meter air (cp. Table 2.1). If the maximum humidity is reached, the air is saturated. No more water can be dissolved. The maximum humidity or the saturation level strongly depends on the ambient temperature, the ambient pressure and the surface, water or ice (cp. Table 2.1). Under similar conditions the saturation level above an ice surface is smaller compared to a water surface because the water molecules are stronger linked with the ice surface. Another commonly known value is the relative humidity  $rF$ . It is the ratio of absolute humidity  $AH$  and maximum humidity  $MH$

$$rF = \frac{AH}{MH}. \quad (2.2)$$

The relative humidity indicates the level of water saturation of the air. A relative humidity of  $rF = 100\%$  means that the air is saturated. The according temperature is the saturation temperature and the dew point is reached. If the air is heated up, the relative humidity decreases (the absolute humidity stays constant but the maximum humidity increases) and the air can assimilate more water. If the saturated air is cooled, water condenses. In the sky clouds occur if condensation nucleus are available. Otherwise the water undercools. On the ground, the precipitated water is called white frost in case of temperatures below zero (Fig. 2.1 a) or dew at temperatures above zero degree Celsius (Fig. 2.1 b).

**Table 2.1:** Air saturation level above water and ice surface [110]

| Temperature [ $^{\circ}\text{C}$ ]            | -20               | -15               | -10               | -5                | 0    | 5   | 10  | 15    | 20    |
|---|-------------------|-------------------|-------------------|-------------------|------|-----|-----|-------|-------|
| Above water [ $\frac{\text{g}}{\text{m}^3}$ ] | 1,08 <sup>1</sup> | 1,61 <sup>1</sup> | 2,36 <sup>1</sup> | 3,41 <sup>1</sup> | 4,85 | 6,8 | 9,4 | 12,82 | 17,29 |
| Above ice [ $\frac{\text{g}}{\text{m}^3}$ ]   | 0,88              | 1,39              | 2,14              | 3,25              | 4,85 | -   | -   | -     | -     |

Within the troposphere clouds, wind and rainfall are generated. At the border to the stratosphere ambient temperatures of  $T = -50^{\circ}\text{C}$  to  $-60^{\circ}\text{C}$  can be found. In the troposphere many different conditions concerning the temperature but also concerning the dissolved water in the air can be found. Both are essential for the formation of the precipitation. Water and its properties highly influence weather conditions. Water occurs in three phases on earth: solid, liquid and gaseous. Every phase can be reached from every other phase (Fig. 2.2). A notable property of the phase diagramm is the negative gradient of the melting curve. According to PETRENKO and WHITWORTH "The negative slope of the melting curve is (...) a consequence of the fact that water expands on freezing, breaking vessels, bursting

<sup>1</sup>Overcooled water





**Figure 2.1:** Grass in nature: Covered with a) white frost and b) dew

pipes and causing icebergs to float'' [91]. The negative gradient of the melting curve also causes the phenomenon of pressure melting. That means that a sufficient pressure increase (at constant temperature) melts the ice surface (cp. Fig. 2.2). At a temperature of  $T = -5\text{ }^{\circ}\text{C}$  the melting pressure is  $P_S = 600\text{ bar}$  for example [26]. In the following, the nomenclature of the different phase transitions is introduced (cp. Fig. 2.3).

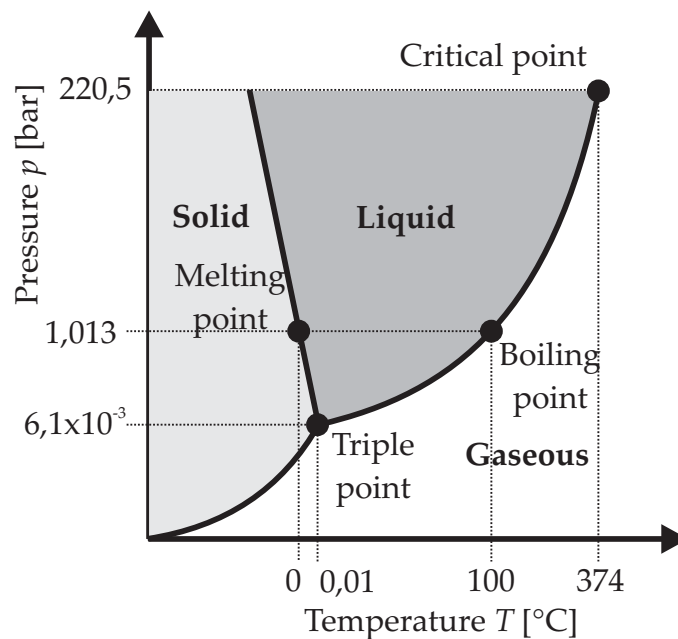


**Figure 2.2:** Phase diagram of water (Not to scale, according to [96])

**Melting** describes the change of the solid state (ice) to the liquid form (water). An energy of  $E_M = 334\frac{\text{kJ}}{\text{kg}}$  is necessary to start the melting process [34].

**Freezing** is the opposite of melting. The liquid water becomes ice. The yielded energy during this process is  $E_F = 334\frac{\text{kJ}}{\text{kg}}$  [34].

**Evaporation / Vaporization** is the change of the liquid phase to the gaseous one. The vaporization process starts at the boiling point of the water. An energy of  $E_M = 2257\frac{\text{kJ}}{\text{kg}}$  is necessary for the vaporization of water [49]. Even if the water does not reach the boiling point, water molecules can leave the surface (cp. Fig. 2.3). This process is called evaporation (Fig. 2.3).

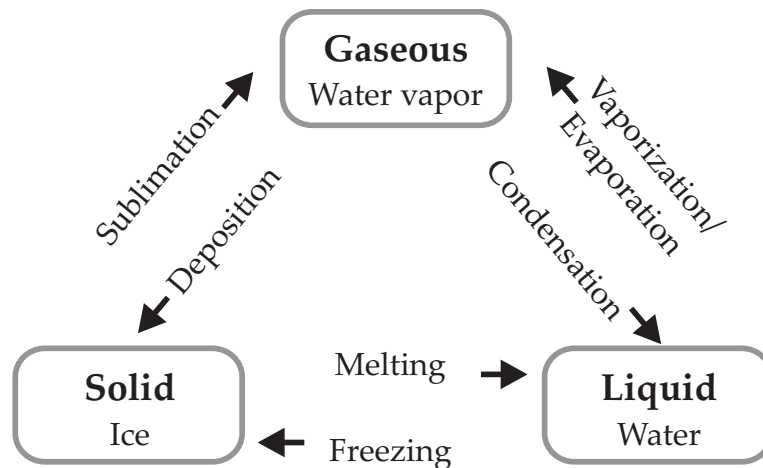


**Figure 2.3:** Different phases of water and the nomenclature for the different phase transitions

**Condensation** is the opposite of evaporation / vaporization: The gaseous phase becomes liquid.

**Sublimation** is the change of the solid phase to the gaseous one. Snow and ice surfaces in nature sublime as well. This mechanism of sublimation leads to a continuously decreasing snow and ice surface thickness outside, too. The challenge of sublimating ice surfaces is picked up later in this work (cp. Chapter 4.4).

**Deposition** is the process of the gaseous phase becoming solid.

After the definition of the basic vocabulary, the evaporation and condensation of water at a phase boundary is visualized (Fig. 2.4), because this effect causes a challenge during the friction measurements. Dry air lies above a water surface (Fig. 2.4 a) and water molecules ( $\text{H}_2\text{O}$ ) evaporate from the water surface (Fig. 2.4 b). At the same time other molecules condensate back to the water (Fig. 2.4 c). The air is saturated when the number of evaporating and condensing molecules is equal (Fig. 2.4 d). The water molecules can leave a snow or ice surface or they can come from a liquid surface like a lake. The single molecules are stronger linked to the surface of solid materials like snow and ice. Due to this the saturation level above solid and liquid surfaces differs (cp. Table 2.1). The amount of water vapour above a surface in thermodynamic equilibrium (evaporating and condensating molecules are equal) influences the vapour pressure above this surface. The vapour pressure is a part of the overall atmospheric pressure. The vapour pressure depends on three parameters:

- The temperature: With an increasing temperature the vapour pressure as well as the maximum humidity increases (cp. Table 2.1). Warmer air assimilates more water molecules.
- The boundary surface: The vapour pressure over an ice surface is lower compared to a water surface because the fixing of molecules of an ice surface is greater than the one of a water surface (cp. Table 2.1).

- The surface bending: Above concave surfaces the vapour pressure is smaller compared to convex surfaces due to the fixing of the single molecules. Concave and convex surfaces can be found at snow crystals for example.

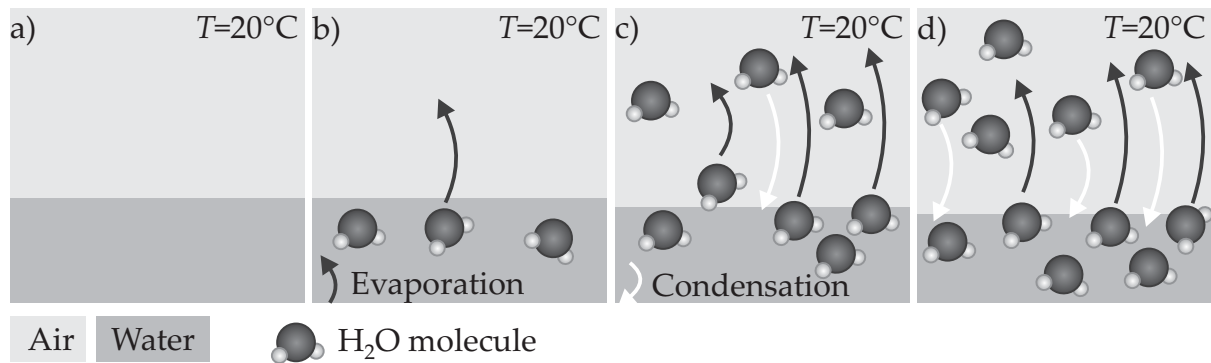


**Figure 2.4:** Process of air saturation: a) Dry air lies above water at  $T = 20^\circ\text{C}$ , b) Evaporation of water molecules into the air begins, c) Condensation back to the water occurs, d) The air is saturated, the water level is lower but remains constant, the number of evaporating and condensing water molecules is equal (According to [2])

A descriptive example for evaporation is the drying of cloths at temperatures under the melting point: Wet cloths which are hung out in freezing weather get dry. The water simply freezes and evaporates. This process can take several time depending on the amount of water which has to sublimate. The calculation of evaporation is complex, for details see e.g. [90].

The process of evaporating and condensating molecules also occurs in the lab. Thus the ice surface is subject of continuously changes. The effect on the results of the friction measurements is pointed out later (cp. Chapter 4). Further information about weather formation, humidity and vapour pressure can be found in [2], [55], [45], [34].

## 2.2 Ice as a contact partner in tire friction

Besides the rubber specimen the contact partner ice has a very big influence on the friction process. To understand the contact partner ice in more detail, the basic physics of ice are introduced while the focus is on the ice surface. A general overview of the material ice has been given by PETRENKO and WHITWORTH [91]. Another detailed book on ice physics is written by HOBBS [51]. The ice surface was investigated by DÖPPENSCHMIDT [26]. A literature review has been given by PETRENKO [92] who considers experimental results as well as theoretical models of ice and its properties. The following chapter is mainly based on these three publications.

## 2.2.1 Formation of ice

"On the atomic scale ice is being made up from water molecules- $H_2O$ " [91].  $H_2O$  consists of one oxygen and two hydrogen atoms (Fig. 2.5). The distance  $O - H$  for a free molecule is  $0,9572 \pm 0.0003 \text{ \AA}$  and the angle  $H - O - H$  is  $104,52 \pm 0,05^\circ$ . The constitution of the molecules characterises the water molecule and plays an important role for the properties of water and ice. "This bent form gives it a dipol moment and determines how the molecules can fit together in a crystal" [91]. The molecules are connected in the ice crystal with hydrogen bonds. Ice occurs under different conditions. Different stable and unstable phases exist, depending on the temperature and the pressure (Fig. 2.6). Ice of type Ih arises under normal atmospheric pressure only<sup>2</sup>. Ice Ih has a hexagonal crystal structure. The orientation of the single water molecules in the ice crystal is completely disordered which causes many of the special properties of ice (for details see [91]).

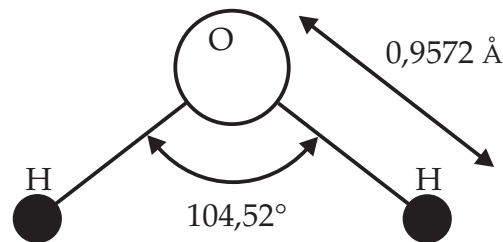


**Figure 2.5:** The geometry of a free  $H_2O$  molecule

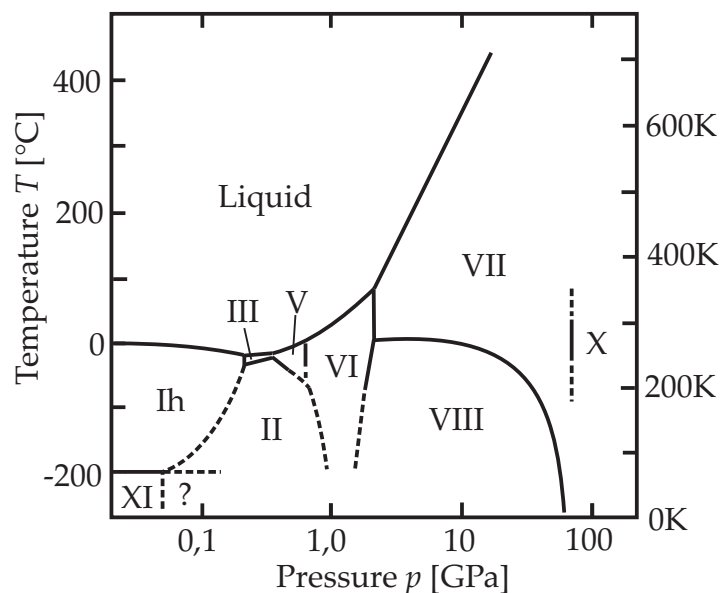


**Figure 2.6:** "Phase diagram showing the stable phases of the ice-water system on a logarithmic scale of pressure" [91]

<sup>2</sup>"The number 'I' was assigned by TAMMANN (1900) following his discovery of the first of the high-pressure phases of ice, and the 'h' is commonly added to distinguish this normal hexagonal phase from a metastable cubic variant called ice Ic." [91]

### 2.2.2 The ice surface: Water layer and surface melting

An ice surface is not only solid material. "Most of the researchers agree that the ice surface is covered with a liquid like layer" [26]<sup>3</sup>. SCHRÖDER concluded that surface melting of ice at the ice-vapor and ice-air interface must exist. "Molecules from the surface are in constant exchange with molecules in the gas phase" [106]. ENGEMANN also mentioned that the humidity "has to be controlled very precisely, otherwise the surface morphology changes rapidly due to sublimation/resublimation" [27]. Numerous work has been done on identifying specific properties of this initial surface water layer (for details see [26], [91] and [92]). And research on the ice surface is still of great interest: "The surface properties have become the largest field of current research within ice physics" [91]. A good overview on the history of the surface water layer research is given by JELLINEK [60]. He also did theoretical and experimental work to prove the existence of the water layer on an ice surface. Disagreement prevails concerning the temperature range in which the layer exists as well as on its thickness and the theoretical explanation of its existence and properties [26]. Many authors investigated the layer thickness and they published different results for the temperature-layer thickness relation depending on the measurement method (Fig. 2.7). "At first glance, the results presented in Figure 2.7 are awesome, so great are the discrepancies" [92]. So estimations of the layer thickness at a temperature of  $T \approx -10^\circ\text{C}$  differ from  $d = 1\text{ nm}$  to  $d = 100\text{ nm}$ . The temperature range in which a layer thickness was observed diverged in the same way (Fig. 2.7). Based on theoretical considerations JELLINEK concluded that the liquid layer vanishes at a temperature of about  $T = -30^\circ\text{C}$  [60].

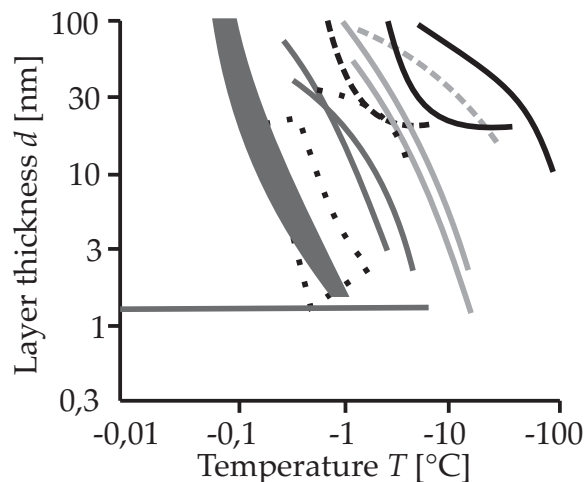


**Figure 2.7:** Temperature-surface layer thickness relation depending on the measurement method: Ellipsometry (dark grey), Nuclear magnetic resonance NMR (black), Electrical conductivity (light grey), X-ray (dashed black), Proton channeling (dashed light grey); (According to [92] and [26])

<sup>3</sup>The following citations of DÖPPENSCHMIDT [26] were translated from German into English by the author of this thesis

A phenomenon of the ice surface, which is strongly linked with the surface water layer, is the extremely small friction coefficient. Normally, the small friction coefficient is explained by a water layer in the contact area. Pressure melting (see Chapter 2.1) does not deliver a significant contribution to the water layer generation. So DÖPPENSCHMIDT gave a rough estimation on the phenomenon of pressure melting. A skier's weight would have to be in the order of an unrealistic  $m = 10^6$  kg at an ambient temperature of  $T = -5^\circ\text{C}$  (melting pressure  $P_s(T = -5^\circ\text{C}) = 600$  bar) for pressure melting. However, this calculation assumed that the real contact area is equal to the surface of the ski which does not correlate with reality. But "an exact estimation of the real contact area on ice is very difficult" [26]. Although the exact size of the contact area is unknown an influence of pressure melting on the macroscale seems to be unrealistic due to the required high pressure increase. However, the influence of pressure melting on the ice friction process can be clarified finally until the size of the real contact area can reliably be determined. A commonly accepted theory for the origin of the water layer in the contact is the fact that it is caused by frictional heat. "A peculiarity in ice friction is, however, that the friction process generates its own lubricant" [10]. So "the influence of the liquid like layer on the friction process, for example, is investigated rarely" [26]. ROBERTS also recommended a deeper investigation of the ice surface properties and not only of the rubber-ice interaction (cp. Chapter 2.6.5). Up to now it is unknown if other factors influence the generation of the water layer and the friction process itself. "So the friction on ice depends on the temperature, velocity, humidity, electrical and thermal conductivity, plastic and elastical properties, impurities, normal pressure, crystal structure and orientation, surface roughness and many more factors" [26]. ROBERTS already mentioned in 1981 that ice plays an important role: "Over the temperature range  $-20^\circ\text{C}$  to  $0^\circ\text{C}$ , which is of considerable practical importance, it is the ice behaviour rather than the rubber that sets the general level of friction" [104]. DOPORTO et al. observed a dependency of tire test results on the day of execution. They concluded that the ice surface properties were hard to reproduce, which caused the variation of the measurement results of different days [25]. They also assumed a high impact of the ice surface on the friction measurements.

### 2.2.3 Properties of ice and their measurement

The question arises of how to characterize the ice surface to be able to determine its influence on the result of the friction measurement, cp. [101]. This would guarantee reproducible results independent of the actual ice surface. This means that the characterization of the ice is essential for a detailed investigation of the rubber-ice friction process because the ice properties also influence the measurement results (cp. Chapter 4.4). Thereby it is important that the methods can be used in the lab and outside on test tracks to guarantee a controlled test environment. The test equipment should be portable (cp. also RIPKA et al. [101]). Stationary methods like atomic force microscopy or X-ray are hard to realize. First of all ambient parameters like temperature and humidity shall be measured which can be realized in a very simple way. The influence of impurities on the friction process

can be eliminated in the lab by using purified water, but outside on the tire test track the dissolved impurities in the water must be considered. So the ice can be characterized by measuring conductivity and pH-value as well as the total dissolved solids [103]. A more detailed characterization of ice can be gained if thermal and electrical conductivity are measured. The surface roughness of ice seems to be of less importance because it is melted away during the first passages with the test specimen. The ice surface is passed several times with the test sample in the lab but also on the tire test track. During the polishing process the ice surface is homogenized (cp. also [26]). The ice grain size as well as the grain orientation shall be considered as well because they vary depending on the freezing process. Both can be observed with polarized light (Fig. 2.8 a). The ice sample is placed between two crossed polarizing filters and illuminated from the bottom. Depending on the orientation of the ice grains the colour varies (Fig. 2.8 b). A requirement for this method is clear ice. Additionally, a test track with a glass bottom was prepared to realize this approach in lab. The usage of this test set-up outside on a tire test track can be difficult to realize because an ice sample needs to be cut off from the surface.

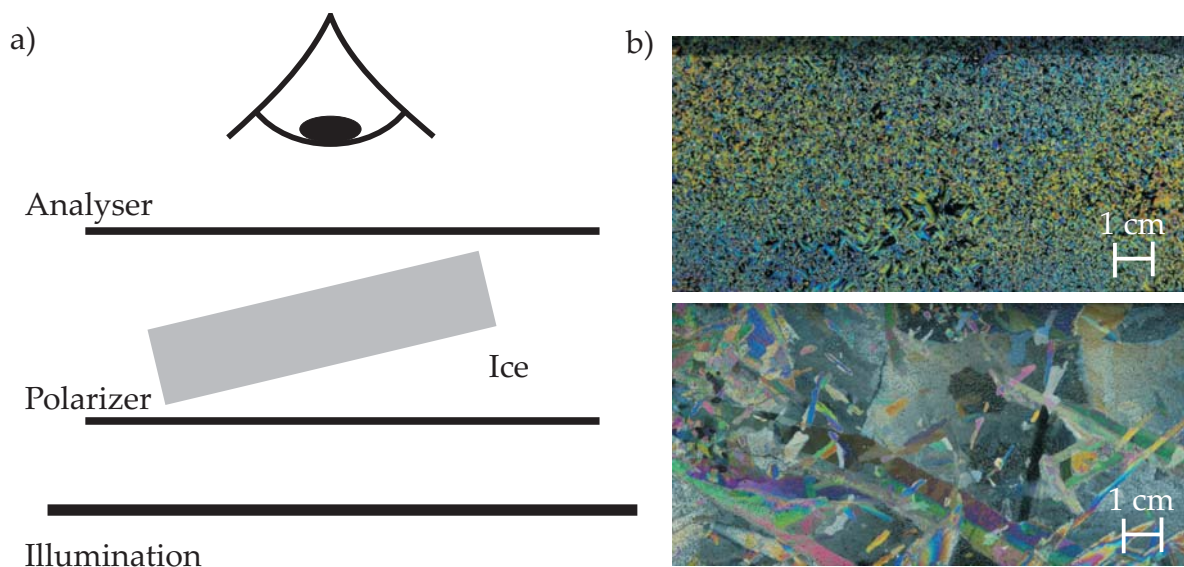


**Figure 2.8:** a) Experimental set-up for observing the ice grain size and orientation with polarized light (According to [91]), b) Ice grain size visualized with polarized light [101]

It is concluded that several methods for characterizing the ice can be used inside the lab and also outside on a test track. In the future various data shall be collected with different methods. With the help of this information basic studies on the ice properties can be done to get an impression of the influences of ice on the friction process.

## 2.3 Properties of rubber

This section gives a short overview on the physics of rubber which is generated by vulcanizing filled caoutchouc. Comprehensive information can be found in the publications of TRELOAR [122], AUSTRELL [5] and SPERLING [112].

Caoutchouc is a plastic material and belongs to the group of elastomers. It consists of long polymer chains which can be acquired naturally or manufactured synthetically. It shows plastic and viscous material properties. Fillers like carbon black or silica can be added in order to change the material properties. In addition the single polymer chains are cross linked by sulphur during the vulcanization process, which results in a complex material structure (Fig. 2.9). Before the vulcanization process the caoutchouc filler mixture is viscous and can be deformed plastically. Afterwards the rubber material becomes elastic. The viscous properties are still unaffected. Depending on the filler and the vulcanization process the material properties can be influenced, and a tire tread compound with arbitrary (in a certain range) material properties can be generated.

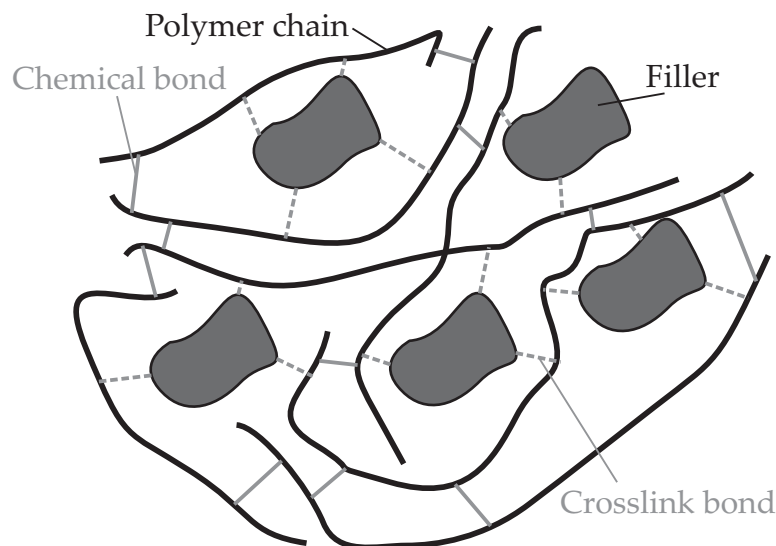


**Figure 2.9:** Molecular structure of filled caoutchouc (According to [5], [52])

The complicated material structure of rubber results in a complex material behaviour. Considering a stress strain diagram of filled rubber (Fig. 2.10) it can be observed that the maximum stress of the first cycle (cp. Fig. 2.10: Cycle 1) is clearly inflated compared to the following cycles. The same behaviour can be observed for the hysteresis of the first cycle. The dissipated energy is clearly reduced for the following cycles. After some cycles a steady state is reached. The observed behaviour is called *stress softening* or MULLINS effect. This effect was investigated by MULLINS [79]. The reason for this material behaviour is a combination of recoverable and unrecoverable configurational changes of the molecular rubber structure.

Another effect which can be observed by comparing different strain levels is the so called PAYNE effect [89]. The gradient of the stationary curve is reduced for increasing strains.



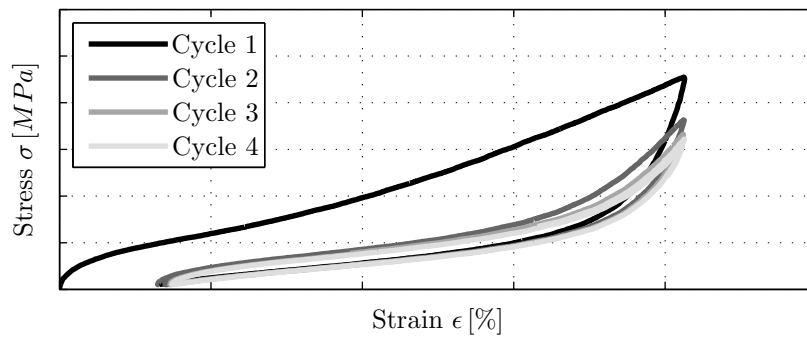


**Figure 2.10:** Stress strain diagramm of filled rubber (Data from CONTINENTAL)

It is caused by the detachment of the cross links between filler and polymer chain (Fig. 2.9). Both effects are negligible for low strains [74]. Additional information concerning the material behaviour and properties of rubber can be found e.g. in [74], [33], [56], [5].

## 2.4 Mechanisms of rubber friction

Besides the rubber material behaviour the friction mechanisms of rubber are very complex as well. The COULOMB friction model is valid in certain limits only. The viscoelastic material properties of rubber cause a complicated friction behaviour which depends e.g. on the contact area, the sliding velocity, the normal pressure and the ambient temperature [98]. The compound of the rubber as well as the structure of the contact partner influences the friction level. Conventional friction theories which were developed for metals do not suffice to describe the rubber friction. For a better understanding the single friction mechanisms are considered in detail. The rubber friction in general is dominated by four single mechanisms:

- Hysteresis  $F_H$
- Adhesion  $F_A$
- Cohesion  $F_C$
- Viscous Friction  $F_V$

The overall friction force  $F_F$  is assumed to be the sum of the single components

$$F_F = F_H + F_A + F_C + F_V. \quad (2.3)$$

A fundamental investigation of the friction mechanisms has been done by KUMMER [66] (see also [72]). With his "unified theory of rubber and tire friction" he investigated the relation between adhesion and hysteresis and the damping properties of rubber. He formulated a general theory of rubber friction mechanisms (cp. Fig. 2.11) based on lab and tire experiments.

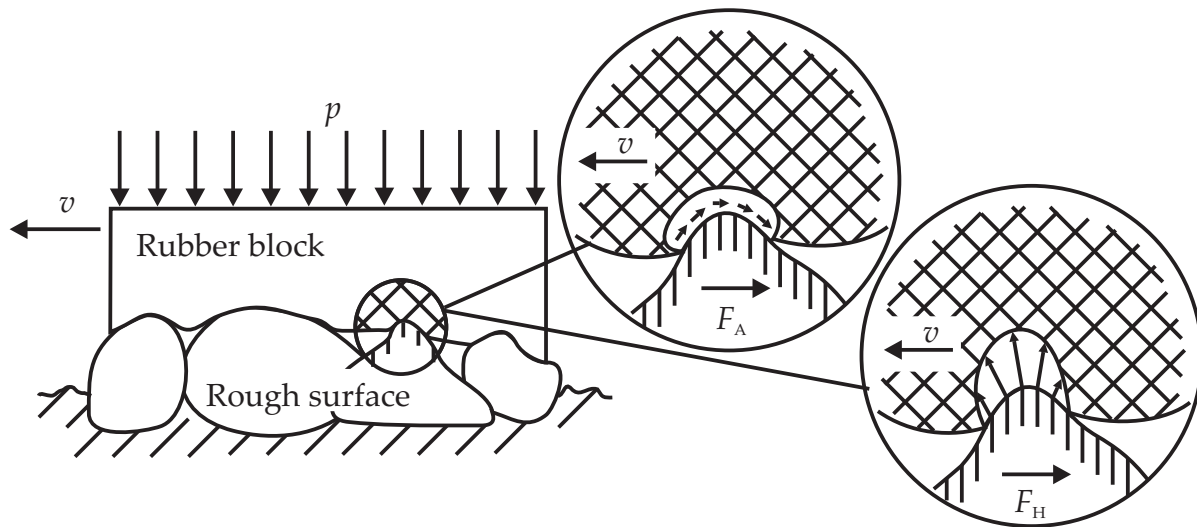


**Figure 2.11:** Rubber block sliding on a rough surface. Friction mechanisms include adhesion and hysteresis and depend on normal pressure  $p$  and sliding velocity  $v$  (According to [66])

### Hysteresis

The friction mechanism called hysteresis is caused by inner damping of the rubber material. So the energy used to deform the rubber can be regained only in a certain range (cp. Fig. 2.10). The dissipated energy results in the hysteresis friction force  $F_H$ . The hysteresis friction mechanism occurs, when a tire tread block slides on a rough surface. The single surface asperities cause a deformation of the tire tread blocks. Hysteresis dominates the so-called "wet friction" on rough surfaces. It depends on the rubber material, surface roughness, sliding velocity, normal load and temperature.

### Adhesion

During the contact of a rubber surface with an arbitrary material a molecular junction is generated. Pulling the rubber back in normal direction or moving the rubber block forward in tangential direction extends the polymer chains of the rubber. If the stress becomes too large the molecular junction breaks and the polymer chain relaxes. Both extending the polymer chain and breaking of the molecular junction dissipate energy which causes another friction force: The so called adhesion force  $F_A$ . It is associated with an energy loss caused by the inner damping during the elongation of the polymer chain and is sometimes called adhesion induced hysteresis. The adhesion dominates the so-called "dry friction" on smooth surfaces. It can be eliminated by lubricants like water or oil in the contact.

### Cohesion

The generation of wear particles or cracks on the rubber surface is associated with the formation of free crack surfaces and needs energy. This energy represents the cohesive part of the friction force  $F_C$ . In general, the generation of new surfaces due to material failure on the tread block is called cohesion.

### Viscous friction

Viscous friction  $F_V$  occurs in lubricated contacts. The movement of the rubber causes shear forces in the lubricant due to viscous flow. Sometimes the lubricating film separates both partners completely so that the total friction force  $F_F$  is equal to the viscous friction force  $F_F = F_V$ . This phenomenon happens during the hydroplaning of a tire. The tire loses the contact to the ground and literally swims on the fluid. The STRIBECK curve is often used to explain the mixed friction phenomena of lubricated systems. It shows the dependency of the friction force  $F_F$  on the sliding velocity (Fig. 2.12). Static friction occurs if there is no relative motion. The STRIBECK curve can be divided into three parts. The first one is the regime of boundary friction where the two solid bodies are in contact (Fig. 2.12, I). The second part (Fig. 2.12, II) is the area of mixed friction. It is characterized by local contact points of the solid materials but also by a lubricant in the contact zone. If both solid materials are completely separated fluid friction occurs (Fig. 2.12, III). The viscous friction force increases with increasing velocity. For more details see [116]. Background information on friction mechanisms and friction theories for ice are introduced later on (cp. Chapter 2.6).

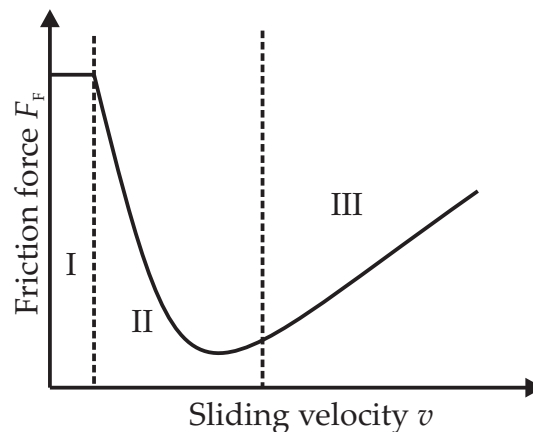


**Figure 2.12:** Different friction regimes depending on the sliding velocity (According to [116]), I: Boundary friction, II: Mixed friction, III: Fluid friction

The tire or tire tread block friction mechanisms are still of great interest. This is proven by many Ph. D. theses coming up within the last years, e.g. GIESSLER [39], VAN DER STEEN [114], MOLDENHAUER [74], GUTZEIT [44], GÄBEL [33], LE GAL [35], LAHAYNE [68], LINDNER [70], BOLZ [14], HOFSTETTER [52], IHLEMANN [56] and AUSTRELL [5] but there are still open questions especially in the case of rubber-ice friction. Some of these questions are formulated in Chapter 3.

## 2.5 Tire and tire tread block testing

The motivation of tire industry to find weather independent tire test methods exists for a long time. The aim is testing tires throughout the whole year. Various approaches were

followed. For example CONTINENTAL tested winter tires in snow proof areas of the Alps already back in the 1950s [40], but these tests could be done in the European winter period only. Therefore possibilities have been evaluated to run tests without natural snow. The use of a snow gun was discarded because the test programs became too expensive and time-consuming due to unstable weather conditions [40]. Performing vehicle tests in the lab could not be done either. Problems with the track preparation and increasing costs due to infrastructural costs and energy consumption made this approach unattractive [40]. This situation resulted in the idea of testing single tires and tire components like tread blocks in the lab. Although several test rigs exist (cp. Chapter 2.5.1) where snowy and icy test surfaces can be used, the vehicle test is essential. Numerous vehicle tire tests fall upon the winter tire performance criteria (cp. [82], [83]). So many tire manufacturers have got their own proving ground(s) where winter tire tests can be done. Additionally, independent organizations run test areas as well.

Within the following pages a general overview of different test rigs is given. Thereby tire test procedures and methods are separated from tire component test rigs and methods. Similar test rigs (test rigs working with the same principle) are introduced within one chapter. It has to be mentioned that the following section gives an overview of existing and commonly used test rigs in the western world only. An additional overview of miscellaneous test rigs was collected by DO and ROE [23].

## 2.5.1 Tire test methods

The following section gives a short overview of tire tests and test vehicles for outdoor tests. It is followed by a review of indoor tire test rigs.

### 2.5.1.1 Vehicle tests

Besides the subjective tire evaluation objective tests are performed. The forces acting on the tire can be measured directly with instrumented wheels or indirectly by measuring acceleration. The test cars used for vehicle tests typically are equipped with special hardware and software to collect the test data. Examples are the Saab friction tester, the CRREL instrumented vehicle [108] and the Smithers drive traction test vehicle [24], [86]. Furthermore, vehicles with a special interface exist using a fifth test wheel like the Uniroyal-Goodrich traction tester [22], [108]. Another possibility to evaluate the tire performance is the so called two vehicle drawbar method [24], [59]: Two vehicles are linked with a drawbar and forces, slip<sup>4</sup> and acceleration of both vehicles are measured. Independent from the test setup all methods allow conclusions concerning the tire properties for passenger cars and trucks. Other instrumented vehicles for tire tests are, for example, a modified snow removing vehicle characterising the road condition to increase the traffic safety [4]. Another institution modified several trailers. The test tire can be mounted on a special interface

---

<sup>4</sup>A velocity difference between two objects is called slip. The slip between tire and surface is  $S = 100\%$  for a sliding vehicle with blocked tires

to test the tire properties [7]. In general, the trailer is a commonly used method for tire testing, e.g. [123]. Furthermore, a bus was converted [69]. The so called "tire measure bus" has a tire test rig between front and rear axle. With this test rig arbitrary tire characteristic measurements can be done. An additional overview concerning different test vehicles was collected by BOLZ [14].

### 2.5.1.2 Tire lab tests

Over the years several different types of indoor test rigs have been developed (Fig. 2.13). Depending on the measuring task one test rig can be more suitable than another. A linear test rig (Fig. 2.13 a) can be used for tests on different road surfaces like e.g. asphalt and snow. Such a test rig can be found at the University of Darmstadt, Germany [7]. The ambient temperature can be cooled down but tests on snow and ice have never been done. A disadvantage of the linear test rigs is the limited friction surface length.

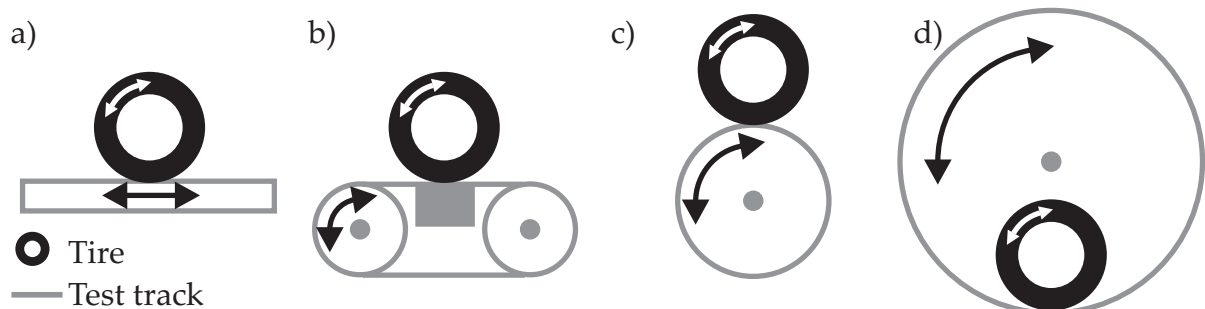


**Figure 2.13:** Different designs for tire test rigs: a) Linear test rig, b) Flat track test rig, c) Outer drum test rig, d) Inner drum test rig

Flat track (Fig. 2.13 b) and outer drum test rig (Fig. 2.13 c) are not practical for other track materials than corundum or steel because asphalt, ice or snow tracks are dismantled due to the centrifugal force. Such test rigs are normally used to measure rolling resistance, side force diagrams or noise characteristics. Another disadvantage of the outer drum test rig is the curved surface which changes the surface-tire contact situation. The same problem exists for the inner drum test rig (Fig. 2.13 d). LEISTER investigated this phenomenon in detail [69]. He analyzed the influence of inner and outer drum surface bending compared to a flat track test rig comparing the influence on slip angle, side force and self aligning torque diagrams. The drum bending influenced the cornering stiffness in a significant way. The inner drum overestimates the cornering stiffness and the outer drum underestimates its value. The righting moment was influenced for small slip angles: The outer drum underestimates and the inner drum overestimates the righting moment compared to the flat track result. Anyhow, the inner drum test rig also has advantages: It can be equipped with arbitrary surfaces because the centrifugal force presses the surface in the drum. Furthermore, an unlimited track length is realized. A large drum can be found at the Karlsruhe Institute of Technology, Germany which allows the execution of snow and ice tests [14], [40] but concrete and asphalt surfaces [31] can also be studied.

## 2.5.2 Tire tread block test rigs

Another important part of the tire development process is the test of single components. The tread compound properties can be evaluated in the lab using a single tread block. A single tread block allows the study of friction mechanisms and contact phenomena [99]. The particular advantage of tire tread block tests is that they allow to concentrate on isolated specific aspects of tread block behaviour under perfectly controlled experimental and environmental conditions. Depending on the demand different types of test rigs exist (Fig. 2.14).

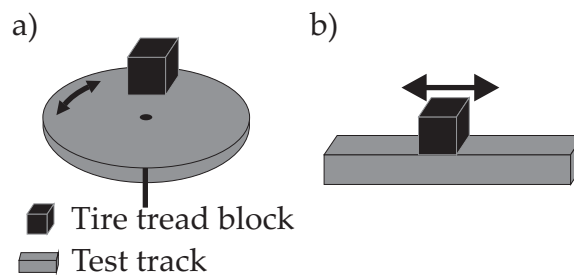


**Figure 2.14:** Different designs for tire tread block test rigs: a) Tribometer, b) Linear test rig

One group of test rigs uses a circular surface with a tread block sliding on it (Fig. 2.14 a). Depending on the construction two types are available: One group presses the tread block element against a rotating table [29], [129]. The rotational speed limits the usage of this type of test rig for friction measurements on ice surfaces because the melted water is pressed to the outer area of the table due to the centrifugal force. At the other type of test rig the sample is rotated while the surface stands still [3]. This type of test rig offers the opportunity of arbitrary rotational speeds especially for ice surfaces because the surface stands still. Both test rigs provide an endless track length. A specific function of the turntable used by ROBERTS and RICHARDSON is the possibility to observe the contact area of the tread block through the tread block sample [103].

The linear test rigs present the second group of equipment (Fig. 2.14 b). Here the tread block element performs a linear motion. A Linear Friction Tester (LFT) is located at the University of Vienna [54], [68]. The University of Helsinki built the "Mini-Mu-Road" [124], [123], [74]. A new linear test rig was built at the University of Edinburgh for investigating rubber-ice friction mechanisms [109]. The test rig used for the present thesis is a linear test rig as well. The high speed linear test rig "HiLiTe" was built by MOLDENHAUER ([74], [76]) and continuously modified and improved [99]. A detailed description of HiLiTe is given in Section 4.2.

## 2.6 Frictional investigation of tires and tire tread blocks

This chapter introduces tire test and tread block test results on ice given in the literature. Already known friction mechanisms and influencing factors are collected and existing friction models of other authors presented. Details on the preparation of the ice and rubber as well as the measurement procedure are given in the cited literature.

The aim of this thesis is the investigation of friction mechanisms of sliding tire tread blocks on ice. Therefore the tire tread block behaviour in the tire footprint is investigated in a first step for getting a detailed impression of the different tread block motions. Based on detailed studies of the tread block movement in the tire footprint with simulations (Fig. 2.15) it can be seen that the parts of sticking and sliding areas within the footprint strongly depend on the slip of the tire. With increasing slip the area where the tread blocks slide through the footprint increases continuously. At slip values between seven to eight percent nearly the whole footprint is under sliding conditions.

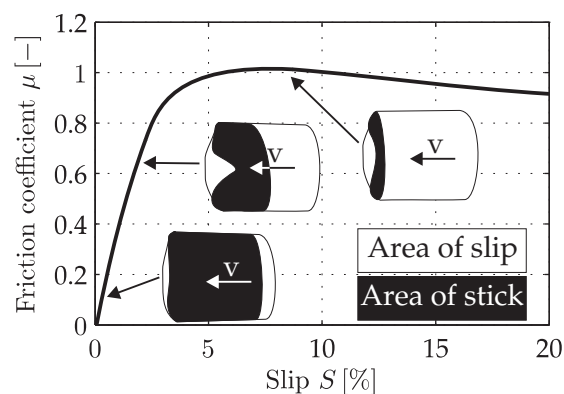


**Figure 2.15:** Sticking and sliding within the tire footprint depending on slip (According to [48], [98])

For the sake of completeness a basic overview of the tire-“rough surface”-contact is given. The contact of tires with dry concrete or asphalt is characterized by high friction coefficients compared to snow and ice (cp. Fig. 2.16). It is caused by the interlocking of the tire tread with the single surface asperities. The dominating friction mechanism is hysteresis, but also adhesion acts in the contact. Wet roads show a smaller friction level (cp. Fig. 2.16). The adhesional component of the overall friction force gets lost. A fundamental work has been done by CLARK [19]. This book covers all topics concerning tires like material, mechanics and testing. An overview of the friction process gives the literature research from BACHMANN [6]. Additional tire characteristics can be found in [30], [7]. The tire tread block-road interaction has been investigated in depth by GÄBEL [33] and MOLDENHAUER [74]. A detailed investigation of the influence of the contact temperature on the sliding and rolling friction has been done e.g. by WANGENHEIM and RIPKA [127] and HOFSTETTER [52]. The influence of the slip on the time dependent friction coefficient was investigated in detail by GUTZEIT [44].

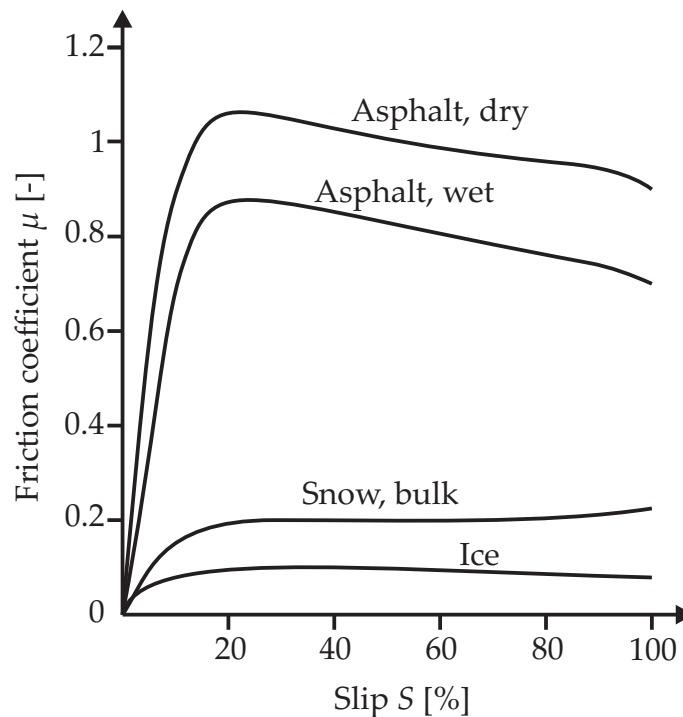


**Figure 2.16:**  $\mu$ -Slip curve measured on different surfaces (According to [130])

### 2.6.1 Performance characteristics of tires on ice

This section gives an overview of basic tire performance measurements on ice based on vehicle tests of CONTINENTAL. Detailed explanations of the single tire friction mechanisms which cause the characteristics are given in [47], [77]. In general every part of the tire (cp. Chapter 1) influences the friction behaviour. The tire test results presented here were originally obtained by CONTINENTAL. Tests with the aim to evaluate the tire performance outdoors are reported in [118], [85], [20]. A commonly used test method is the so-called traction test. A standard test method is defined by ASTM [119]. An overview on tire traction testing has been given by KING [62]. In general, this test is performed with special test vehicles (cp. Section 2.5.1.1) which are equipped with an additional fifth tire used for the tests. The constant rolling test tire is accelerated and forces and velocities are measured while the vehicle velocity is kept constant. The friction coefficient can be calculated for every slip phase. The so called  $\mu$ -slip curve is generated (Fig. 2.16). It shows the dependency of the friction coefficient on the slip<sup>5</sup>. It is used to judge the quality of a tire and to compare the quality of different tires respectively. Instead of the friction coefficient the traction force can be plotted against the slip. This test can also be done with a normal passenger car to avoid the need of a special test vehicle. A disadvantage is the increasing velocity of the vehicle during the acceleration process which makes the calculation of the slip level more complex. Particular attention has to be paid to the effects resulting from the evaluation of the winter traction measurement as shown by SHOOP et al. [107]. A typical  $\mu$ -Slip curve of

<sup>5</sup>During a braking manoeuvre the ABS tries to match this curve near the maximum of the  $\mu$ -Slip curve to keep the stopping distance as short as possible



a winter tire on ice shows a decreasing trend with increasing slip (Fig. 2.17). Depending on the tire properties, a certain characteristic can be adjusted.

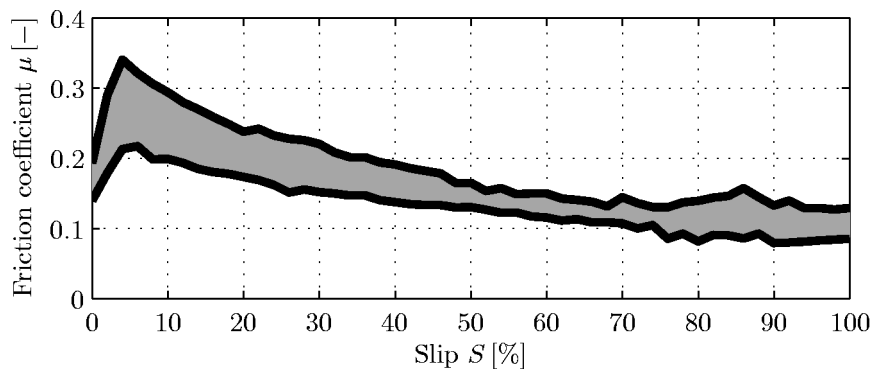


**Figure 2.17:** Range of measured  $\mu$ -Slip curves of different winter tires on ice (Based on internal tire test results of CONTINENTAL)

The level of friction depends on the number of sipes per tread block (Fig. 2.18). The friction characteristic shows a maximum due to the optimized interaction of tread compound and block geometry. It seems that an optimum number of sipes per tread block can be found to maximize the friction potential. Other publications where the tread block geometry and the number of sipes have been investigated are [73] and [133].

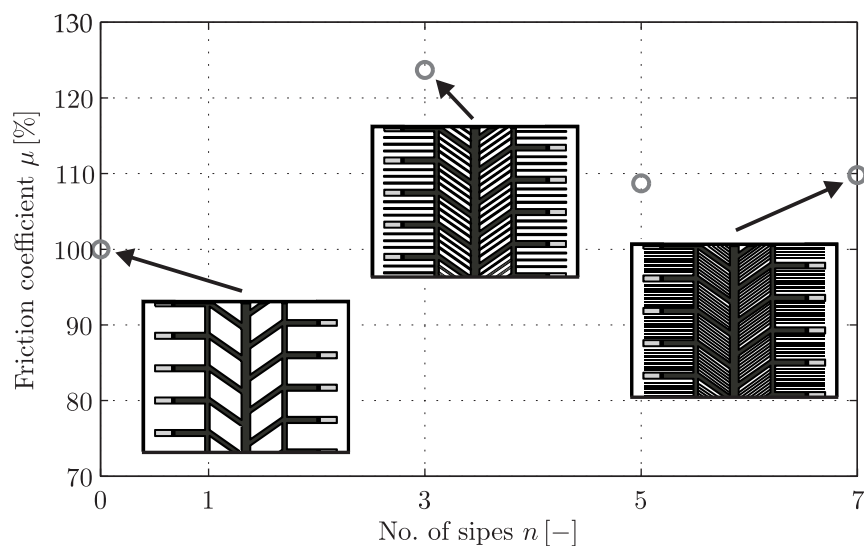


**Figure 2.18:** Influence of the number of sipes per tire tread block on the friction coefficient on ice [99]

The following subsections show different investigations, measurements, theoretical approaches and simulations of ice friction by several authors. A selection of the main relevant papers has been made and the section is structured in such a way that each author or group of authors and their results are presented in a separate subsection. This structure has been chosen because different authors developed theoretical models and validated them with their measurements. For a better overview the different parameters influencing the rubber-ice friction are divided into three groups:

- **Test parameters:** These parameters are linked with the test rig like sliding velocity and normal pressure. They also include ambient parameters like temperature and relative humidity.
- **Ice properties:** This group is related to ice. It also includes the surface water layer although it is influenced by test parameters like temperature and humidity, but also the frictional power (sliding velocity, normal pressure).
- **Rubber properties:** These parameters describe the single rubber blocks. They include material as well as design parameters. The contact area is influenced by both materials, rubber and ice. Mostly on rough surfaces a difference between nominal contact and real contact area can be found. The nominal contact area is similar to the cross sectional area of the tread block sample. Depending on the contact partner the real contact area can be much smaller. Therefore the nominal dimension of a tire footprint is comparable with the size of a post card but the real contact area is much smaller depending on e.g. surface structure and normal load (Fig. 2.19, see also [33]).

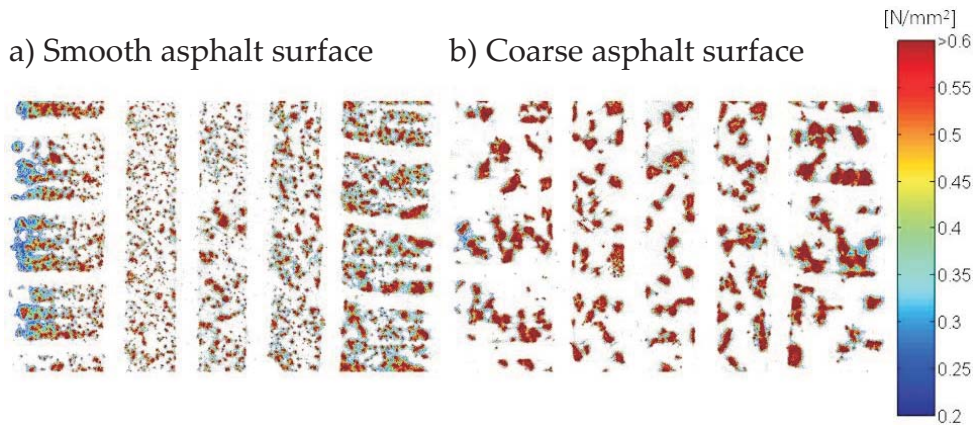


**Figure 2.19:** Real contact area of a tire: a) on smooth asphalt, b) on coarse asphalt (See also [33])

## 2.6.2 Mechanisms of sliding on ice investigated by F.P. BOWDEN and T.P. HUGHES

The following section is based on a work of BOWDEN and HUGHES and deals with the mechanisms of sliding on ice and snow [15]. At the beginning they considered the friction on ice and snow theoretically to explain the low friction coefficients. "The suggestion has often been made that, in skating or skiing, the surfaces are lubricated by a layer of water formed by pressure melting" [15]. They made simple calculations of the skiing process by considering temperature, mass and contact area to get an impression of the pressure melting theory. They concluded that the pressure melting theory cannot be neglected due to their theoretical calculations, "but if it is true it means that the real area of contact is extremely small" [15]. As already mentioned DÖPPENSCHMIDT also gave a rough

estimation on the possibility that pressure melting occurs. In her opinion pressure melting does not deliver a significant contribution to the water film thickness (cp. Chapter 2.2.2). The pressure melting was not sufficient to cause the lubrication film so BOWDEN and HUGHES considered melting due to frictional heat. The heat generation is concentrated on the points in contact with the surface. Based on different assumptions concerning contact area ("Again we do not know the real area of contact" [15]) and ambient temperature, different water layer thicknesses were calculated. Based on the electrical conductivity between two electrodes they determined the water film being about  $70 \mu\text{m}$  thick during the sliding process. Besides the theoretical estimation of the friction process they presented experimental results of solids sliding on ice and snow. The experiments were done using a turntable test rig. Based on their measurement results they concluded that the low friction coefficients on ice at temperatures near the melting point were caused by a lubricating water film. This water film occurred at the contact points of the surfaces. They also found out that the friction coefficient of sliding friction is independent of load, apparent contact area and speed of sliding over a certain range. A decreasing temperature resulted in an increasing friction coefficient because the more frictional heat must be generated to melt the ice. Their measurements with skis have shown that the friction strongly depended on the thermal conductivity of the ski. This indicated that frictional heating played an important role to melt the ice and therefore to form the water film. Former approaches considered the pressure melting to be responsible for the formation of the water film.

### 2.6.3 Investigation of the kinetic friction on ice by D.C.B. EVANS, J.F. NYE and K.J. CHEESEMAN

EVANS et al. mentioned that the theory of BOWDEN and HUGHES is widely accepted "but it has not been developed analytically to a point where it can fully explain the effects of temperature, velocity, load and slider material on the coefficient of friction" [28]. EVANS et al. also derived an analytical solution of the frictional melting theory under consideration of the heat flows occurring in the contact area due to friction. "This means that, instead of considering the friction as a resistive force we may consider it as heat produced at the surface per unit displacement" [28]. Their theory contains three terms: The heat which melts the ice surface and causes the water film, "the heat which diffuses into the ice" and the one which "is conducted through the rod" [28]. The sum delivered the friction force or, by dividing by the load, the friction coefficient. A detailed consideration of each part followed, and the analytical calculation of the friction coefficient was compared with experimental data. Analytical and experimental results differed within a factor of two. EVANS et al. assume that the difference between theory and experiment was caused by the overestimation of the contact area.

In their experiments EVANS et al. considered the influence of the sliding velocity on the friction process. They believed that the friction coefficient decreases approximately with:  $\mu \sim v^{-\frac{1}{2}}$ . Furthermore, an increasing temperature resulted in a decreasing friction

coefficient. Additionally, the authors observed that the wear of the ice track increased rapidly at higher temperatures. Their investigations on the influence of the normal load  $L$  showed the tendency to  $\mu \sim L^{-\frac{1}{2}}$ , but "further work would be needed to establish the friction-load relation more precisely" [28]. Their investigations on the contact area gave strong indications that water is formed there. Based on their experiments they confirmed the view of BOWDEN and HUGHES that the contact area is lubricated with a water layer and EVANS et al. expand the mechanisms in the contact area: "mixed lubrication exists: the lubricant supports much of the load between the surfaces, but at high points the surfaces come into contact or are separated by a film only a few molecules thick..." [28]. These contact points delivered most of the frictional force. The authors also took into account that an area of dry friction could be found at the leading edge of the specimen where the ice temperature is rapidly raised to the melting point. They summarized that the formation of the liquid layer within their experiments was caused by the frictional heating and not by pressure melting: "If the film were produced by pressure melting, heat would have to flow to it not away from it: the temperature gradients are the wrong way round for this" [28]. The pressure melting theory could be taken into account as a reason for the formation of the water film at temperatures above  $T = -2^\circ\text{C}$ . EVANS et al. also took a dry area in the front of the specimen into account for the generation of friction: "We conclude that, in the range of our experiments, the main contribution to the observed friction comes from a large lubricated area at the melting point rather than from a small dry area in front, but of course at low enough temperatures or small enough velocities the dry area would certainly become the significant one" [28].

Although the authors made comprehensive experiments and derived a detailed analytical model, they mentioned that there is still much work to do: "Precisely how the heat is generated in the lubricated area, and what is the detailed mechanism that produces the frictional drag are questions that are not answered by our experiments. ... if we know that the contact is at the melting point and  $\mu_m$  (the heat loss by melting the ice) is small, we can calculate the friction but to understand why these conditions hold would need a deeper insight into the frictional mechanism" [28].

#### 2.6.4 Friction measurements of S. VENKATESH

VENKATESH investigated rubber-ice friction with a turntable. He used a rubber specimen with cylindrical shape,  $A = 10\text{ cm}^2$  cross sectional area and  $h = 10\text{ mm}$  thick [125]. Based on his measurements he found out that the friction of rubber-ice depends on the normal load [125]. With increasing normal pressure the friction coefficient decreased. The measurements confirmed that the friction coefficient  $\mu$  on ice followed the law

$$\frac{1}{\mu} = A\left(1 + \frac{Bp}{E_0}\right). \quad (2.4)$$

The constant  $A$  depended on the type of rubber material with values between  $A = 1\text{...}8$ , and the constant  $B$  "is almost the same for all rubber like materials and averaged around"

[125]  $B = 15$  for all rubber-like materials. The compression modulus is  $E_0$  and the overall normal pressure is called  $p$ . The constants  $A$  and  $B$  vary depending on the type of ice surface. A temperature influence of the friction of rubber-ice could be found as well: A decreasing temperature caused an increasing friction coefficient [125].

The friction process also depends on the chemical composition of the rubber specimen. In general an increasing amount of softener resulted in an increasing friction coefficient. The age of the rubber seemed to influence the friction behaviour clearly but its shape seemed to have no influence on the friction process. The smoothness of the test specimen affected the friction process just like the age of the ice. How the friction process was influenced and which changes occur was not mentioned. The conditioning time of the rubber sample at test temperature could be another influencing factor. It sometimes affected the friction coefficients just like the smoothness of the ice surface and the age of the ice. Details concerning the impact on the friction process have not been given in [125].

### 2.6.5 Investigation of rubber-ice friction by A.D. ROBERTS and co-authors

The rubber-ice friction has been investigated at the Malaysian Rubber Producers' Research Association to improve winter tires, e.g. [41], [111]. ROBERTS and RICHARDSON investigated the contact interface between rubber and ice surfaces with a newly developed test rig [103]. The aim of their research was the understanding of tire grip on icy roads by observing the interface. Therefore, they used a turntable and a rubber hemisphere as test sample. The contact situation could be observed through the transparent smooth-surfaced rubber sample [103]. The transparent rubber seems to be promising for gaining a deeper view into the contact mechanisms although the missing fillers like carbon black influence the rubber material properties. The investigations of ROBERTS and RICHARDSON on the temperature influence in a range of  $T = -32^\circ\text{C}$  to  $T = -1^\circ\text{C}$  showed "a sharp fall (of friction) for all speeds at temperatures above  $-10^\circ\text{C}$ . The fall was dramatic, 20 times or more" [103]. They compared the measurements on ice with those on glass surfaces. Based on these measurements they concluded that "there is a special phenomenon on the ice surface itself because near its melting point "lubrication" is so much better than that of water on glass " [103]. Within their investigations of adhesion of ice they calculated the surface energy based on the observed contact areas. They observed "an apparent increase (of the surface energy) as the melting point of ice was approached" which "might be an artefact associated with the ice surface" [103]. They noticed a circular mark in the ice after a dwell time of some minutes of the rubber hemisphere. A smaller load caused smaller marks. The investigation of the separating force showed a decreasing characteristic the nearer the ice melting point was reached. Based on their results they assumed the existence of a water film although it could not be seen. At temperatures above  $T = -10^\circ\text{C}$  the pull-off force measurements indicated a reduced adhesion compared to colder temperatures.

They concluded their work with the recommendation that future investigation should be focused not only on the rubber-ice interaction but also on the ice surface properties.

In addition ROBERTS investigated the adhesion in more depth and also studied some other factors influencing the friction of rubber-ice [104]. He again studied the contact interface optically and considered rolling and sliding. Again he compared a wet glass surface with the ice surface. He found evidence that the water is squeezed out (at slow sliding velocities) on glass surfaces which resulted in the high friction coefficient. Ice near the melting point was much more slippery than wet glass. In his opinion this was caused by "a thin aqueous film bound to the ice surface" [104]. In contrast to the glass surface this film "is not squeezed away and so it provides a very effective lubrication" [104]. The friction showed again the strong decline while approaching the melting point of the freshly prepared ice track. He also predicted the friction potential with the help of the sliding friction stress (friction force/contact area) with a good correlation to the measurements on cold ice. Other measurements showed a small rubber pull-off force on ice near the melting point which indicated again that water is in the contact. In general, the low friction and adhesion of rubber-ice near the melting point was caused by the ice surface. Its influence on the friction process was shown again by comparing polished ice and an ice surface covered with frost (at low temperatures). The polished ice surface showed a high friction level ( $\mu = 1,8 \pm 0,2$ ). Stick slip phenomena could be observed as well "-an indication of good adhesion" [104]. In contrast, the frosty surface delivered friction coefficients of  $\mu = 0,5 \pm 0,005$ . As a result all subsequent measurements had been performed on polished ice to ensure the comparability between different measurements. The age of the ice track also influenced the friction. An old ice track showed a much smaller friction level compared to a newly prepared one. This phenomenon was explained with the concentration of impurities at the ice surface of the old track. The conductivity of the water also verified this theory<sup>6</sup>. ROBERTS concluded that the "compound softness benefits the grip to ice, probably because the softer rubber can come into more intensive intimate contact with the ice" [104]. In relation to the tire grip he concluded that "the grip of rubber to ice near its melting point appears largely to depend upon the surface properties of the ice" [104].

ROBERTS and LANE investigated the influence of ionic contaminations (such as salt) of ice on the friction process [105]. They varied the concentration of the salt and also showed the influence of different salts. The friction characteristic declined and the friction curve was shifted to other temperatures depending on the concentration and the type of salt. In relation to the friction of winter tire compounds they found out that "the harder the compound the more easily a liquid surface can be penetrated at asperity high spots" [105]. Based on the result that their hardest compound was worst (at  $T = -23^{\circ}\text{C}$ ) they concluded that an optimum hardness for best friction in a wide temperature range exists.

---

<sup>6</sup>An increasing number of impurities (normally different ions like e.g. salt) in the water increase the conductivity of the water and reduces the friction coefficient, cp. Section 4.3.5.1

### 2.6.6 Friction measurements and modeling by P. OKSANEN and J. KEIONEN

OKSANEN and KEIONEN investigated ice-ice friction with a turntable. They found out that the coefficient of friction depended on the sliding velocity, the normal load and the temperature [87]. They also developed a mathematical model to calculate the friction coefficient based on the assumption that the frictional heat melts the ice into water. They further assumed that the friction force was caused by the water film only. So the friction force was generated by the viscous shear of the water layer. Based on the theoretical approach they pointed out that the friction coefficient decreased with  $\mu \sim v^{-\frac{1}{2}}$  at low temperatures. At temperatures near the melting point the friction coefficient increased with  $\mu \sim v^{\frac{1}{2}}$ . Depending on the temperature two mechanisms could be found: At low temperatures the frictional heat flows into the ice. An increasing velocity causes a reduced contact time which results in a shorter heat conduction phase. The heat penetration depth was smaller "so that a greater fraction of the heat produced remains for melting the ice" [87]. At temperatures near the freezing point "the main part of the frictional heat is consumed in the melting of ice" [87]. They showed that the thickness of the water layer  $d$  followed the law  $d \sim v^{\frac{1}{2}}$ . They also linked the thickness of the water layer  $d$  and the friction force  $F_F$  which results in the previously mentioned relation between friction coefficient  $\mu$  and sliding velocity  $v$ . The frictional behaviour of ice near the melting point could physically be described as follows: With an increasing velocity "the shear force increases more rapidly than the thickness of the water layer" [87]. The temperature range in between showed a mixed region where the friction was influenced by heat conduction. For further details see [87] and [88].

Additionally, OKSANEN investigated the adhesion strength of ice to several other materials like ice, steel, wood and polyethylene [88]. He made experiments and developed a mathematical model based on the fracture mechanics of ice. With both methods he investigated the behaviour of fresh-water and sea ice. The differentiation between fresh and sea water is done with the help of physical parameters like e.g. elastic modulus. The mathematical model explained the dependency of the adhesion strength on the strain rate. The reason for this dependency "is the creep of ice, which again depends on time, temperature, stress and grain size" [88]. He concluded his work with the statement that both mathematical models (for the kinetic friction of ice and the adhesion of ice) were in general agreement with the experiments. Some exceptions had to be accepted when using simplified models. Furthermore, he noted that "it is typical of measurements of ice properties that the scatter is very large" [88]. It is influenced e.g. by the structure of ice, the preparation of specimens and the experimental arrangements. He concluded that the mathematical models could be improved but also "carefully designed experiments are needed for verification" [88].

### 2.6.7 Arctic Friction Research Study ARTTU

The "Arctic Friction research study" was an interdisciplinary project of different Finnish institutions: Universities, tire manufactures and the Technical Research Centre of Finland (VTT) [123]. The aim of the project was the generation of detailed knowledge of friction phenomena on snow and ice and therefore "maintain the leading position in arctic friction research in the world" [123]. Besides the detailed literature review of friction phenomena of rubber-ice they studied friction mechanisms in the field and in the lab. They built test rigs and correlated field and lab tests. This section gives a brief introduction of this work, for details see [123].

The literature review is a condensed introduction in the topic of ice friction. It begins with a general overview of friction mechanisms on dry and wet road. Hence, the authors pointed out that the morphology of the rubber surface plays an important role, and also that the micro scale roughness of rubber influences the friction on lubricated surfaces significantly. On ice, combined friction phenomena can occur. The authors claimed that the high friction values at cold temperatures and low velocities represent dry friction while the mechanisms of wet friction have to be taken into account when the ice is wet. In their opinion the rubber properties should be marked with low hysteresis and low hardness to improve the rubber-ice friction. The thermal conduction of heat into ice and slider also influences the friction process. "This provides an interesting perspective to control friction on ice by the choice of the slider material (e.g. tire) based on its thermal properties" [123]. Based on the theory of EVANS et al. (cp. Chapter 2.6.3) and OKSANEN et al. (cp. Chapter 2.6.6) VAINIKKA and PIRJOLA developed a numerical model to calculate the friction coefficient. They added the influence of pressure melting and slip to the model to increase the accuracy of results. For the calculation of friction coefficients the model "requires the size  $a$  of the contact asperities as an input. This parameter cannot be readily measured" [123]. This is the reason why quantitative comparisons between model data and laboratory and field results could not be made. In general, the model data agreed qualitatively with field and lab tests. At the end the authors concluded that the rubber friction on ice decreases with increasing load. They also pointed out, that the friction coefficient  $\mu$  was  $\mu \sim v^{-\frac{1}{2}}$  for cold temperatures and  $\mu \sim v^{\frac{1}{2}}$  for temperatures near the melting point.

Besides the theoretical view on ice friction phenomena and their modeling, VAINIKKA and PIRJOLA investigated tire friction on an outside test track with a trailer. One aim of the field test was the generation of reference measurements which were compared to lab measurements. All tests were validated with vehicle tests. Furthermore, the influence of the climatic conditions on ice friction was studied. After every measurement in the field the temperature of tire and ice surface was recorded just like the hardness (Shore-D) and the pH-value of the ice. For the evaluation of the measurements the authors used three different methods. The influence of the evaluation method on the measurement result was investigated also. "The order of the tyres varies from day to day. Yet, no clear dependency on climatic conditions to the rank of the tyres could be perceived. The rank of



the tyres depends also according to which friction value is studied (Peak, ABS, Locked)'' [123]. One result which was pointed out is that the friction coefficient increased with decreasing temperature. The comparison of field tests and tests in an ice arena showed similar results, though some differences could be found. The same behaviour could be found when comparing lab and field tests: A correlation existed but the ranking of samples could change sometimes. As a result it could be said that a sliding speed below  $v = 1 \frac{\text{m}}{\text{s}}$  correlated best with outdoor measurements. Furthermore, the normal pressure influenced the friction process significantly. Another challenge which had to be solved was the preparation of homogeneous ice surfaces with similar frictional properties.

Another research topic of ARTTU was the prediction of road weather. Different tools to improve the forecast of the weather were developed and also the influence of electrical forces on the friction process was studied. A device based on this mechanism has been patented by VTT. Considering their measurements ''with practical surface pressures did not show any increase or decrease in friction gives us the assumption that the phenomenon is irrelevant for tyre application'' [123]. Furthermore, they investigated tires with a thermal camera to demonstrate the temperature distribution on its surface. They also studied the production of ice surfaces to ensure similar and homogeneous quality of the ice. For detailed results and further research activities within ARTTU see [123].

### 2.6.8 Friction measurements and simulation of L. BÄURLE

BÄURLE investigated the sliding friction of polyethylene blocks on ice with the aim to reduce the friction in skiing [8], [10], [9]. For the experimental investigations he used a turntable and a polyethylene sample with a size of  $A = 40 \times 40 \times 9 \text{ mm}$  [10]. One measurement period lasted for three minutes and showed a slowly increasing friction force characteristic which was caused by the polishing of the ice surface. The smoothed surface resulted in an increase of the real contact area [10] and therefore the friction force increased. Depending on the ambient temperature, an increasing sliding velocity resulted in a decreasing friction coefficient (for temperatures  $T \leq -10^\circ\text{C}$ ). It followed the law  $\mu \sim v^{-\frac{1}{2}}$  (see also Section 2.6.3 and 2.6.6). The frictional heat melted the ice and increased the thickness of the lubricant film which reduced the friction. At intermediate temperatures ( $T = -5^\circ\text{C}$ ) the friction coefficient was independent on the investigated velocity in a range between  $v = 0 \frac{\text{m}}{\text{s}}$  and  $v = 10 \frac{\text{m}}{\text{s}}$  although the measured slider temperature depended on velocity. An increasing friction coefficient could be observed for an increasing sliding velocity at temperatures close to the melting point. This was explained by the thicker water films enlarging the real contact area. Furthermore, the friction coefficient decreased for increasing loads for all investigated temperatures. Based on experiments with surface variations on polyethylen BÄURLE concluded that the friction can be influenced with defined surface structures of the test sample [8]. Due to water film thicknesses between  $h = 100 - 200 \text{ nm}$  and some microns, further research should be done on the surface topography to reduce the polyethylene ice friction.

Besides the measurements BÄURLE also developed a numerical model to simulate the friction of polyethylene on ice and snow [8], [9]. He also compared the simulation results with measurements [8], [10]. The model included dry friction, heat conduction, phase changes and the shearing of water films [9]. The first basic consideration was done for ice surfaces while the numerical model considered the friction process of polyethylene sliders on ice. In principle it could also be used to simulate friction on snow surfaces [9]. The model is based on the transfer of translational kinetic energy into heat. This heat is unevenly distributed because it is generated at the contact spots. BÄURLE investigated snow surfaces which had been passed by a slider. Electron microscopy and X-ray computer tomography were used to estimate the real contact area. These measurements were static and therefore yield rough estimates only. "Flattened regions that have seen contact are clearly visible and are evidence of melting. They are very unevenly distributed" [9]. Based on the simulations it could be seen that the "thermal conductivity has quite a large influence on friction at lower temperatures, but none close to the melting point" [9].

As a conclusion BÄURLE summarized that the friction process on ice was mainly influenced by "the thickness of the water films and the relative real contact area" [9], depending mostly on temperature and sliding velocity [8]. An increasing thickness of the water film caused an increasing real contact area which then increases the friction. Furthermore, the size of the contact spots played an important role in snow and ice friction [9]. For more details see [8], [9], [10].

### **2.6.9 Investigation of rubber-ice friction of SCHRAMM et al.**

SCHRAMM et al. investigated the mechanisms of rubber on snow and rubber-ice friction. They built a test rig which adopted the sliding of tire tread blocks. They considered the passage of a tire tread block through the tire footprint. They presented lab measurements on snow as well as a friction model which displayed the tread block snow interaction. Their ice friction model was based on the idea of a dry sticking part in the front section of the tire footprint which is followed by a wet sliding phase in the back part which showed a clearly reduced friction coefficient. The model based on a thermodynamical approach. It assumed a stationary heat flow to the ice. Most of the energy was conveyed into the ice which results in a water layer. The authors set up the heat balance for an infinitesimal small part of tread block which allowed the derivation of a non linear differential equation for the layer thickness. So the shear force distribution in the water layer could be calculated which caused the frictional force. For further details on the model set up and the interpretation see [106].

### **2.6.10 The analytical thermodynamical approach to calculate rubber-ice friction by WIESE et al.**

WIESE et al. derived an analytical approach of rubber-ice friction. According to this theory the frictional energy for melting the ice was caused by the shear of the water layer only. Considering the microscopic scale the authors assumed a smooth ice surface and a rough rubber surface based on the GREENWOOD-WILLIAMSON contact theory. As a basic approach they used the thermodynamical conservation law which describes the distribution of the generated energy for melting the ice on the one hand, and for heat conductivity in the ice on the other hand. Step by step the model was extended with the surface roughness and a "squeeze-out" term which is strongly linked with the properties of the rough rubber surface. The non-linear differential equation was solved analytically. The model was loaded with material stiffness parameters, surface parameters and contact area parameters including the contact diameter (measured statically on glass), all gained from experimental results. The calculated friction coefficients had been compared with experimental data. "The calculated  $\mu$  values show a very good agreement with the experimental results" [131]. Due to the smooth ice and a rough rubber surface the effect of hysteresis was neglected. For further details see [131].

### **2.6.11 The analytical thermodynamical approach to calculate rubber-ice friction by SKOUVAKLIS et al.**

The influence of sliding velocity, normal load, ambient temperature and the rubber compound has been investigated with a new linear friction machine [109]. A decreasing friction coefficient was observed for an increasing load, sliding velocity and temperature. Detailed studies were performed on the influence of the glass temperature of the rubber compound on the friction process. The highest friction was determined for the softest rubber (lowest glass temperature) which corresponds to the largest real contact area and thus, resulted in higher friction. For their theoretical calculations the authors used a heat flow model based on the instationary heat flow equation. Model and measurements were in good agreement. For the explanation of different levels of friction they hypothesized "that the values of  $\mu < \approx 0.3$  will be lubricated by melt-water layer, while the higher values (low velocity and low temperature) will have progressively more solid-solid contact. We suggest that there may be a continuum in the friction mechanism behaviour from solid-solid to fully lubricated contact, with different amounts of mixed lubrication within the continuum" [109].

### **2.6.12 Additional publications of other researchers**

As seen before a commonly used model is the assumption that the frictional heat melts the ice, the water acts as a lubricant and therefore the friction coefficient decreases. This theory

was also used by several other authors, e.g. KISHIMOTO [63], SOUTHERN and WALKER [111] and SPRING et al. [113]. Experimental and numerical investigation of rubber blocks on ice were used to calibrate FE models, c.p. HUEMER et al. [53]. The dynamic tire friction potential on ice has also been investigated experimentally by IVANOVI et al. [58]. It was influenced by the vehicle speed, the applied force rate on the wheel (change of applied motor torque per second) and the length of contact time of each tread block element in the contact area. Additionally a clear tire pattern print was observed on the ice surface after a standstill of the tire for about one minute.

The influence of thermal conditions of a rolling tire on the transmittable forces was also a subject of recent research programs [38]. In these investigations a rolling tire had been investigated on a drum test rig with an infrared camera. Besides the measurements a theoretical model had been developed describing the time depending temperature behaviour in the footprint. As a result, a thermal force transmission limit on ice and snow had been introduced. It explained the measured force maxima on ice and hard packed snow tracks. Additionally, the theoretical approach verified that increasing ambient temperatures reduced the transmittable forces [38].

KISHIMOTO mentioned that NIHEI et al. investigated the influence of rubber surface roughnesses on ice friction [63]. They found out that the friction coefficient reaches a maximum at a tire surface roughness of about  $50 \mu\text{m}$ . They concluded that the water is probably removed due to this surface unevenness. Based on this study KISHIMOTO focused a "systematic investigation and detailed analysis of these behaviors to improve the performance of studless tires"[63]. Therefore, he investigated the contact behaviour between rubber for tires and ice [63] by X-ray refraction contrast imaging in depth. He prepared four rubber samples with surface roughnesses of  $20 \mu\text{m}$ ,  $45 \mu\text{m}$ ,  $60 \mu\text{m}$  and  $90 \mu\text{m}$ . The first sample was completely in contact with the ice surface. No clearance could be observed. With an increasing rubber surface roughness the clearance increases as well, and space for dewatering could be generated. On the other hand, a small friction coefficient could be observed due to the decreasing real contact area. Thus, it is very important to observe the contact behaviour between rubber and ice to improve the tire performance [63].

KUROIWA investigated the mechanisms of skiing and skating [67]. He used a test set up where a slider with two speed skates was ejected from a specially designed catapult. The overall sliding distance was measured and plotted against the temperature. With increasing temperature the sliding distance increased as well. He found a maximum of the sliding distance at temperatures near the melting point.

A brief overview of friction on ice was given by PETRENKO [91]. He also considered the adhesional effect of ice. In his opinion the adhesional bonds are the reason for the strong link of ice on a solid body e.g. on a car windshield.

Meanwhile first publications can be found where the tire tread block-ice contact is investigated in more depth. RIPKA et al. visualized the tread block ice interaction with a special

glass bottom test track [98]. They took pictures of sliding tire tread blocks under different conditions with a camera through the clear ice surface. They explained the observed differences in the friction coefficient with the changes of the local contact pressure which has been calculated based on the contact area photos. RANTONEN et al. investigated the contact between studded rubber samples and an ice surface with the help of a glass bottom track [95]. Again a basic requirement for their investigations was the preparation of a clear ice. They used a high speed camera for image recording. Based on the films they visualized the ice particle movement which were cutted out of the ice with the stud and calculated the velocity vector field of each particle.

## **3 Analysis of the state of the art and research objective**

The following analysis of the state of the art points out open questions in rubber-ice friction. The following research objectives formulate the aim of this thesis to close some of the existing gaps in rubber-ice friction knowledge.

### **3.1 Analysis of the state of the art**

With the help of temperature and relative humidity the environment can be characterized and its influence on the rubber-ice friction process can be pointed out. The temperature is a very important factor because it strongly influences the saturation level of the air above an ice surface (cp. Tab. 2.1). Depending on the temperature more or less water molecules evaporate or condensate and therefore influence the condition of the ice surface. This theory is supported by many scientists who investigated the temperature - surface water layer relation of ice surfaces. Although the measured values for the temperature-layer thickness relation vary within a factor of 100 (depending on the measurement method) all investigations show an increasing layer thickness with increasing temperature (cp. Fig. 2.7). The existence of publications where the influence of the humidity on the surface water layer thickness on the rubber-ice friction process is investigated are unknown.

Over the years mostly the influence of test parameters and the contact material and geometry on the friction process has been investigated with different test rigs. The influence of sliding velocity and normal load on the friction coefficient are investigated very detailed. An increase of each parameter results in a reduction of the friction coefficient. A temperature raise reduces the friction. This behaviour can be explained by considering the frictional heat which melts the ice and therefore leads to a lubricating film in the contact. This model is widely accepted and used by different scientists for calculating the friction level. The pressure melting theory is in contrast to this. Up to now it is not finally clarified if pressure melting occurs in the contact or not. The result of different estimations strongly depends on the adopted size of the real contact area. Measuring the size of the real contact area for arbitrary contact situations in general would give the possibility to improve the reliability of theoretical models and to understand the friction mechanics in more depth. So several researchers claim that detailed knowledge on the real contact area would improve their theoretical calculations significantly. First investigations of the real contact area seem

to be promising but considering the rubber-ice contact through a glass bottom track has a significant disadvantage: The camera always notices the rubber sample no matter if it is in contact with the ice or not. This effect has to be optimized in the future to guarantee a clear differentiation between contact and no contact. The influence of different slider materials has also been studied. In the case of rubber the hardness of the compound has a big influence on the friction: The softer the compound the higher the friction.

Although some ideas exist which describe the development of the water layer (pressure melting and melting due to frictional heat) the condition in the contact area is unknown. Different ideas exist: Some researchers claim that the water layer prevails all over the contact. Other scientists think about wet and dry regions but the location of these is not clarified in depth. Some favor dry contact spots which are surrounded by water. Others again assume a dry run-in area in the beginning of the tire footprint which is followed by a water layer in contact. So it can be concluded that a consistent, widely accepted model of the prevailing mechanisms in the contact area is missing.

Friction is a process which is influenced by both partners. So in this case the ice and its surface cannot be neglected. This has been shown by different investigations where the influence of the level of salinity has been shown. The level of salinity influences the friction process clearly: An increasing level of salinity results in a reduced friction coefficient. However, there are many more factors which can be used for characterizing the ice like pH-value, conductivity, ice grain size as well as the mechanical properties like shear resistance, modul of elasticity and so on. So several scientists assumed an influence of the ice on the friction result and many recommended a deeper investigation but nobody did. By choosing parameters for characterizing the ice it has to be kept in mind that these methods should also be applicable to be used outside the tire test track and not only inside the lab.

## 3.2 Research objective of this thesis

The analysis of the state of the art has shown that the following mechanisms influence ice friction:

- ambient temperature
- sliding velocity
- normal load / pressure
- slider material
- slider geometry
- level of salinity of ice surface
- thickness of water layer in the contact zone

The basic mechanism which is responsible for the low friction is a water layer in the contact area. The water layer is caused by melting the ice due to frictional heat which is a widely accepted theory. The influence of the phenomenon of pressure melting is not finally clarified. Different theoretical calculations exist and all strongly depend on the size of the real contact area which is one of the most important factors. A method which offers an insight in the contact could help to answer many questions, e.g. the distribution of wet and dry parts, the influence of pressure melting and the size of the real area of contact in general. Additionally the influence of the humidity on the friction has not been answered up to now and the contribution of the ice has also not been investigated in more detail. Based on the following hypotheses some of these questions should be answered with the help of this thesis:

- A variation of humidity has no influence on the rubber-ice friction process. This hypothesis has been formulated because the humidity differs depending on the weather and it cannot be controlled on the test track.
- The rubber-ice friction process is dominated by a water layer in the contact. No dry areas exist. This hypothesis is analyzed with the help of a friction model which is derived based on the state of the art and experimental data. With the help of the experimental data different dependencies of the friction coefficient can be studied in depth.
- Pressure melting has an influence on the rubber-ice friction process. This hypothesis shall be answered by providing a method which offers a possibility to visualize the real contact area of sliding tire tread blocks on ice. A major problem of contact investigation is the unknown size of the real contact area because the real contact pressure cannot be determined. Based on the size of the real contact area the phenomenon of pressure melting is reconsidered. Furthermore, the reliability of existing friction models increases with the help of this data.

The complexity of the ice and its surface leads to the following hypotheses:

- The level of salinity has an influence on the friction process. This will be investigated because the composition of the water which is used for preparing the ice surface differs from test track to test track.
- The ice grain size has no influence on the friction process. This parameter will be investigated because the ice grain size is a property which obviously differs depending on the freezing process.

As mentioned in the beginning of this thesis, friction phenomena can be studied with experiments but also with simulations. Besides the investigation of the friction phenomena with experiments different analytical models are presented which allow the investigation of different factors like e.g. velocity or sliding on rough surfaces. The decision of developing analytical models has been made because this gives the possibility to fully control the model behaviour and also to reduce the model complexity depending on which influence



---

shall be investigated. Thus, different analytical approaches for simulating tire tread block movements are introduced to be used as an alternative for the FEM models. In a first step rigid body models are considered. Later on the EULER-BERNOULLI as well as the TIMOSHENKO beam theory are used to simulate sliding tire tread blocks. The models are characterized by a simple but still flexible structure. They shall consider all important properties of the tread block like material parameters and geometry as well as the contact to the ground and between the single block elements. Additionally, different friction laws can be implemented in the model. These models can also take instationary tread block movements into account. The models are evaluated, advantages and disadvantages are pointed out and compared to each other. The model behaviour is checked with simulations and validated against friction measurements.

## 4 Experimental investigation of friction mechanisms of rubber on ice

The following chapter shows the experimental investigation of rubber-ice friction. In a first step, the adhesional properties of ice and rubber are investigated. Afterwards, the high speed linear test rig "HiLiTe" is introduced (cp. Section 4.2). The measurement method and the evaluation of the test results is explained. The process of ice track preparation is shown. Furthermore, the high speed linear test rig HiLiTe is validated using outdoor tire test results obtained in outdoor vehicle tests. In a second step, the influencing parameters of rubber-ice friction are investigated. A basic variation has been done with the test parameters which includes sliding velocity and normal pressure, but also influences like ambient temperature and humidity. These measurements have been carried out with different rubber samples to investigate the influence of the rubber sample geometry. Basic investigations have also been done with varying ice properties to analyze their influence on the friction process. The chapter is completed with a discussion of the measurement results. Based on these measurements and the state of the art, a physical model of the tire tread block on ice friction is derived and already presented measurement results are explained with the existing model.

### 4.1 Investigation of adhesion

Adhesion belongs to the most important friction mechanisms in tire-road contact [65]. It dominates the friction under dry conditions and low sliding velocities. However, that does not exclude an influence of the adhesional effect on rubber-ice friction. Different authors considered mixed friction in the contact, e.g. EVANS et al. [28] (Chapter 2.6.3) and OKSANEN et al. [87], [88] (Chapter 2.6.6).

The following section investigates the role of adhesion in the rubber-ice contact. It is based on RIPKA et al. [99]. The following measurements were done with the adhesion pendulum test rig (Fig. 4.1) which was first introduced by KRÖGER et al. [65]. The motion of the rubber sample was guided by a bifilar pendulum and the impact velocity was controlled by the initial height (approx. 10 cm) of the adhesion pendulum probe (diameter of approx. 1 cm, height of ca. 1 cm). The rubber sample impacts an ice hemisphere. The shape of a hemisphere had been chosen to eliminate edge effects during the impact. The hemisphere was frozen in a special mold made of aluminium with a diameter of approx. 2 cm. The

adjustment of the ice hemisphere and the rubber specimen played an important role to guarantee a centered contact. The hemisphere was fixed on a force sensor which measured a compressive force during impact. If tensile forces occurred after the impact, rubber and ice have been linked due to adhesional forces. They were cut off while the pendulum swings back which becomes visible due to the tensile forces. The horizontal displacement of the pendulum was recorded with a triangulation laser. Based on both data series a force-displacement diagram could be plotted (Fig. 4.2). The energy loss due to the impact of the rubber on the ice was proportional to the included surface area of the force-displacement curve (cp. Fig. 4.2). For details on the test setup and the measurement evaluation method see KRÖGER et al. [65].

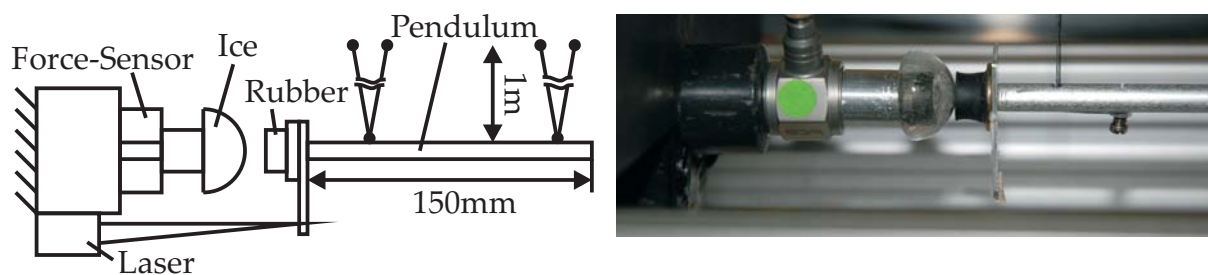


**Figure 4.1:** Schematic diagram of the adhesion pendulum test rig [99]

In a first experiment, the rubber sample was protected by a foil to eliminate the adhesional forces. Only a compressive force was measured (Fig. 4.2 a). The enclosed area in the force-displacement curve corresponded to the energy loss due to hysteresis, which was caused by the deformation of the rubber sample during the impact. In a second experiment the foil was removed. A compressive force as well as a tensile force were measured (Fig. 4.2 b). The energy loss was the sum of hysteresis and adhesion. The energy loss due to the adhesional forces could be calculated by subtracting both results. The adhesional effect was studied for different ambient temperatures (Fig. 4.2 c). The measurements showed an increasing energy loss due to adhesion with a decreasing ambient temperature. That meant the colder the ambient temperature the more distinctive were the adhesional forces.

The existence of the initial water layer on the ice surface (cp. Chapter 2.2.2) plays an important role for the interpretation of the measuring results. The reason for the increasing adhesion (cp. Fig. 4.2 c) with decreasing ambient temperature is the reduction of the surface water layer at lower temperatures. Its thickness strongly depends on the temperature (cp. Fig. 2.7). The reduced initial water layer in the contact between rubber and ice allows the enhanced development of adhesional bindings.

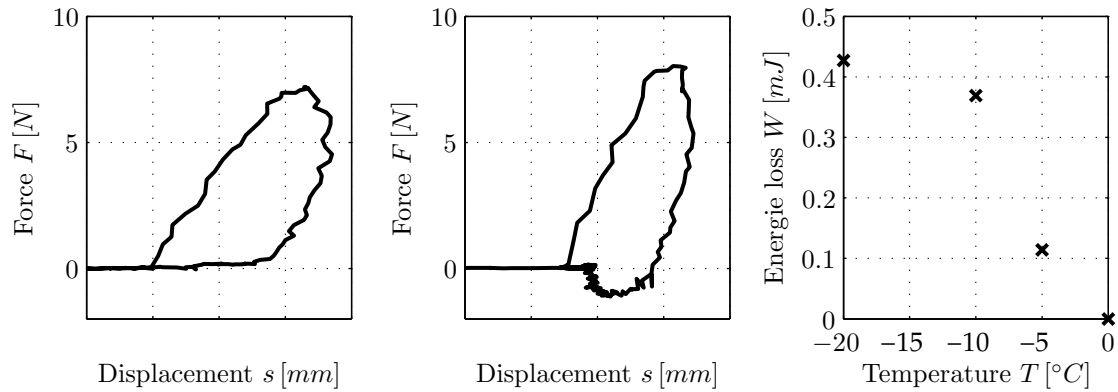


**Figure 4.2:** Adhesion in rubber-ice contact: a) Rubber specimen was covered with a foil during the impact, no adhesional force occurred, b) Tensile force occurs during the contact of rubber and ice, adhesional forces exist, c) Measured rubber-ice adhesion depending on the ambient temperature (According to [99])

## 4.2 The High Speed Linear Test Rig "HiLiTe": Design features, execution, evaluation and validation of measurements

The High Speed Linear Test Rig "HiLiTe" was built at the Institute of Dynamics and Vibration Research by MOLDENHAUER [74], [76] in 2006 and since then continuously improved to satisfy the increasing requirements of the experimental work of the Institute [97], [99], [102]. The test rig allows to perform a linear motion covering the typically wide parameter range of normal force  $F_N$  and sliding velocity  $v$  which can be found within the tire road contact. The most contributing factor which supported the decision of building a test rig which performs a linear motion was the knowledge that most of the tire tread blocks slip through the footprint at higher slip rates (cp. Section 2.6).

**Table 4.1:** Design parameters of HiLiTe

|                                 |   |
|---------------------------------|---|
| Sliding velocity                | $v = 10 \frac{\text{m}}{\text{s}}$          |
| Normal load                     | $F_N = 1000 \text{ N}$                      |
| Power                           | $P = 15 \text{ kW}$                         |
| Maximum friction surface length | $\ell_{\text{max}} = 5,5 \text{ m}$         |
| Temperature range               | $-20^\circ\text{C} < T < +60^\circ\text{C}$ |

### 4.2.1 Design features of HiLiTe

The High Speed Linear Test Rig is located in an environmental chamber. The temperature range is between  $-20^\circ\text{C} < T < +60^\circ\text{C}$ . Therefore research can be done on icy and snowy test surfaces, but also under summerlike conditions. The test rig is powered with a synchronous servo motor with a maximum power of  $P = 15 \text{ kW}$  and a nominal torque of  $T = 53 \text{ Nm}$ . The motor drives a tooth belt which is linked to the carriage (cp. Fig. 4.3 a).

The carriage performs a linear motion along the test track. It is connected to a guide rail to ensure the horizontal movement. The test rig is mounted onto a concrete bedding with a mass of approx.  $m = 3000$  kg. The overall length of the test rig is  $\ell_{max} = 5,5$  m. Due to safety reasons, the maximum test surface length is  $\ell = 4$  m. HiLiTe can be equipped with arbitrary friction surfaces like corundum, safety walk, glass or aluminium but also with concrete, asphalt, snow and ice. The maximum sliding velocity can be set to  $v = 10 \frac{m}{s}$ .

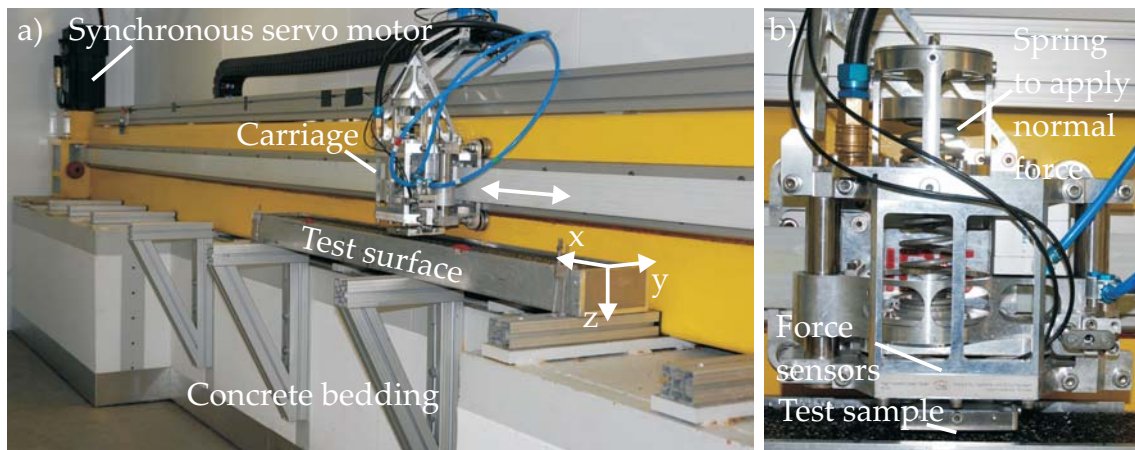


**Figure 4.3:** Layout of High Speed Linear Test Rig: a) Overview, b) Detailed view of the carriage

This test rig's most important part is the carriage (Fig. 4.3b). The challenge which had to be solved during the phase of design was to find a proper compromise between mechanical stability and weight to ensure a sufficient acceleration, but also in order to avoid undesirable deformations of the test rig during measurements. The carriage comprises the test sample, the 3D piezoelectric force sensors and the normal force application. The normal force  $F_N$  (force in positive  $z$ -direction (cp. Fig. 4.3 a)) is applied to the test specimen with a prestressed coil spring. Surface height variations are compensated due to the small spring constant and the initial load. A bellows cylinder can also be used to apply the normal force. The maximum load is  $F_N = 1000$  N. Besides the normal force  $F_N$ , the 3D piezoelectric force sensors measure the friction force  $F_F$  (in positive  $x$ -direction) and the side force  $F_Y$  if desired. The test specimens are vulcanized or glued on a metal plate with a maximum size of  $A = 80 \times 80 \text{ mm}^2 = 6400 \text{ mm}^2$ . The commonly used samples (Fig. 4.4 b) have a tread block length of  $L = 20$  mm and a tread block width of  $w = 80$  mm. Like typical winter tires, the used test specimen can have different numbers of sipes (Fig. 4.4 b). The samples can be fixed under the carriage with two different types of sample holders. One special sample holder allows the rotation of the sample around the  $x$ -axis to compensate small gradients of the test surface (Fig. 4.4 a). Sometimes it is important that the rubber specimen is fixed to avoid undesirable sample movements. For that case the second holder can be used. Additionally, a special device was built which allows the design of arbitrary tread block element arrangements (4.4 c). This device can be compared with a bench vise. It has one static flange and a flexible one. Between both flanges the newly designed tread block is clamped. Different block and block element lengths can be combined, the block

width can be changed, the deformation of chosen elements can be avoided or fixed to a defined value, and the sipe length and sipe depth can be varied (Fig. 4.4 d). This flexible tread block holder allows the specific study of different rubber-ice friction influencing parameters (see Chapter 4.3).

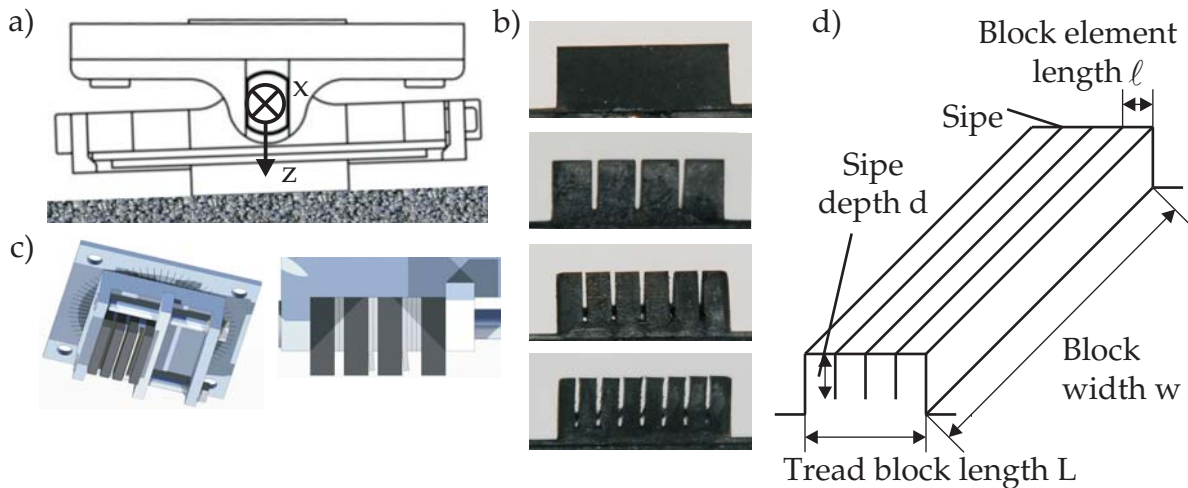


**Figure 4.4:** a) Tread block sample holder of HiLiTe, b) Commonly used tire tread block samples from CONTINENTAL, c) Flexible tread block holder, d) Nomenclature of tire tread block

## 4.2.2 Ice surface preparation

A detailed instruction for the preparation of single ice crystals for ice research purposes was given by PETRENKO [91]. In the context of this thesis icy surfaces with a length of up to  $\ell = 4$  m were produced. Depending on the size and the character of the test track several points have to be considered. So a smooth ice surface structure is aspired to reduce the effort of flattening the ice before the measurement starts. A flat surface guarantees the holohedral contact between ice and rubber sample. It can be reached by freezing the water very slowly at temperatures near the melting point so the dissolved gases can escape. Otherwise, bubbles can be observed in the ice (Fig. 4.20). In the worst case, the ice surface bursts due to embedded air. The result of this slow freezing method is a smooth surface structure with relatively large ice grains. Small ice grains can be achieved at colder temperatures. In some cases a clear ice surface is necessary as it can be observed in nature (Fig. 4.5). For instance image and video based contact area investigations require clear ice surfaces, otherwise the pictures are hard to evaluate (see Section 4.3.6). The method of preparation varies depending on the test track. Up to now lots of research has been done at the Institute of Dynamics and Vibration Research in order to produce clear ice in the lab.



**Figure 4.5:** Clear ice in nature

### 4.2.3 Execution of measurements

Basically the measurement starts by configuring the velocity profile of the servo motor. Therefore the acceleration and deceleration as well as the maximum sliding velocity and the measurement length have to be adjusted. Additionally the desired normal force has to be adjusted by prestressing the coil spring. During the experiment sliding velocity  $v$ , normal load  $F_N$ , friction force  $F_F$ , temperature  $T$  and humidity  $rF$  are measured. Before the measurement starts the rubber sample is set on the ice surface. Afterwards the carriage is accelerated until the maximum sliding velocity is reached. The carriage automatically starts braking and stops at the afore defined position which is the maximum friction length. During the measurement all variables are recorded with a sample rate of  $f = 50000$  Hz. After the measurement is completed the tread block sample is lift off the surface automatically.

Independent of the method of production, all tracks were polished for several minutes before the measurement started. The polishing process is always done with the same sample. Thus, the influence of different conditioning states of the measurement samples can be avoided. The polishing procedure guarantees a homogeneous and smooth surface. Existing micro roughnesses are removed from the ice surface. Every sample is measured for ten times which is an acceptable measuring expenditure but also ensures the quality of the measurement result. Details on the evaluation of measurement results can be found in Chapter 4.2.4.

The temperature control of the cooling process of the climate chamber varies in a range of  $T = \pm 1^\circ\text{C}$  which also influences the humidity  $rF = \pm 7\%$  (cp. Fig. 4.6 a+b). A method has to be found to avoid the influence of the fluctuating temperature and humidity on the friction measurement. By alternating the single tread block samples during the measurement (The different test specimens are measured one after another, this procedure is repeated for ten times) the average temperature and humidity of each group ("Spec. 1 to Spec. 4", Table 4.2) are homogenized. Compared to the average temperature and humidity of all measurements ("Average", Table 4.2) it can be seen that alternating the samples during the measurement reduces the fluctuation of temperature and humidity of each group clearly

(cp. Table 4.2) thus the effect of changing ambient parameters on the friction measurement was eliminated.

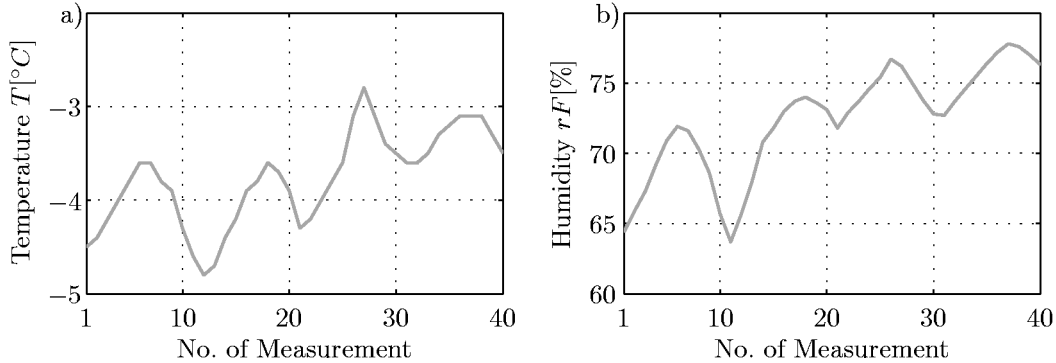


**Figure 4.6:** Example for recorded temperature and humidity characteristic during a measurement run (approximately 45 minutes) in the climate chamber

**Table 4.2:** Average values of ambient temperature and relative humidity for friction measurement of different tread block samples

| Specimen                        | Average | Spec. 1 | Spec. 2 | Spec. 3 | Spec. 4 |
|---------------------------------|---------|---------|---------|---------|---------|
| Temperature $T^{\circ}\text{C}$ | -3,9    | -3,9    | -3,8    | -3,7    | -3,8    |
| relative humidity $rF\%$        | 72,4    | 71,9    | 72,4    | 72,4    | 72,8    |

#### 4.2.4 Evaluation of measurements

The LabView program which is used to control the test rig also provides different functions for a basic data evaluation. The data evaluation is always done after the measurement is completed. For a more detailed data analysis a MATLAB based script was programmed. The result which is used to evaluate the friction measurement is the average friction coefficient  $\bar{\mu}$ . It is used to characterize the friction process because it is less susceptible for stochastic deviation compared to the time depending friction coefficient  $\mu(t)$ . Due to the interaction of tread block and surface each friction process fluctuates. On ice the deviation is very small but on asphalt highly dynamical forces can be measured. In general, two evaluation methods can be used:

- In a first step the friction coefficient  $\mu(t)$  is determined for every time step via the quotient of friction force  $F_F(t)$  and normal force  $F_N(t)$ :  $\mu(t) = \frac{F_F(t)}{F_N(t)}$ . Afterwards the average friction coefficient  $\bar{\mu}$  is calculated:  $\bar{\mu} = \frac{1}{T} \int_0^T \mu(t) dt$
- The second possibility for measurement evaluation begins with the calculation of average normal and friction force:  $\bar{F}_N = \frac{1}{T} \int_0^T F_N(t) dt$  and  $\bar{F}_R = \frac{1}{T} \int_0^T F_R(t) dt$ . Afterwards the average friction coefficient is calculated:  $\bar{\mu} = \frac{\bar{F}_R}{\bar{F}_N}$



Note that both methods can be used in parallel<sup>7</sup> but method one has an essential advantage: The dynamic of the friction process is also displayed by the friction coefficient  $\mu(t)$ . The analysis of the dynamics can be important in case of investigating the influence of e.g. fluctuating normal load on the friction process. GUTZEIT investigated the influence of abrupt changing slip states on the rolling friction process [44]. It also allows the evaluation of the friction process dynamics.

For both methods the part of the friction coefficient time plot which corresponds to the phase of constant sliding velocity (cp. Fig. 4.7) is evaluated with the arithmetic mean value. The result is a single value of the friction coefficient which characterizes the friction process. The so called steady friction coefficient can be calculated for each adjustable parameter combination of sliding velocity, normal load, temperature, rubber sample compound and geometry as well as friction surface. The result is a steady friction characteristic. A commonly used evaluation is the friction coefficient  $\mu = \bar{\mu}$  depending on the sliding velocity  $v$  and/or the normal pressure  $p$ . Additionally, a temperature dependency can be considered (cp. Chapter 4.3.2). Every value of the steady friction characteristic is generally based on up to ten single measurements to ensure a statistical reliability.

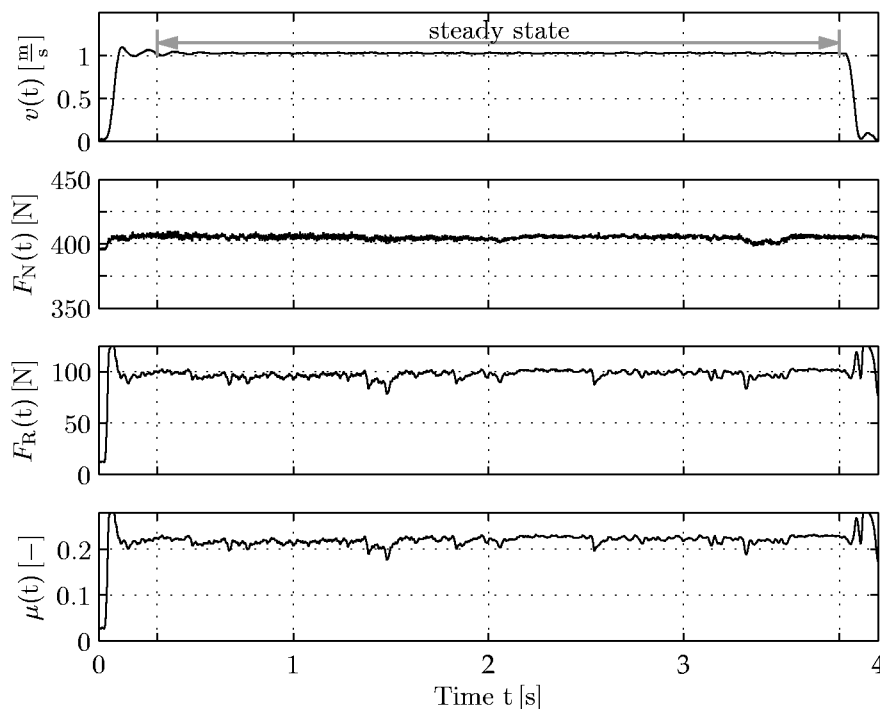


**Figure 4.7:** Sample measurement with constant sliding velocity  $v(t)$ , normal force  $F_N(t)$  and friction force  $F_F(t)$ , calculated friction coefficient  $\mu(t)$  [98]

<sup>7</sup>For the evaluated measurements the friction coefficients calculated with both methods differ in a range smaller than 0,2%

## 4.2.5 Validation of HiLiTe measurements with outdoor tire test results

The high speed linear test rig HiLiTe was built to investigate the tire tread block road contact under typical passenger car conditions. Therefore, it is important to judge the quality of HiLiTe measurement results. A detailed validation of HiLiTe measurements with outdoor passenger vehicle test results (cp. Section 2.6.1) was performed in order to gain confidence on HiLiTe's performance (see also RIPKA et al. [98] and [99]). Therefore the influence on the friction coefficient of the rubber compound on the one hand and the influence of the tread block geometry on the other hand as well as the interaction of compound and geometry is evaluated in detail. Both aspects are very important in tire development because they influence the tire performance clearly. For judging the quality of new prototypes the mechanisms which can be identified outside on the test track must be represented by the lab test as well. Due to the uncontrollable boundary conditions during the tests outside like ice quality, humidity and temperature a perfect agreement of absolute values cannot be expected. Therefore, the validation is judged successful if HiLiTe measurement and outdoor test show the same ranking. The measurements have been done with five different rubber compounds (Table 4.3). For all of the five compounds non siped and three siped samples were available (Table 4.4). Additionally samples with more sipes exist for the reference compound (REF, cp. Table 4.4)

**Table 4.3:** Specification of tread block compounds used for HiLiTe validation and following rubber-ice friction research





| Compound marking | Compound character | ShA hardness |
|------------------|--------------------|--------------|
| REF              | winter reference   | 60           |
| A                | nordic soft 1      | 49           |
| B                | winter             | 63           |
| C                | nordic soft 2      | 51           |
| D                | all season         | 67           |

### 4.2.5.1 Validation of rubber compound measurements

For the rubber compound validation process different rubber compounds (REF, A-D, cp. Table 4.3) have been measured with HiLiTe. Due to the large variety of sliding velocities in the footprint during an ABS braking maneuver three different sliding velocities have been measured indoor:  $v = 1, 3, 5 \frac{\text{m}}{\text{s}}$  at a temperature of  $T = -3, 5^\circ\text{C}$  (see also Section 4.3.1). The ranking obtained from HiLiTe measurement was compared with the ranking gained from outdoor vehicle tests (Fig. 4.8). It is expected that the nordic winter compounds (A,C) are best, the standard winter compound (B) as well as the reference compound (REF) show smaller friction coefficients and the all season compound (D) is worst.

Differences between the nordic winter compounds (A, C) and the standard winter compound (B) as well as the winter reference (REF) can be identified clearly with HiLiTe. The all season compound (D) delivers the smallest friction coefficient. Comparing indoor lab measurements and outdoor vehicle test results (Fig. 4.8), the highest correlation can

**Table 4.4:** Specification of tread block geometry used for HiLiTe validation and following rubber-ice friction research

| Geometry marking | Geometry character   | Availability |
|------------------|--|--------------|
| G0               | no sipes<br>    | REF, A-D     |
| G3               | three sipes<br> | REF, A-D     |
| G5               | five sipes<br>  | REF          |
| G7               | seven sipes<br> | REF          |

be found for a sliding velocity of  $v = 5 \frac{m}{s}$ . The only difference which can be found in the ranking is the result of the winter compound (B) where the results obtained on the HiLiTe shows a different behaviour compared to those of the other compounds. Although the HiLiTe results do not match exactly with the outdoor tire test results, the compound validation process is judged as successful because the general tendency between nordic soft compound, winter compound and all season compound can be identified. The differences might have been caused by the uncontrollable parameters (ice quality, humidity, temperature) during the vehicle test.

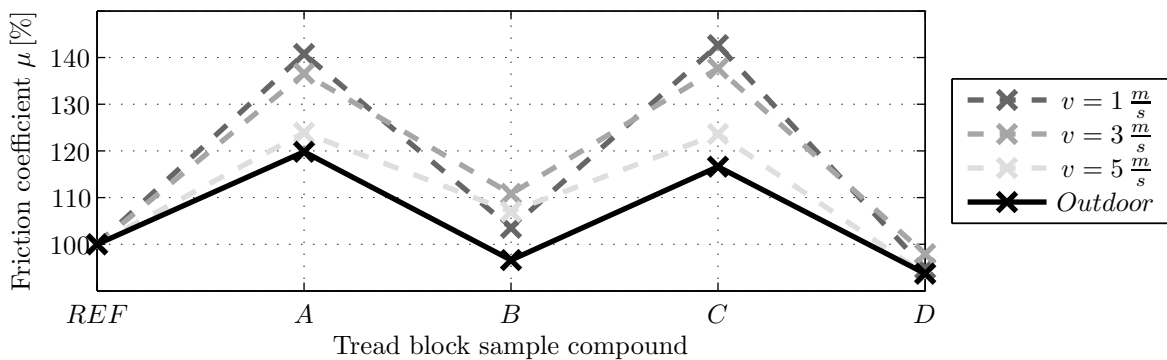


**Figure 4.8:** Variation of rubber compound: HiLiTe measurement vs. outdoor tire test (According to [98])

#### 4.2.5.2 Validation of rubber geometry measurements

In a second step the influence of the number of sipes on the rubber-ice friction was investigated (cp. Table 4.4). Therefore, four different tread block samples (Fig. 4.4 b) with reference compound have been measured at two different sliding velocities ( $v = 1$  and  $5 \frac{m}{s}$ ). These measurements are compared with the results of an outdoor vehicle test (cp. Fig.

2.18). The tread blocks have a constant length of  $L = 20$  mm. With an increasing number of sipes the effective length of the single tread block elements  $\ell$  is reduced. This results in very thin tread block elements for the seven siped sample (Fig. 4.4 b). Considering the results, a maximum friction coefficient can be observed for the three siped tread block for both lab experiments and vehicle test (Fig. 4.9). The friction potential decreases for five sipes per sample for all data series. Large differences between lab and outdoor results can be found for the seven siped sample. The outdoor result shows a small increase compared to the five siped sample. The friction value in the lab is much smaller for the seven sipes. This behaviour can be explained as being the result of large bending deformation of the thin lab test specimen. Due to the large deformation the last tread block element loses the contact to the ground and the contact area becomes very small (see also RIPKA et al. [99]). The tire tread block element is supported by the following block so that the bending deformation is limited which results in the higher friction level of the outdoor test for the seven siped sample. It seems that the tread block elements in the footprint support each other which reduces the bending deformation and therefore increases the friction. Basically the increased sliding velocity of  $v = 5 \frac{\text{m}}{\text{s}}$  results in a vertical shift of the friction characteristic which means that the sipes increase the friction at higher sliding velocities. However, the differences within the absolute values of the friction can be caused by various other factors which cannot be controlled outside on the test track. So the humidity as well as the temperature influence the friction process (cp. Chapter 4.3), but also the ice properties will most likely be different between indoor and outdoor. In addition the block element lengths varies from indoor test sample to outdoor test tire. The difference of the tread block element length also causes a shift of the friction coefficient in the vertical direction. In the lab a clear trend could be found, the observed mechanisms could be explained. Additionally, the differences of outdoor test results increase due to the varying test conditions. In general, it can be concluded that studies of the effect of geometry parameters can be done with HiLiTe.

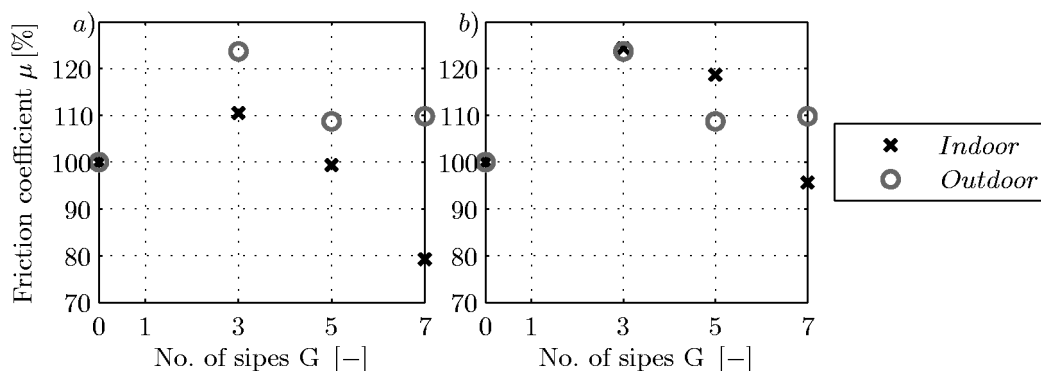


**Figure 4.9:** Variation of number of sipes per tread block (Reference compound for indoor measurement): Outdoor tire test vs. HiLiTe measurement ( $T_{in} = -3^\circ\text{C}$ ,  $rF_{in} = 70\%$ ), a)  $v = 1 \frac{\text{m}}{\text{s}}$ , b)  $v = 5 \frac{\text{m}}{\text{s}}$

Additionally, a basic investigation has been done on the interaction of the tread block geometry and the tread block compound. Therefore, a non siped and three siped tread

block were used because these geometries represent typical tire tread patterns (Fig. 1.2 a+b). This part of the validation process is judged successful if the siped sample shows the higher friction coefficient compared to the non siped sample because the siped structure always delivers a higher friction level in vehicle outdoor tests under normal conditions. The interaction of the tread block geometry and the tread block compound on the ice friction was investigated with the already known compounds "REF" and "A-D" (see also Table 4.3) which are available with no sipes and three sipes (cp. Table 4.4 and Fig. 4.4 b). For this measurement three different sliding velocities ( $v = 1, 3, 5 \frac{m}{s}$ ) and two different ambient temperatures ( $T = -3, -8^\circ C$ ) have been investigated at constant humidity. As it is known from passenger car tests, the siped tread blocks deliver a higher friction coefficient compared to the non siped blocks (see Fig. 2.18). This behaviour shall be found in the lab as well. The result of the friction measurement is presented as the ratio of the friction coefficient of the three siped sample divided by the friction coefficient of the non siped sample for a better understanding (Fig. 4.10). This method of presenting the results allows a simple interpretation: A ratio of  $\frac{G_3}{G_0} > 100\%$  means that the friction coefficient of the siped sample is higher than the one of the non siped sample, as it can be found for tire tests. Additionally, a major influence of sliding velocity and temperature can be identified (Fig. 4.10). At cold temperatures (Fig. 4.10 b) the non siped tread block showed higher friction for the nordic compounds (A and C). At temperatures closer to the melting point ( $T = -3^\circ C$ , Fig. 4.10 a), the expected geometry ranking can be found for sliding velocities larger than  $v = 3 \frac{m}{s}$ . As observed during the geometry effect measurements the sipes improve the friction at higher sliding velocities. It is concluded that geometry effects can be investigated with HiLiTe for temperatures near the melting point and sliding velocities of  $v > 3 \frac{m}{s}$  independent of the tread compound because there the siped sample delivers higher friction coefficients compared to the non siped one. A more detailed investigation of sliding velocity and temperature influences on the rubber-ice friction is given in Chapter 4.3. An interpretation of the results and a rubber-ice friction model can be found in Chapter 4.5.

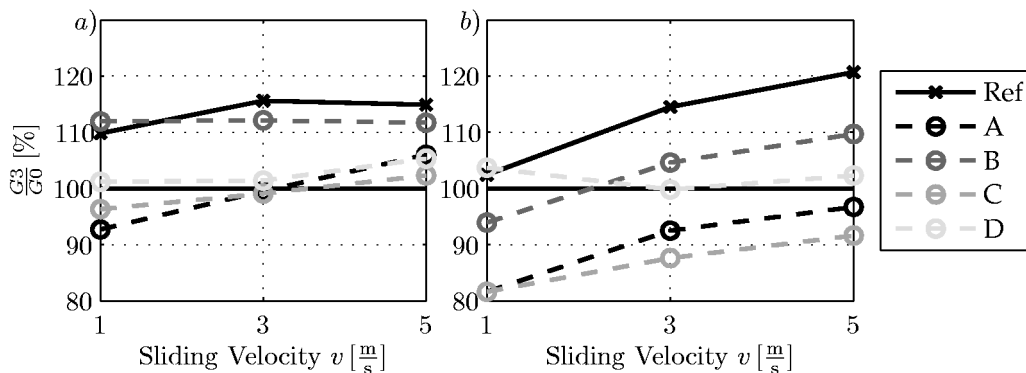


**Figure 4.10:** Variation of number of sipes per tread block: Influence of rubber compound and temperature on ranking between siped tread block (G3) and non siped tread block (G0), a)  $T = -3^\circ C$ , b)  $T = -8^\circ C$

### 4.3 Friction measurements of tire tread blocks on ice

Simulations have shown that an increasing slip enlarges the area of sliding in the contact zone (cp. Fig. 2.15). This is why the sliding process is investigated in more depth now. Additionally the results of the measurements are used to define the mechanisms which shall be displayed by the friction model (cp. Section 4.5.1). The following section shows the influence of different parameters on the rubber-ice friction process. The influence of the test parameters like sliding velocity and normal pressure is investigated in depth although the general dependency of those parameters has already been pointed out in Chapter 2.6. The repetition of these measurements is used for validating HiLiTe measurement results in another way. Additionally the influence of rubber and ice properties as well as that of the humidity on the friction process is investigated in depth. Furthermore, a method is presented which allows the observation of the real contact area of a tread block sample during sliding on ice.

#### 4.3.1 Variation of sliding velocity and normal pressure

The local contact pressure in the contact zone strongly depends on the real contact area. With an increasing real contact area the constant normal force is distributed on a larger area, which results in a decreasing contact pressure. First investigations of the real contact area under static conditions on asphalt by GÄBEL showed local contact pressure peaks due to the asperities of asphalt [33]. Although it is assumed that the ice surface is smooth, it can be postulated that the local contact pressure is higher due to a deformation and surface irregularities of the tire tread block. This assumption was checked with a high speed camera during a HiLiTe experiment. In a corresponding a tread block sample passed the high speed camera during the friction measurement and was filmed (Fig. 4.11 a). From an instantaneous photograph, it can be seen clearly that all four tread block elements are deformed (Fig. 4.11 b) which results in an unknown pressure distribution in the contact, depending on the tread block element deformation. As a result of this analysis it is determined that the influence of the contact pressure on the friction coefficient shall be investigated for more than the standard pressure of approx.  $p = 2,5$  bar. The measurement range was extended to higher (up to  $p = 5$  bar) and lower pressures ( $p = 1$  bar).

For the following friction measurements with HiLiTe three different sliding velocities ( $v = 1, 3$  and  $5 \frac{\text{m}}{\text{s}}$ ) and three different normal pressures ( $p = 1, 2,5$  and  $5$  bar) have been chosen to cover the wide parameter range. The measurements have been made with the three siped sample (reference compound) at an ambient temperature of  $T = -4$  °C and a humidity of  $rF = 73$  % according to the procedure described in Section 4.2. It could be observed that an increasing sliding velocity resulted in a decreasing friction coefficient as it is described in the literature (Fig. 4.12 a, cp. Chapter 2.6). Additionally, it could be seen that the gradient of the curves becomes smaller with increasing sliding velocities. It can

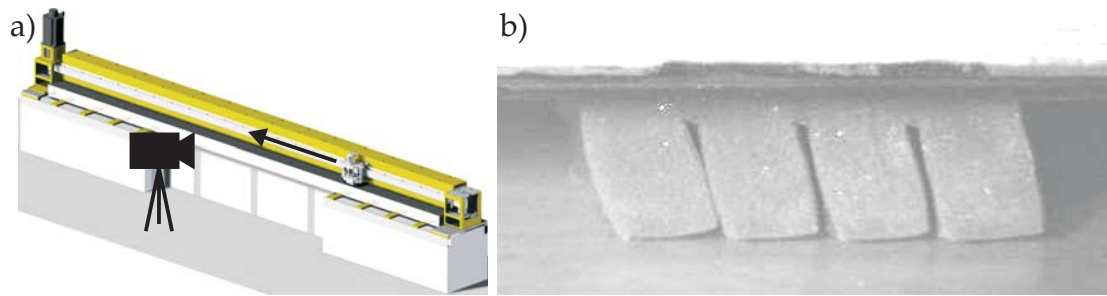


**Figure 4.11:** Film of camera-passing tire tread block: a) Test set up at HiLiTe with high speed camera, b) Picture of sliding tire tread block

also be observed that an increasing normal load results in a decreasing friction coefficient (Fig. 4.12 b). The gradient of the characteristic decreases with increasing pressure, too.

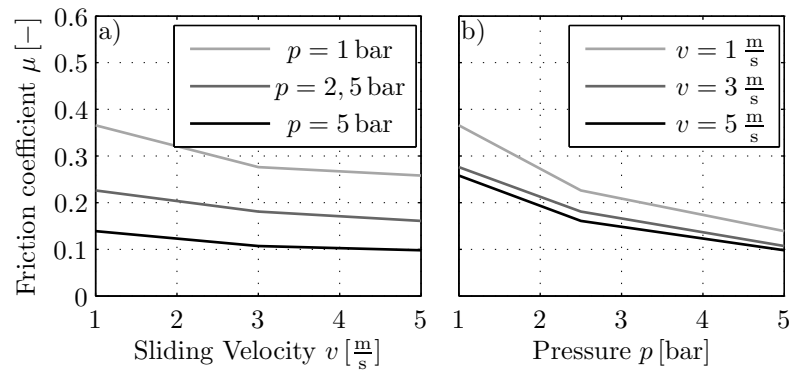


**Figure 4.12:** Sliding tire tread block on ice: Three sipes, reference compound,  $T = -4^\circ\text{C}$ ,  $rF = 73\%$ , a) Friction coefficient depending on sliding velocity  $v$  with varying normal pressure  $p$ , b) friction coefficient depending on normal pressure  $p$  with varying sliding velocity  $v$

A changing normal pressure results in a vertical shift of the curve of the velocity depending friction coefficient (Fig. 4.12 a). An increasing normal pressure reduces the friction level. The offset between the single pressure levels (in vertical direction) at a constant sliding velocity decreases with increasing sliding velocities (Fig. 4.12 a). The same behaviour could be observed at the pressure depending friction coefficient where the sliding velocity was varied. An increasing sliding velocity causes a reduction of the pressure depending friction coefficient (Fig. 4.12 b). Plotting both pictures (Fig. 4.12 a+b) in a 3D-characteristic it can be seen that the friction process depends more on pressure than on sliding velocity (Fig. 4.13).

### 4.3.2 Variation of the ambient temperature

The aforementioned variation of sliding velocity and normal load has been repeated under different ambient temperatures ( $T = -1, -4, -8^\circ\text{C}$ ) for investigating the temperature influence on the rubber-ice friction process. The humidity has been kept constant. The average humidity was  $rF = 73\%$  during the measurements. A temperature change results in a vertical shift of the friction characteristic (Fig. 4.13). The colder the ambient temperature

the higher is the friction level of the tire tread block sample. For slow sliding velocities and a small normal pressure noticeable differences in the friction coefficient can be observed when the temperature is varied (cp. Fig. 4.13). These differences are smaller or even disappear for high sliding velocities and high normal pressures (cp. Fig. 4.13). It also seems that the influence of changes of sliding velocity and normal pressure are more distinctive at lower temperatures.

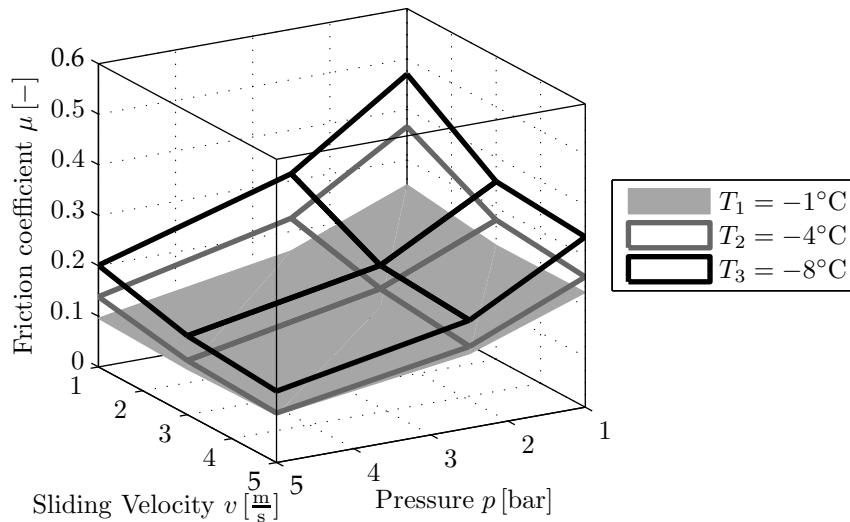


**Figure 4.13:** Sliding tire tread block on ice: Three sipes, reference compound: Steady friction characteristic of rubber-ice-friction depending on sliding velocity  $v$ , normal pressure  $p$  and ambient temperature  $T$  [98]

### 4.3.3 Variation of the humidity

The humidity (which is strongly linked with the equilibrium of evaporation and condensation of water molecules, just like the ambient temperature) is influenced by many boundary conditions like the ambient temperature (cp. Chapter 2.1) and the surface (water or ice). The constant exchange of water molecules between surface and surrounding air also influences the top layer of the surface (cp. Fig. 2.4). With increasing humidity more water molecules evaporate and condensate which results in an increasing initial water layer on the ice surface. The influence of the humidity on the rubber-ice friction and its interaction with other parameters has been analyzed in depth with different HiLiTe friction experiments. Therefore the sliding velocity was varied in a range of  $v = 1, 3, 5, 7 \frac{\text{m}}{\text{s}}$ , the normal load has been set to  $p = 2,5 \text{ bar}$  and  $p = 5 \text{ bar}$ , the rubber sample geometry (reference compound) was G0 and G3. Because of the temperature influence on the amount of dissolved water in the air, the ambient temperature range for the measurements was set to  $T = -1, -3, -5^\circ\text{C}$ . In addition two different states of humidity have been investigated for all parameter combinations: low ( $rF < 50\%$ ) and high ( $rF \approx 90\%$ ). The measurements have been executed on one ice surface to eliminate its influence on the results. For a better overview the measurement results are presented in blocks (Fig. 4.14). Each horizontal line belongs to the same sample geometry. Pictures on the left hand side



show the state of low humidity while the middle vertical column shows the measurement results of high humidity. The column on the right shows the combination of high and low humidity for a better comparison of both states with each other. In a first step the three siped sample (G3) was used (Fig. 4.14 a-c). The normal load has been set to  $p = 2,5$  bar. The humidity was adjusted to a value of  $rF < 50\%$  (Fig. 4.14 a). The velocity depending friction coefficient shows the well known decreasing friction characteristic (cp. Chapter 4.3.1) for temperatures of  $T_1 = -5^\circ\text{C}$  and  $T_2 = -3^\circ\text{C}$ . At temperatures near the melting point ( $T_3 = -1^\circ\text{C}$ , cp. Fig. 4.14 a) a decreasing behaviour of the friction coefficient can be observed first. For higher sliding velocities the friction coefficient increases. The condition of high humidity  $rF \approx 90\%$  shows a completely different characteristic (Fig. 4.14 b): The friction coefficient measured under cold conditions ( $T_1 = -5^\circ\text{C}$ ) shows the decreasing characteristic again. The behaviour of the friction coefficient at a medium cold temperature ( $T_1 = -3^\circ\text{C}$ ) is similar to the one near the melting point with low humidity. In the beginning the values decrease and at higher sliding velocities a continuous increase can be observed. The friction coefficient at temperatures near the melting point ( $T_1 = -1^\circ\text{C}$ ) increases even at small sliding velocities. The influence of humidity on the rubber-ice friction can be identified by combining low and high humidity measurements (Fig. 4.14 c). For low temperatures ( $T_1 = -5^\circ\text{C}$ , dashed and solid black lines) a difference between the friction coefficients obtained for different humidity levels can be observed for low sliding velocities. At higher sliding velocities both curves converge. At a sliding velocity of  $v = 7 \frac{\text{m}}{\text{s}}$  nearly no difference can be found. The characteristic for medium temperatures ( $T_2 = -3^\circ\text{C}$ , dashed and solid dark grey lines) differs in the beginning where the dry condition shows higher friction compared to the state of high humidity. However, the curve measured under wet conditions crosses the dry condition curve at a sliding velocity of  $v = 5, \frac{\text{m}}{\text{s}}$  due to its increasing characteristic. For temperatures near the melting point ( $T_3 = -1^\circ\text{C}$ , dashed and solid light grey lines) the crossing is at a sliding velocity of  $v \approx 2 \frac{\text{m}}{\text{s}}$ . From here, the curve measured at high humidity increases continuously up to the level of the medium temperature ( $T_2 = -3^\circ\text{C}$ , dashed and solid dark grey lines). It seems that all curves approach each other for higher sliding velocities (cp. Fig. 4.14 c).

In a second step the parameter variation was done with the non siped sample (Fig. 4.14 d-f). At low humidity the friction characteristic decreases in general. A smooth increasing is observed at a temperature of  $T = -1^\circ\text{C}$  for a sliding velocity of  $v > 5 \frac{\text{m}}{\text{s}}$  (Fig. 4.14 d). At high humidity the friction characteristic decreases for cold ( $T_1 = -5^\circ\text{C}$ ) and medium cold temperatures ( $T_2 = -3^\circ\text{C}$ ). At temperatures near the melting point ( $T_3 = -1^\circ\text{C}$ ) the friction coefficient increases for a sliding velocity of  $v > 3 \frac{\text{m}}{\text{s}}$  (Fig. 4.14 e). The comparison of both states (high and low humidity) show that the curves approach each other (Fig. 4.14 f), but compared to the siped sample larger differences can be observed. Additionally it can be observed that the friction coefficient of the non siped sample decreases stronger than the friction coefficient of the siped sample does.

In a third step the influence of normal load on the rubber-ice friction has been investigated with the three siped sample (Fig. 4.14 g-i). Therefore the normal load was adjusted to

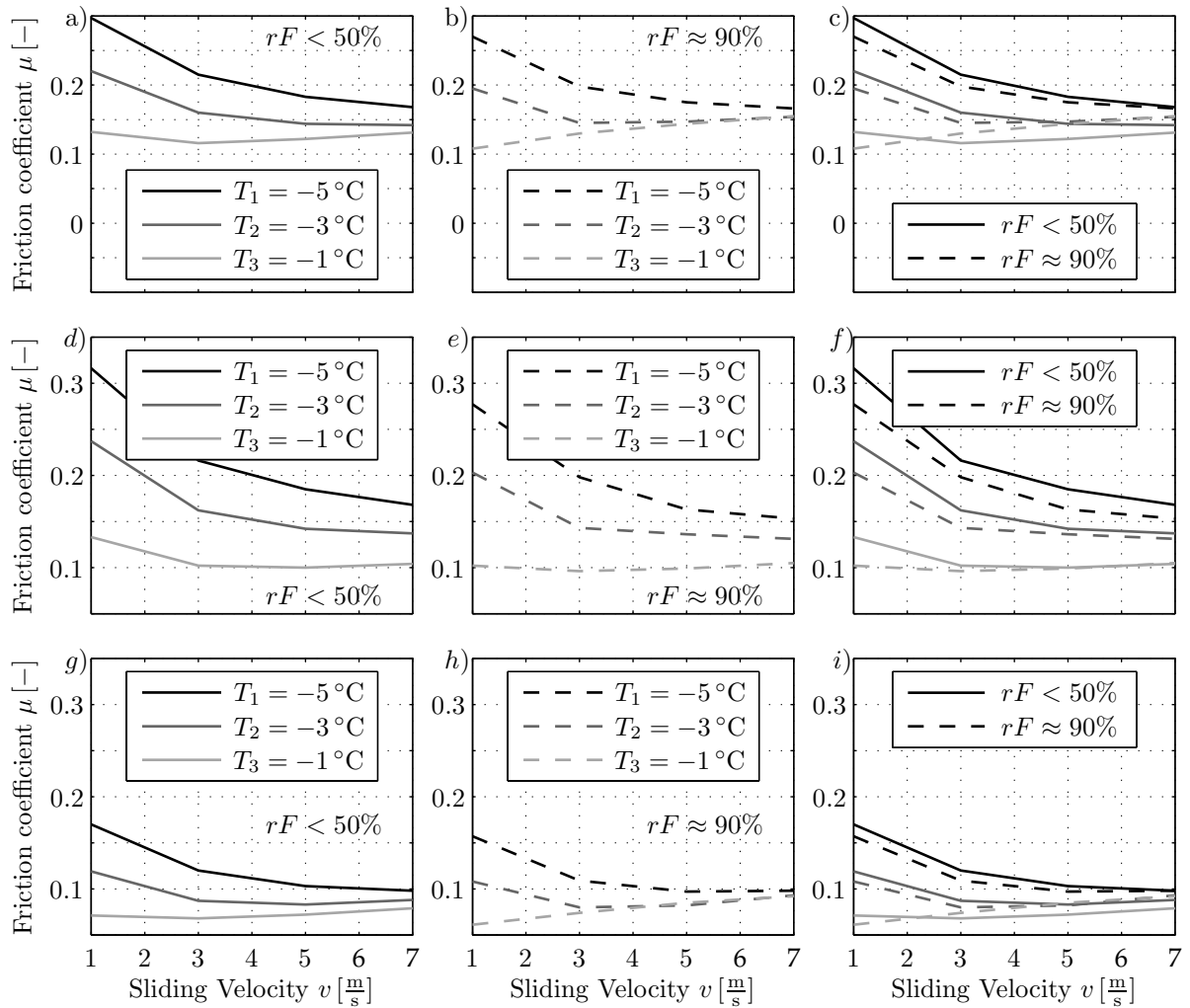


**Figure 4.14:** Rubber-ice friction measurement with varying sliding velocity, normal pressure, temperature, humidity (high and low) and tread block geometry: a-c) Three sided sample G3,  $p = 2,5\text{bar}$  (cp. Fig. 4.14), d-f) Non sided sample G0,  $p = 2,5\text{bar}$ , g-i) Three sided sample G3,  $p = 5\text{bar}$

$p = 5\text{bar}$ . The characteristic at low humidity ( $rF < 50\%$ ) shows a decreasing friction coefficient for cold temperatures ( $T_1 = -5\text{ °C}$ , Fig. 4.14 g). In contrast to the lower pressure the friction coefficient shows an increasing behaviour at medium cold temperatures for a sliding velocity of  $v > 5\frac{\text{m}}{\text{s}}$ . At temperatures near the melting point the friction coefficient decreases first and starts increasing for  $v > 3\frac{\text{m}}{\text{s}}$ . In general the friction values are much smaller for the higher pressure compared to the sided and non sided sample characteristics at lower pressure (cp. Fig. 4.14 a, d, g). The friction characteristic measured at high humidity shows a slight increase at cold temperatures ( $T_1 = -5\text{ °C}$ ) for sliding velocities  $v > 5\frac{\text{m}}{\text{s}}$ . At a medium cold temperature the increase of friction starts for sliding velocities of  $v > 3\frac{\text{m}}{\text{s}}$  as it can be observed for the sided sample under lower pressure also (cp. Fig. 4.14 b, h). For temperatures near the melting point ( $T_3 = -1\text{ °C}$ ) the friction characteristic continuously increases (Fig. 4.14 h). And as observed for low humidity the level of friction is smaller

compared to the lower pressure level (Fig. 4.14 b, h). The comparison of high and low humidity shows that all curves approach each other for high sliding velocities (Fig. 4.14 i).

At lower temperatures, the condensation of the water on the test surface caused great problems at higher humidity. The surface became extremely rough. Thus, friction coefficients similar to those of concrete or asphalt could be measured on the virgin surfaces. However, the friction coefficients also decreased quickly after passing the test surface several times due to the polishing effect of the ice surface (asperities were melted away, see also [26]).

#### 4.3.4 Influence of tread block geometry and inclination angle

The number of sipes per tread block was varied for validation purposes of the HiLiTe test rig (cp. Chapter 4.2.5). The tread block element length  $\ell$  became smaller with an increasing number of sipes due to the constant block length  $L$ . Now the influence of the tread block element length  $\ell$  on the friction process is investigated in depth. Therefore, three different element lengths were measured ( $\ell_1 = 6 \text{ mm}$ ,  $\ell_2 = 10 \text{ mm}$ ,  $\ell_3 = 2 \times 6 \text{ mm} = 12 \text{ mm}$ ). The different rubber samples were manufactured out of rubber plates with different thicknesses. Their velocity depending friction behaviour was investigated with the help of the flexible tread block holder (Fig. 4.4 c). In the back of each sample, a small metal plate was mounted to eliminate potential bending deformation during the friction experiment. The normal load was adjusted for each sample to a constant normal pressure. All three samples show a strongly decreasing friction coefficient for an increasing sliding velocity (Fig. 4.15). It can be seen that the friction characteristic of the small element ( $\ell_1 = 6 \text{ mm}$ ) delivers higher values compared to the friction of the other samples. The characteristics of the larger samples ( $\ell_2 = 10 \text{ mm}$ ,  $\ell_3 = 2 \times 6 \text{ mm} = 12 \text{ mm}$ ) are nearly the same. It seems that the difference in the friction coefficient of these two samples vanishes at high sliding velocities.

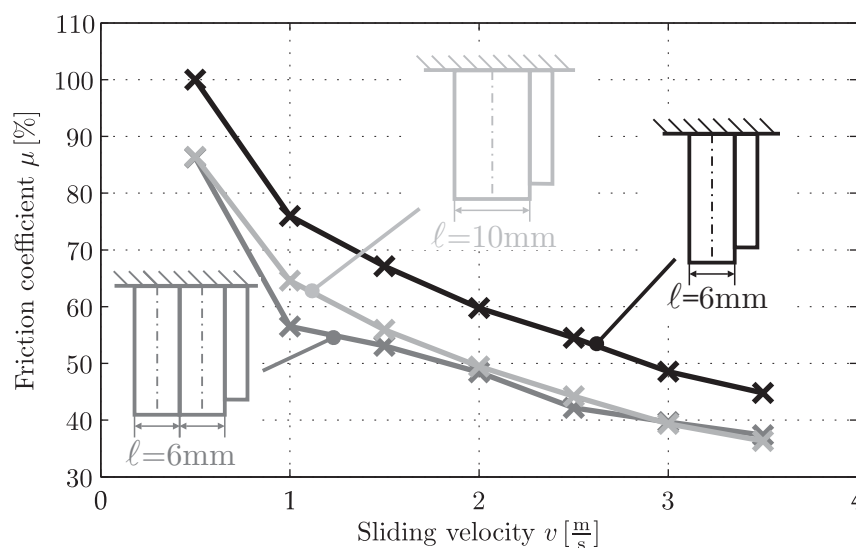


**Figure 4.15:** Influence of the tread block element length  $\ell$  on the friction coefficient (According to RIPKA et al. [98])

The increasing block element length results in a decreasing friction coefficient although the normal pressure is kept constant. For a better understanding of this behaviour the corresponding friction force characteristic of each measurement shall be considered (Fig. 4.16). A gain of friction force can be observed within the first step from  $\ell_1 = 6\text{ mm}$  to  $\ell_2 = 10\text{ mm}$ . For the third block length the friction force stays constant. Although the friction force increases the friction coefficient is reduced (cp. Fig. 4.15). This is a result of the increasing normal load which was adjusted for every sample in order to guarantee a constant global normal pressure. The friction force did not raise to the same degree as the normal load did and therefore the ratio of normal and friction force decreased. It seems that a frictional limit exists for certain parameter combinations.

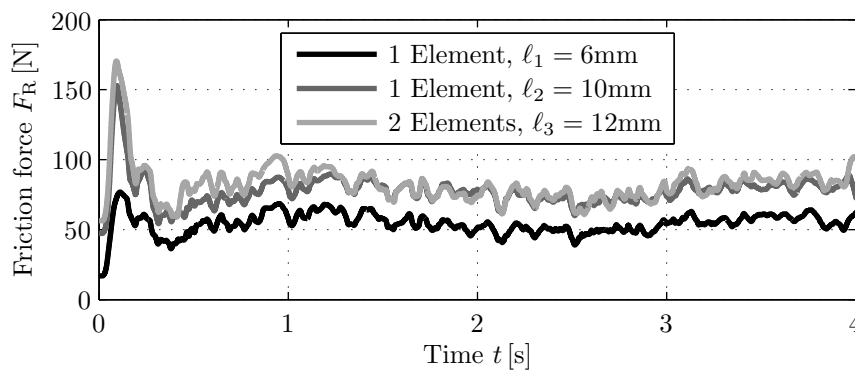


**Figure 4.16:** Friction force as a function of time for different block element lengths (According to [98])

In a second step the influence of the bending deformation of the tread block element on the friction process is investigated. Therefore the flexible tread block holder was used again. Two different bending angles were investigated. The first set up was blocked with a metal plate which resulted in an angle of  $\alpha = 0^\circ$ . The second sample set up consisted of a rubber sample in which the whole sample was fixed with a special device to  $\alpha = 20^\circ$  (cp. Fig. 4.17). Considering the measurement results of the velocity dependent friction coefficient (Fig. 4.17), it can be seen that both set-ups show again the decreasing characteristic. The biggest difference can be found for small sliding velocities. The gradient of the curve of the sample with  $\alpha = 0^\circ$  is higher compared to the sample with  $\alpha = 20^\circ$ . Additionally, the level of friction of the vertically mounted sample ( $\alpha = 0^\circ$ ) is located above the friction level of the inclined one ( $\alpha = 20^\circ$ ).

### 4.3.5 Influence of different ice properties on the friction process

During outdoor tire tests the nature of ice cannot be influenced. The composition of the water is unknown and it is difficult to prepare the whole track surface with a defined water composition. Additionally, the ice grain size and its growths are unknown. The grain size depends on the temperature, but also on the character of the track: The ice grains developed in a lake differ from the grains occurring on land. In a lake the grains grow on a single crystal nucleus. On land the water freezes at many different places

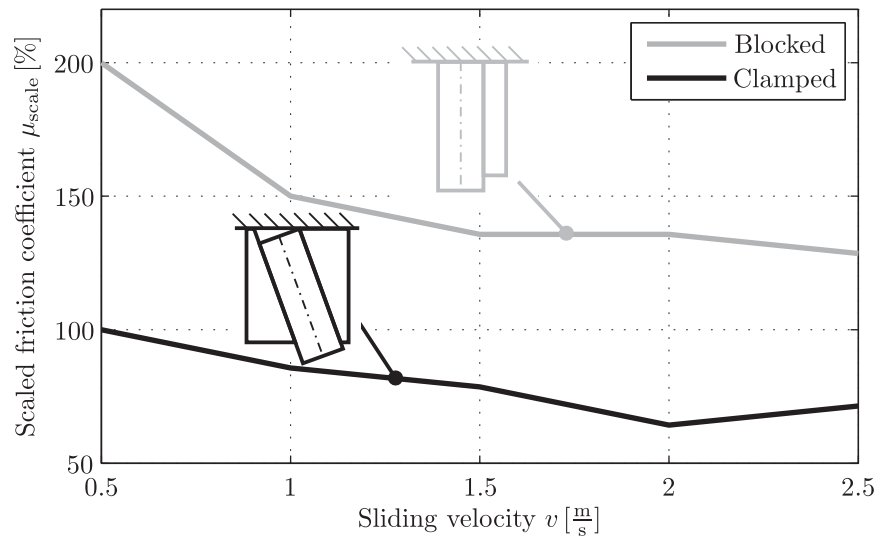


**Figure 4.17:** Influence of the block element inclination on the friction coefficient (According to RIPKA et al. [98])

which results in smaller ice grains. Details on the ice formation were given in Chapter 2.2. However, knowing the ice's influence on the friction process helps understanding the friction mechanisms. Additionally, differences between tire test results from lake tracks and land tracks can sometimes be explained due to the differences in the water composition and ice grain quality. The following subsections aim at identifying the influence of the water composition and the ice grain size on the rubber-ice friction.

#### 4.3.5.1 Influence of ice impurities on the friction process

The influence of the water composition on the friction process was investigated by comparing rubber-ice friction measurements performed on ice made of purified water and saline water. Identifying this influence on the rubber-ice friction helps understanding the friction phenomena but also to interpret differences in tire test results. The saline water had a level of salinity of  $K = 0,05\%$ . It was produced by mixing purified water with salt. The level of salinity of  $K = 0,05\%$  has been chosen to guarantee a clear influence on the friction process compared to purified water. The geometry of the samples was G0 and G3 (cp. Table 4.4), both with reference compound (cp. Table 4.3). The investigated temperature was in a range between  $T = -4^{\circ}\text{C} - -5^{\circ}\text{C}$ . The humidity was at about  $rF = 72\%$  for the measurements on ice from purified water and near  $rF_{salt} = 63\%$  for the measurements on saline ice. The difference in the humidity levels in principle influence the measurement results (cp. Chapter 4.3.3). A higher humidity results in a smaller friction coefficient compared to lower humidity, but this influence can be neglected here because the friction measurements on salt water show smaller friction coefficients although the humidity is smaller. The influence of the salt on the friction process can be seen clearly. A more detailed understanding can be gained from the discussion of the results (see Chapter 4.5.2).

The measurement results for the non siped block G0 and the siped block G3 show again the well known decreasing friction coefficient with an increasing sliding velocity on both ice surfaces (Fig. 4.18 a+b). In general the ice made of purified water delivered a higher friction coefficient (cp. Fig. 4.18 a+b). The gradient of the curve measured for the saline ice is smaller compared to the gradient of the friction characteristic of the purified water. In general, the level of friction of the track made from saline water is smaller than the friction level of the track made from ice out of purified water. The siped sample delivers higher friction coefficients than the non siped sample independent from the sliding velocity (Fig. 4.18 c). The difference between both results increases for higher sliding velocities on the purified water. For the saline water it stays nearly constant.

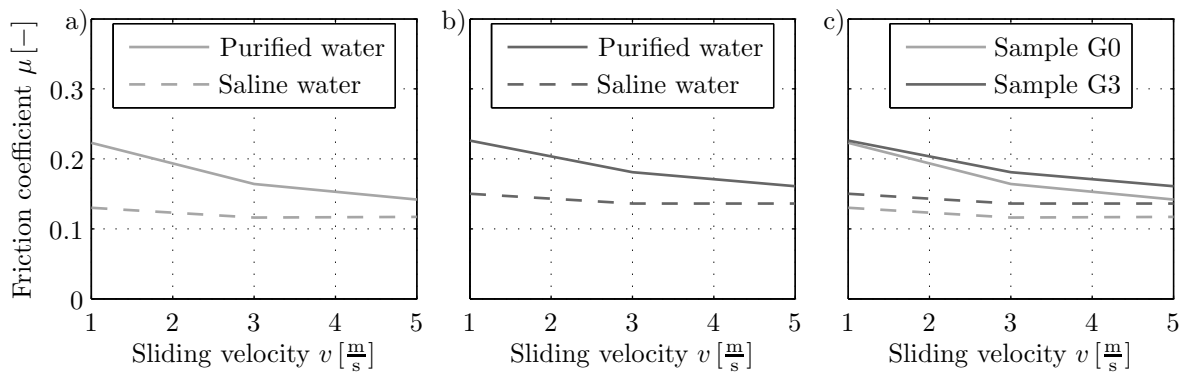


**Figure 4.18:** Influence of saline ice on the friction process with reference compound: a) Sample geometry G0, purified vs. saline water (Level of salinity  $K = 0,05\%$ ), b) Sample geometry G3, purified vs. saline water (Level of salinity  $K = 0,05\%$ ), c) Overall dependency of block geometry and level of salinity on the friction process (Purified water marked with solid lines, saline water marked with dashed lines)

#### 4.3.5.2 Influence of the ice grain size on the friction coefficient

The ice grains can be visualized with polarized light (cp. Chapter 2.2.3 and Fig. 2.8). This allows a judgement of the ice grain size. For the following experiments different methods for generating different grain sizes were developed (cp. Chapter 4.2.2). Afterwards, velocity depending friction measurements were done on these surfaces (Fig. 4.19) with the three siped sample (reference compound). The average humidity was  $rF = 66\%$ , the temperature was  $T = -5,5^\circ\text{C}$  and the normal pressure has been adjusted to  $p = 2,5$  bar. Additionally, other friction influencing parameters like rubber sample and track conditioning process has been kept constant. The friction coefficient shows the well known decreasing characteristic for all three test tracks. Thereby a clear difference could be found between ice made from small and large grains: Ice with small grains shows a higher friction level compared to ice with large grains. A surprising result was observed when the measurements were performed on ice with small and large grains. Among all measurements, those on ice with small and large grains showed the smallest friction level. It can be concluded that the ice grain size influences the friction process clearly. This effect, however, was not studied further in this thesis.

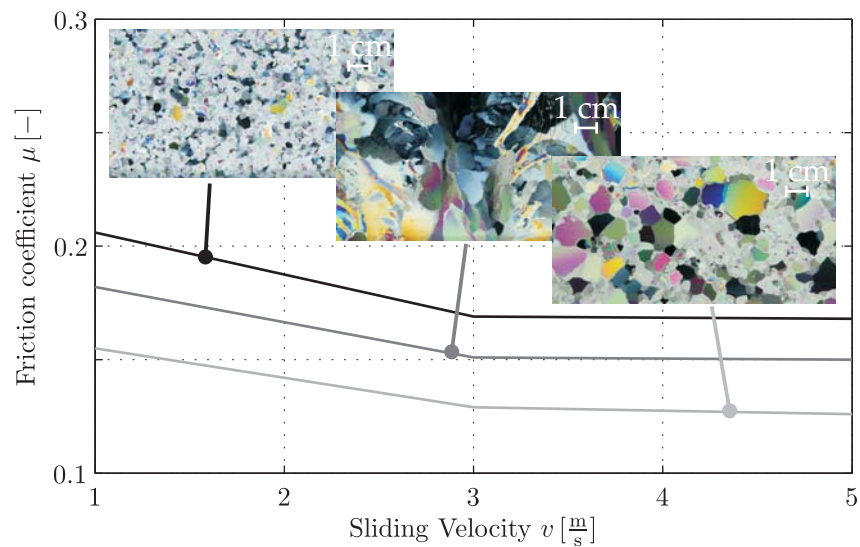


**Figure 4.19:** Influences of the ice grain size on the friction process measured with the three siped sample,  $T = -5,5^{\circ}\text{C}$

### 4.3.6 Determination of the contact area of sliding tire tread blocks on ice

Information on the tire footprint is very important for the tire development because footprint shape and size clearly influence the tire performance. Additionally, the pressure distribution in the contact is very important for the tire performance. Knowing the size of the real contact area between tire and ice surface would greatly increase the accuracy of simulation results because most models need the real contact area as an input parameter. It also helps understanding the friction mechanics in more depth. Different techniques exist for visualizing the actual contact situation, e.g. [32], [126], [64], [11]. A commonly used approach is the total internal reflection method (cp. e.g. [117]) which was also used here to study the contact area of sliding tire tread block samples on ice. A disadvantage of this method is the high effort of adjusting camera and illumination in a way that the total internal reflection occurs but the major advantage of this technique is that only contact regions can be seen on the picture.

After the experimental setup has been introduced basic measurements are shown. The method of total internal reflection works only if the ray of light comes from the optically dense medium and enters the optically rare medium. This method can be used here because the index of refraction of acrylic glass is larger compared to the one of ice  $n_A > n_I$  (cp. Table 4.5).

Basically the determination of the contact area with total internal reflection is done as follows: A prism is illuminated for using the effect of total internal reflection. The camera position has to be chosen in a way that the appearing picture can be recorded. The camera as well as the light have to be adjusted in a way that total internal reflection occurred in the prism. The test tire or tire tread block was set on a prism and loaded. The camera

**Table 4.5:** Index of refraction of selected materials [50]

| Material      | Index of refraction |
|---------------|---------------------|
| Air           | $n_L = 1,0003$      |
| Acrylic glass | $n_A = 1,491$       |
| Ice           | $n_I = 1,31$        |
| Water         | $n_W = 1,333$       |

only recorded the contact area of the tire. At points with no contact the light was still totally reflected and no tire or tire tread block could be seen. Due to the tire, the boundary conditions were changed at the border of the prism and the surrounding air. The required boundary condition for total internal reflection is not achieved any more. At the contact points of tire and ice reflection occurred and showed the tire footprint.

All previous researches directly measured the static contact area on a prism with the help of total internal reflection. This method shall be adjusted now to measure the contact area of sliding tire tread blocks on ice dynamically during a friction experiment at HiLiTe with a high speed camera (cp. Fig. 4.20 a). Therefore it is necessary to prepare an ice surface on top of the prism. The illumination is adjusted in a way that total internal reflection occurs in the prism and the camera position is chosen in a way that the picture can be recorded (cp. Fig. 4.20 a). The range where total internal reflection occurred at this test set-up has to be considered to reach the desired result as well. A basic challenge which also had to be solved was the preparation of a clear ice surface on top of the prism. Otherwise the total internal reflection method does not work any more. After the test set-up is completed the ice surface can be loaded with the tire tread block. In a first step the method was tested statically. The ice surface was free and the effect of total internal reflection could be seen clearly (Fig. 4.20 b). Only some bubbles in the ice were observed in the image. When a tire tread block came into contact with the ice surface its footprint was visualized clearly (Fig. 4.20 c).

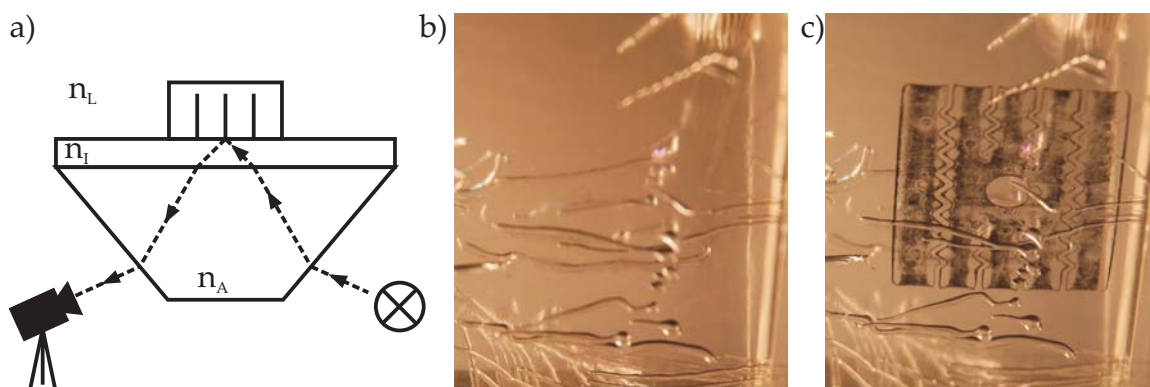


**Figure 4.20:** Sample measurement of static contact area: a) Test setup, b) Total internal reflection at free surface, c) Real contact area of tire tread block sample

In a second step the contact area of the reference samples was measured dynamically. Therefore, a friction experiment was performed with HiLiTe and the contact area was recorded with a high speed camera (Fig. 4.21). The sample slid from right to left. All



samples lost the contact to the ice in the back. With an increasing number of sipes the contact area was reduced. The darker line at the front edge indicates a pressure peak there (cp. Fig. 4.21 a-e). It is notably developed at the non siped and the three siped sample (dark black line at the front edge of the rubber sample), on the left side of the samples. The single block elements of the six and the seven siped sample show linewise contact only (cp. Fig. 4.21 d+e). The contact area is reduced clearly which results in a rising local pressure. The contact area of the non siped sample (Fig. 4.21 a) is approximately 70 % of the original sample size. Even for the seven siped sample the real contact area is about 25 % of the original sample size. While considering the results it has to be kept in mind that the ice preparation has to be done carefully because the flatness of the ice surface strongly influences the contact area measurement result.

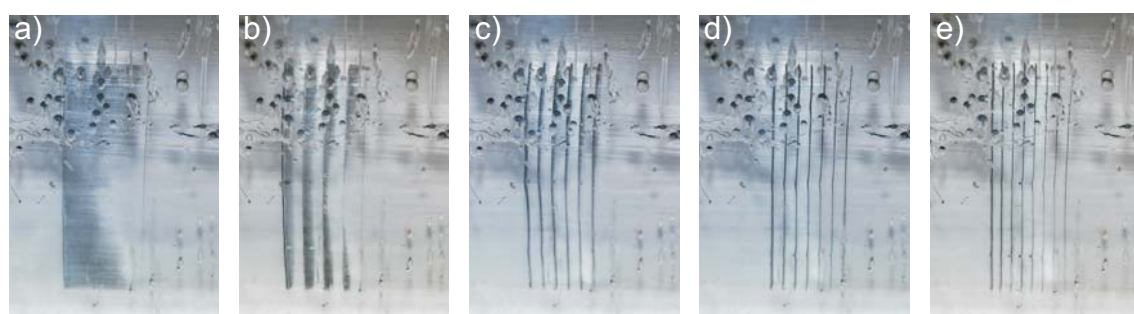


**Figure 4.21:** Contact area of reference samples (sliding direction from right to left): a) Non siped sample G0, b) Three siped sample G3, c) Five siped sample G5, d) Six siped sample G6, e) Seven siped sample G7

## 4.4 Post-processing of measurements on ice

This chapter outlines basic challenges which had to be solved during the development of the test method for investigating rubber-ice friction. So different boundary conditions can influence the measurement results significantly, see also [101].

During the ice surface preparation a smooth surface shall be provided to avoid an unknown variation of the local pressure in the footprint. A smooth surface can be achieved by homogenizing the ice surface by scraping-off the top layer with a blade, but the direct preparation of a smooth surface would be more time effective. During the past years the ice surface preparation process was continuously improved at the Institute of Dynamics and Vibration Research with the result of a smooth surface [101], [98]. It must be polished only before the friction measurements start.

A second challenge which has to be kept in mind is that the friction process is influenced by both partners. The influence of the ice surface cannot be neglected. Due to its nature, ice is a very unstable material. There is a continuous exchange of water molecules with the surrounding air called evaporation (cp. Chapter 2.1). Although the climate chamber is a confined room, sublimation can be observed if the ice surface rests there for a longer

time. The ice surface is a subject of permanent changes. This effect is also influenced by the temperature which impacts the saturation level of the surrounding air. After a few weeks, the ice surface is completely dissolved. Covering the ice surface can help to reduce the evaporation process. Other researchers also hold the ice surface responsible for variations in the measurement results, cp. DOPORTO et al. [25] (Section 2.2.2). VENKATESH identified an influence of the ice surface on the friction process. Two constants of his friction model vary "with the type of ice surface" [125], cp. Chapter 2.6.4. OKSANEN found a very large scatter during ice property measurements [88], cp. Chapter 2.6.6. ROBERTS observed an influence of the age of the ice track on the friction process (cp. Chapter 2.6.5). Probably the reasons are still the same as mentioned before. Due to the large influence of the ice surface on the friction process extensive investigations on the frictional properties of different ice surfaces have been done. Amongst others, the influence of the preparation method was investigated. Based on this knowledge an instruction for the preparation of ice surfaces has been developed. Additionally a reference sample was added to the tread block samples. With the help of the reference sample the friction level of the ice surface can be determined to guarantee the comparability of different friction measurements on different ice surfaces with each other. However, changing the ice surface during one test is avoided up to now.

Another reason for the spread of results are wear effects of the ice surface. They play an important role. After several measurements a groove can be observed on the ice surface where the sample slid on the ice (Fig. 4.23 b+c). Wear effects prevail at temperatures near the melting point. So the temperature variation is normally started with the coldest temperature to minimize the influence of surface wear on the measurement data.

Another field of activity is the evaluation of the measured footprints. Many tasks had to be solved to achieve the goal of measuring the contact area of sliding tire tread blocks on ice. The production of clear, nearly bubble free ice with a smooth surface initially allowed the observation of the contact area. In the course of time the test track and the method of ice preparation have been improved continuously. Finding out the position and the adjustment of high speed camera and light source as well as the illumination level in relation to the test track and the sliding velocity took a lot of time. As shown before, these challenges have been solved successfully. For sure the evaluation of the recorded pictures has to be improved. Therefore the definition of the contact area should be enhanced. This can be done with different methods of image data processing like filters, different average procedures, etc. On the other hand, the illumination level could be improved as well to make the evaluation easier because the difference between contact and no contact would be better. The total internal reflection lights the ice while the contact area of the tread block is still dark. A second advantage of a better illumination level is the possibility to record the contact area of samples sliding with velocities larger than  $v = 3 \frac{\text{m}}{\text{s}}$ .

At the end of this chapter the measurement procedure should be considered critically. The steady state evaluation of the measurements is very time-consuming because every possible combination of parameters is measured up to ten times. A variation based on three different sliding velocities and three different normal loads with four different rubber

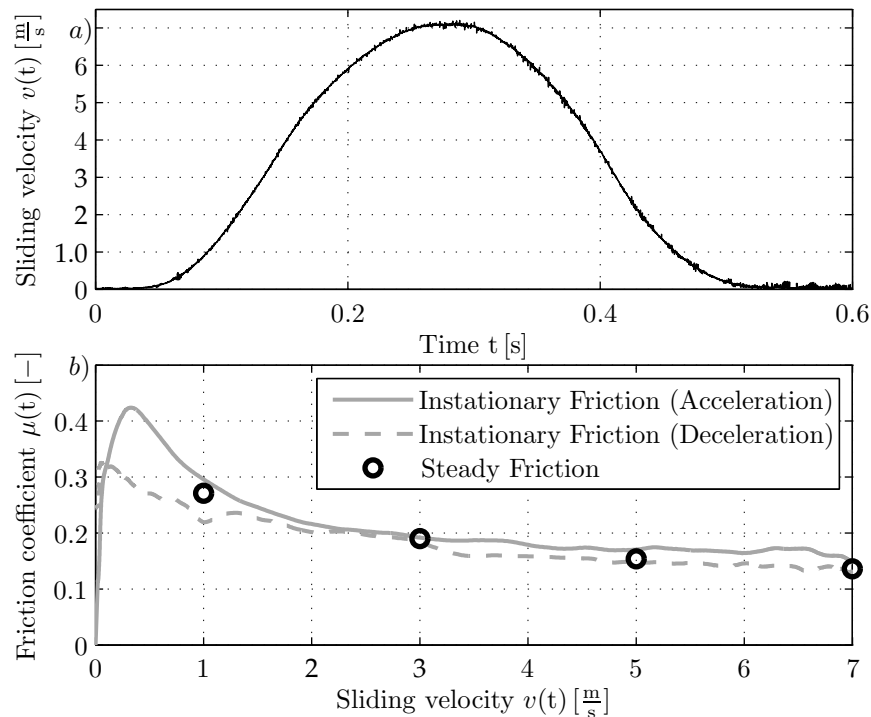


**Figure 4.22:** Method of instationary measurement for determining the friction coefficient: a) Sliding velocity during instationary measurement, b) Instationary friction characteristic vs. Steady measurement (According to [98])

samples results in a measurement effort of 360 single measurements. One possibility to avoid such a huge measurement effort can be the method of instationary measurements, cp. RIPKA et al. [98]. Therefore, the measurement is performed with a constant acceleration followed by a constant deceleration. The sliding velocity never reaches a constant level (Fig. 4.22 a). After the mass inertias of the tread block sample and the HiLiTe carriage are removed from the friction force characteristic during the acceleration phase, the friction coefficient can be calculated. The plot of friction coefficient and sliding velocity delivers the instationary friction characteristic (Fig. 4.22 b). It displays a friction coefficient for every sliding velocity in the investigated range. It can be seen that acceleration and deceleration phase do not perfectly fit together. The deceleration phase has a smaller friction coefficient compared to the acceleration phase. It seems that the rubber sample is heated up due to the frictional heat which reduces the friction coefficient during the experiment. For judging the quality of the instationary measurements these results are compared with the results of steady friction measurements (Fig. 4.22 b) which have been performed under the same climatic conditions and on the same ice track. It can be seen clearly that the friction coefficients of the investigated velocities fit together very well. The steady measurements hit the instationary curve of acceleration and deceleration very well. This first comparison delivers a promising result for the execution of future measurements.

## 4.5 Results and discussion

Friction is a phenomenon which is influenced by both contact partners. Especially rubber-ice friction is very complex. Besides the different dependencies of the friction process on the process parameters like temperature and humidity, the ice surface and its changes play an important role (cp. Chapter 4.3). So the existence of the water layer (cp. Chapter 2.2.2) has to be considered for the interpretation of the measured results. Based on the state of the art and the rubber-ice friction measurements a model is introduced which explains the observed phenomena. Subsequently the influence of the different parameters like sliding velocity, normal load, temperature and humidity as well as rubber geometry is analyzed and explained with the model. The effect of ice properties on the friction process is also considered.

### 4.5.1 The rubber-ice friction model

The analysis of the rubber-ice friction measurements shall help to define the illustratable range of mechanisms of the model. The measurements showed the following dependencies:

- **Velocity dependency:** Most of the experiments show a decreasing friction coefficient with increasing sliding velocity. Sometimes an increasing friction could be observed also.
- **Pressure dependency:** An increasing pressure normally results in a decreasing friction coefficient. However, sometimes an increasing friction coefficient could be observed.
- **Temperature dependency:** In most cases a decreasing temperature results in an increasing friction coefficient but on the other hand there have been done a few measurements which show an opposite behaviour: In this case a temperature near the melting point resulted in an increasing friction coefficient.
- **Humidity dependency:** An increasing humidity results in a reduction of the friction but a high level of humidity supports an increasing friction coefficient.
- **Tread block length dependency:** An increasing tread block length results in a decreasing friction coefficient (at constant normal pressure).
- **Ice impurity dependency:** An increasing level of salinity of the ice reduces the friction coefficient.
- **(Ice grain size:** Different grain sizes result in a changing friction coefficient.)<sup>8</sup>

During the observation of friction measurements with HiLiTe with a high speed camera (cp. Section 4.3.1) it could be seen that under certain parameter combinations each tread block element of the single tread block behaves in a different way: A clear squeal noise

---

<sup>8</sup>The influence of the ice grain size on the friction process cannot be explained by the model

could be heard. The vibrations of single block elements have been visualized with the high speed camera (cp. Fig. 4.11). The first two block elements vibrated while the last two block elements stood still. This allows the conclusion that the conditions in the contact area differ between the single tread block elements. Additionally it is assumed that the friction potential is continuously reduced from the first to the last block element due to the described observations. The presence of vibrations during the rubber-ice friction measurements have always been observed at high friction coefficients.

Additionally different hints on the water layer in the contact have been found during the numerous friction measurements. Although the water layer could not be measured directly during the past years of rubber-ice friction research at the Institute of Dynamics and Vibration Research, lots of indirect proves have been found which will be presented in detail subsequently. It is remarkable that the following observations are more distinctive at temperatures near the melting point or at high humidity. So frozen water can be found on the tread block sample at the end of the friction experiment (Fig. 4.23 a), which is an indication for water in the contact. It is remarkable that most of the frozen water can be found on the front edges of the last block elements. It seems that the water layer thickness is increased in the back part of the contact area. Additionally, wear phenomena of the ice track have been observed at temperatures close to the melting point. The tread block sample displaces that much water that a canal was formed on the test track (Fig. 4.23 b). The sample moved the water to the end of the test track where an ice bump was formed (Fig. 4.23 c). The water rests and freezes at the end of the track because the sample is lifted off there after the measurement is complete. Wear effects of the ice track have been observed also by EVANS et al. (cp. Chapter 2.6.3). The aforementioned observations resulted in the idea of an indirect proof of the water layer: If the tread block sample displaces water and the water is coloured a coloured tail must be visible on top of the ice surface. For checking this assumption two holes have been drilled into the ice surface. Both holes were filled with Na-Flourescin coloured water and frozen. After sliding above the coloured points in the ice with a tread block sample a red tail was visible on top of the ice surface (Fig. 4.23 d, marked with the white circle). The coloured water was melted and the tread block sample wiped the melted water away which results in the red tail which is another clear evidence of water in the contact area.

Many researchers emphasize the meaning of the ice surface water layer for the rubber-ice friction. A commonly accepted theory is the melting of ice due to frictional heat but it seems that an ice surface is always covered with a thin water layer (cp. Section 2.2.2). The estimates for the ice surface water layer thickness differ by an order of magnitude depending on the measurement method and its theoretical explanation is also not manifested (cp. Section 2.2.2). For the following theoretical consideration of the rubber-ice interaction the exchange of water molecules between ice surface and surrounding air as mentioned by SCHRÖDER is picked up (cp. Section 2.2.2 and [106]) again. A decreasing temperature reduces the water molecule movement in the ice surface as well as the water saturation level of the surrounding air (cp. Table 2.1). The number of evaporating and condensating molecules

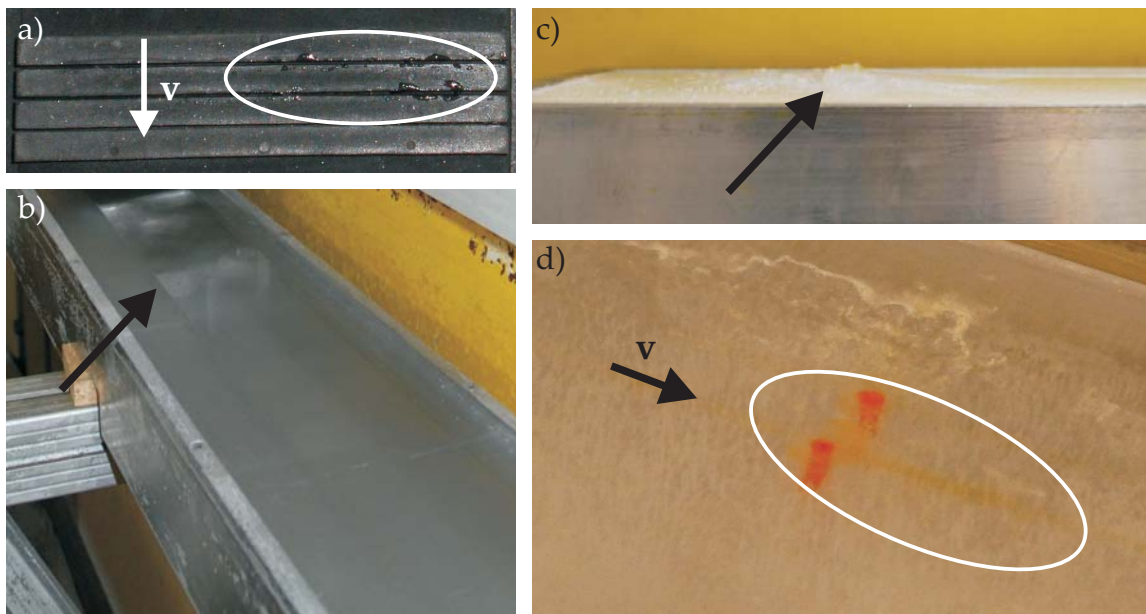


**Figure 4.23:** Indirect proof of water layer in the rubber-ice contact: a) Tread block sample with frozen water at the run-out area (white circle), b) Worn out ice test track due to melting, c) Ice bump at the end of the test track where the sample is lifted of, d) Red tail of melted Na-Flourescin ice

is reduced (cp. Fig. 2.4) which results in a reduction of the water layer thickness on the ice surface. The equilibrium of evaporating and condensing molecules is attended at a smaller layer thickness which leads to one of the temperature influences of the rubber-ice friction (cp. Fig. 4.13). A variation of humidity also changes the number of evaporating and condensating molecules which results in a change of the water layer thickness. Depending on the number of exchanging water molecules between ice surface and surrounding air the initial height of the surface water layer is influenced. This effect leads to the strong dependency of the humidity on the rubber-ice friction as observed during the measurements (cp. Fig 4.14). This result shows that the hypothesis that humidity has no influence on the friction process is wrong (cp. Section 3.2).

As already mentioned in the state of the art (cp. Section 2.6) some scientists assumed mixed friction, viscous and dry, in the rubber-ice contact (cp. Chapter 2.6.3, 2.6.8 and 2.6.9). Based on the observations during the rubber-ice friction measurements there is no doubt that water is in the contact. Beside this the initial surface water layer of the ice has to be kept in mind which results in a wet contact even if its thickness corresponds to the height of some molecules only. Additionally the theory of the existence of a "dry area" is picked up as well. A local contact of the rubber with different asperities of the ice seems to be unlikely because they were melted away (cp. [26]). The melting process shall be clearly visible in the friction characteristic due to a continuously decreasing friction coefficient from measurement to measurement but there was no evidence found during the experiments. Based on these considerations the following assumptions are done: There is a zone in the front of the tread block where the friction coefficients are in the range of dry friction

because of the very thin initial water layer. This zone is called dry run-in area. If the water layer is thicker, the tread block element edge wipes away the water which again results in a reduction of its thickness and the dry run-in area is generated. During the sliding process the ice is heated up due to the frictional power generated at the dry run-in area. The result is a water layer with increasing thickness in the back of the tread block (Fig. 4.24 a).

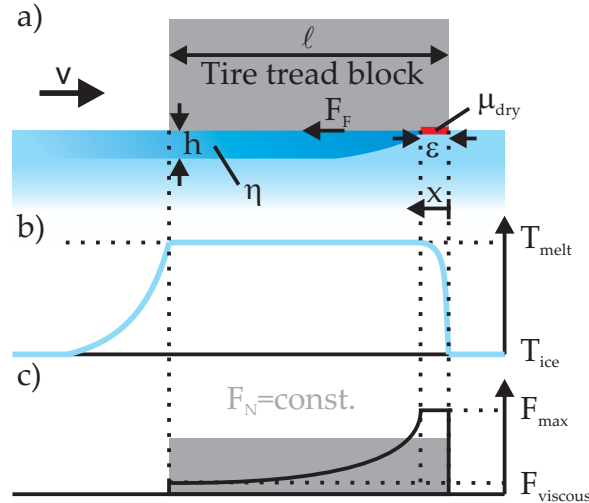


**Figure 4.24:** Model of rubber-ice friction: a) Schematic diagram of the process in the footprint with dry ( $A_{dry}$ ) and wet ( $A_{wet}$ ) part of contact, b) Temperature distribution in the contact area, c) Shear force distribution in the contact area (from RIPKA et al. [98])

The contact area consists of a dry run-in area and a wet part in the back:

$$A = A_{dry} + A_{wet} = \varepsilon w + (\ell - \varepsilon) w \quad (4.1)$$

with the length of the dry area  $\varepsilon$ , tread block width  $w$  and tread block length  $\ell$ . After the tread block has left the ice, the contact temperature decreases to the level of the ice temperature (Fig. 4.24 b) and the melted water layer refreezes up to the level of its natural thickness which is caused by the equilibrium of evaporating and condensating molecules.

In case of a siped tread block the single block elements influence each other (Fig. 4.25). The first tread block element wipes away the initial water layer (caused by condensating and evaporating water molecules) and heats up the ice due to the frictional heat generated in the dry run-in area. The ice temperature increases and a water layer arises. Its thickness is influenced by the frictional heat on the one hand but also by ambient temperature and humidity due to the changing number of condensating and evaporating water molecules on the other hand. Due to the small sipe the ice surface cannot cool down to the initial temperature. The following block element wipes away the water layer and continues heating up the ice due to the frictional heat generated in the dry run-in area which leads to a reduction of the dry run-in area (cp. Fig. 4.25). The following block element again wipes away the water layer and continues heating up the ice which further reduces the length of

the dry run-in area. This effect continues for the following tread block elements and leads to the inhomogeneous contact situation within the contact area.

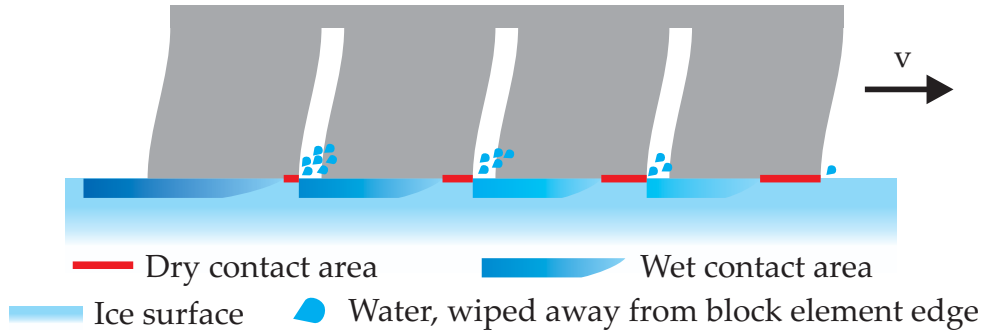


**Figure 4.25:** Siped tread block on ice friction model: Contact area of single block elements with dry run-in area followed by wet area. Due to the heating of the ice the length of the dry run-in area is reduced for each following tread block element and water is wiped away by the leading block element edge.

Independent from the number of sipes the mechanisms for each block element are generally the same. Only the length of the dry run-in area varies depending on the number of block elements in the front, the temperature and humidity. The generated friction force in the contact  $F_F$  is the sum of dry  $F_{F,dry}$  and viscous friction force  $F_{F,viscous}$  as observed by STRIBECK (cp. Section 2.4 and Fig. 4.24 c)

$$F_F = F_{F,viscous} + F_{F,dry} \quad (4.2)$$

The viscous shear force  $F_{F,viscous}$  can be calculated by the product of sliding velocity  $v$ , the viscosity of the water layer  $\eta$  and the real contact area  $A_{wet}$  divided by the water layer thickness  $h$  [78]:

$$F_{F,viscous} = v \eta \frac{A_{wet}}{h} \quad (4.3)$$

The friction force generated at the dry run-in area  $F_{F,dry}$  is calculated via the product of local friction coefficient  $\mu_{dry}$  multiplied with the normal force  $F_{N,dry}$  or the normal pressure  $p_{dry}$  and the dry part of the contact area  $A_{dry}$ :

$$F_{F,dry} = \mu_{dry} F_{N,dry} = \mu_{dry} p_{dry} A_{dry}. \quad (4.4)$$

Inserting Equation 4.3 and Equation 4.4 in Equation 4.2 delivers:

$$F_F = v \eta \frac{A_{wet}}{h} + \mu_{dry} p_{dry} A_{dry} = \frac{v \eta}{h} w (\ell - \varepsilon) + \mu_{dry} p_{dry} w \varepsilon. \quad (4.5)$$



The geometry of the tread block, i.e. its length  $\ell$  and width  $w$  are constant. The viscosity of the water layer  $\eta$  and the sliding velocity  $v$  are also constant during the experiment. The height of the water layer  $h$  is constant as well if the friction process is stationary due to the equilibrium between supplied and discharged frictional heat. Additionally, it is assumed that the pressure distribution in the contact area is constant within the dry as well as the wet part because of the homogeneous contact situation of each area on the macroscopic scale. This assumption is supported by the measurements of the real contact area of sliding tire tread blocks (cp. Fig. 4.21). The contact situation on the microscopic scale has to be investigated in depth in the future. The homogeneous contact situation also leads to a constant dry friction coefficient  $\mu_{\text{dry}}$ . It can be seen clearly that the friction force is strongly influenced by the length of the dry run-in area  $\varepsilon$ . It corresponds to the size of the dry part in the front which directly affects the size of the wet part of the contact area. The contribution of dry and viscous friction to the overall friction force depends on the ratio of dry to wet contact area. A critical size of the wet contact area needs to be passed so that viscous shear forces can be activated in the water layer. This is the case if the dry friction part is so small that it does not dominate the friction process any more. Depending on the combination of test parameters, rubber and ice properties in the beginning of the rubber-ice measurement, the friction force decreases due to the decreasing length of the dry run-in area. If the critical size of the wet part of the contact area is reached viscous shear forces are activated and result in an increasing friction coefficient. If the size of the wet part of the contact area suffice in the beginning of the measurement cycle the friction force increases directly. For understanding the impact of the different parameters like sliding velocity  $v$ , normal load  $p$  and ambient temperature  $T$  on the rubber-ice friction process in more detail their influences on the length of the dry run-in area  $\varepsilon$  are considered in depth. The length of the dry run-in area  $\varepsilon$  can be calculated with the heat conductance equation solved by BLOK [13] and used by MUNDL [134] to calculate the temperature increase during a dry braking manoeuver (see also RIPKA et al. [98]):

$$\Delta T(x = \varepsilon) = 2 K \mu_{\text{dry}} p \sqrt{\frac{\varepsilon v}{\pi \lambda_{\text{ice}} \rho_{\text{ice}} c}}. \quad (4.6)$$

Solving Equation 4.6 for the length of the dry run-in area  $\varepsilon$  delivers

$$\varepsilon = \left[ \frac{\Delta T}{2 K \mu_{\text{dry}} p} \right]^2 \frac{\pi \lambda_{\text{ice}} \rho_{\text{ice}} c}{v}. \quad (4.7)$$

The thermal conductivity of ice is  $\lambda_{\text{ice}} = 2,2 \frac{\text{W}}{\text{mK}}$ , the density of ice is  $\rho_{\text{ice}} = 917 \frac{\text{kg}}{\text{m}^3}$  and the specific heat capacity of ice is  $c_{\text{ice}} = 2,09 \frac{\text{kJ}}{\text{kgK}}$ . Nearly 100 % of the frictional heat is dissipated from the ice (due to the much smaller thermal conductivity of rubber  $\lambda_{\text{rubber}} = 0,16 \frac{\text{W}}{\text{mK}}$ ), so the heat flow into the ice is set to  $K = 1$ . The following parameter variation gives a more detailed impression of the sensitivity of the length of the dry run-in area  $\varepsilon$  (Fig. 4.26). The ambient temperature or the temperature difference  $\Delta T$  to the

melting point dominates the lengths  $\varepsilon$ . This seems to be plausible because, depending on the temperature, ice has to be heated more or less to generate a water film. For example heating a defined ice volume from  $T = -10^\circ\text{C}$  to the melting point needs ten times more energy (specific heat capacity of ice  $c_{\text{ice}} = 2,09 \frac{\text{kJ}}{\text{kgK}}$ ) compared to a temperature of  $T = -1^\circ\text{C}$ . This seems to be much energy but compared to the heat of fusion of ice  $q_{\text{ice}} = 334 \frac{\text{kJ}}{\text{kg}}$  which is needed to melt the ice it is very small. At colder temperatures a change of the sliding velocity or the normal pressure results in a clear reduction of the dry run-in area because only heating up the ice to the melting point needs only a little more frictional heat in contrast to melt more ice for increasing the water film height significantly, e.g. for activating viscous shear forces.

This difference in specific heat capacity and heat of fusion is also the reason why pressure or velocity changes at temperatures near the melting point do not noticeably change the length of the dry run-in area (cp. Fig. 4.26 a). The frictional heat which is generated does not suffice to melt more ice. Additionally, it has to be kept in mind that the initial water layer thickness on the ice surface increases at higher ambient temperatures and high humidity due to the larger amount of evaporating and condensating water molecules. The molecules are less fixed on the ice surface. The length of the dry run-in area is strongly influenced by the dry friction coefficient  $\mu_{\text{dry}}$  as well. Especially small friction coefficients have a high impact on the dry length  $\varepsilon$  (cp. Fig. 4.26 b), but due to the assumption that the first part of the tread block contact area is dry it can be assumed that the friction coefficient is in a range around  $\mu_{\text{dry}} = 1,5$  as it can be found for rubber friction on dry glass. Adopting a temperature difference of  $\Delta T = 8 \text{ K}$ , a contact pressure of  $p = 2,5 \text{ bar} = 0,25 \text{ MPa}$ , a dry friction coefficient of  $\mu_{\text{dry}} = 1,5$  and a sliding velocity of  $v = 1 \frac{\text{m}}{\text{s}}$ , the length of the dry run-in area can be calculated to  $\varepsilon = 1,5 \text{ mm}$  (see also RIPKA et al. [98]).

It is concluded that the rubber-ice friction is dominated by the length of the dry run-in area  $\varepsilon$  (cp. Fig. 4.27). It defines the ratio of dry and wet part of the contact area. The dry length influences the friction coefficient directly. If the dry part is small enough the viscous shear forces in the wet part of the contact area dominate the friction process and the friction coefficient increases (cp. Fig. 4.27). The dry run-in area is supported if the front edge of the tread block or the front edge of each tread block element wipes away the water layer. The length of the dry run-in area is affected by the melt water layer on the one hand and by the initial water layer on the ice on the other hand. The initial water layer increases for an increasing ambient temperature and for increasing humidity. The thickness of the melt water layer is influenced by the ambient temperature and the frictional heat. At constant ambient temperature an increasing sliding velocity or normal load results in increasing frictional heat which melts more ice and therefore increases the melt water layer thickness which results in a reduction of the dry length  $\varepsilon$  (cp. Fig. 4.27). Based on the ratio of wet and dry area a limit of transmittable friction forces can be reached (Fig. 4.16). A stationary state is approached where a change of the parameters does not affect the friction coefficient any more. The friction coefficients of each parameter variation tends to move against this limit. Sometimes this trend can be seen clearly, in other cases the

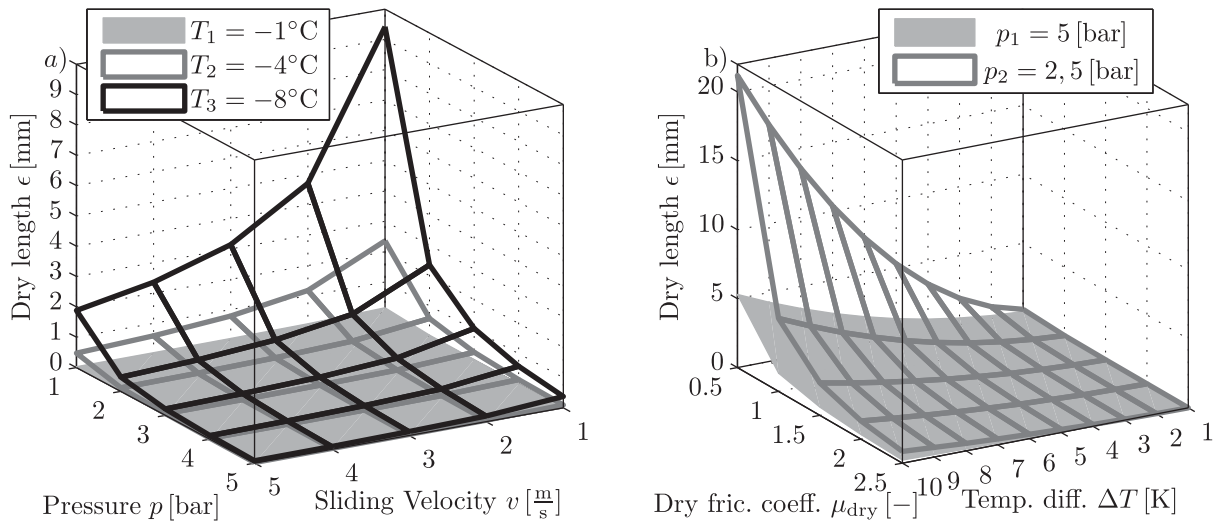


**Figure 4.26:** Parameter variation on the length of the dry run-in area: a) Dependency of sliding velocity  $v$ , normal pressure  $p$  and temperature  $\Delta T$  on the length of the dry run-in area  $\epsilon$  (According to RIPKA et al. [98]), b) Dependency of Temperature  $\Delta T$ , dry friction coefficient  $\mu_{\text{dry}}$  and normal pressure  $p$  on the dry run-in area  $\epsilon$

frictional limit seems to be far away. The upper limit is defined by dry friction, the wet area disappears:  $A = A_{\text{dry}} \Rightarrow \mu_{\text{max}} = \mu_{\text{dry}}$ . The lower limit is dominated by viscous friction:  $A = A_{\text{wet}} \Rightarrow \mu_{\text{min}} = \mu_{\text{wet}}$ . It seems that the maximum viscous friction (lower limit) is similar to the state of minimum dry friction where the viscous friction is not just activated (cp. Fig. 4.14 i). So the rubber-ice friction phenomena can be described sufficiently with a dry run-in area followed by a wet part. The second hypothesis which has been formulated (cp. Section 3.2) has to be expanded with a dry run-in area otherwise the decreasing behaviour of the friction coefficient cannot be explained.

In oposite to the third hypothesis which has been formulated in the beginning (cp. Section 3.2) the pressure melting phenomena can be neglected here because the reduction of the contact area during sliding on 70 to 25% of the original size does not suffice to melt the ice due to increasing pressure in the contact. Note that this result is valid for the macroscopic scale only. A future determination of the microscopic contact situation can result in another pressure distribution. Maybe the pressure melting can have an influence there.

#### 4.5.2 Impact of the ice properties on the friction process

After explaining the friction model in detail, the influence of the ice surface on the friction process is considered in more depth. The results play an important role for tire tests because the water composition which is used there for track preparation can also influence the test results which affects the comparability of results of different test days. Different water compositions make it hard to compare between lab test and tire test results. The reason why the impurified water influences the friction process is the change of the melting point

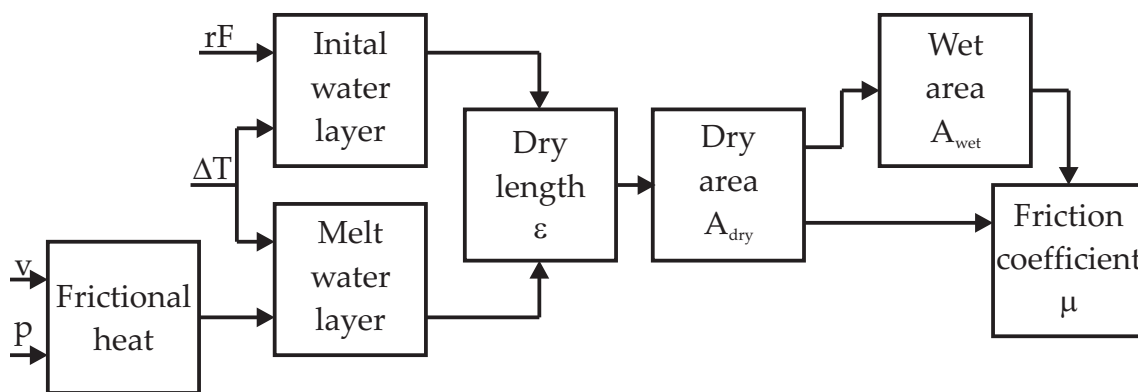


**Figure 4.27:** Flow chart of rubber-ice friction mechanisms

of the ice. The ice melts earlier, the friction coefficient is reduced and therefore the friction characteristic is vertically shifted. The purified water, for example, has a higher melting point compared to impurified water which can be seen on the comparison of friction of purified and saline water (cp. Chapter 4.3.5.1). The measurement results support the theoretical considerations in its entirety. The measurement results also show the advantage of siped tire tread blocks compared to non siped tread blocks. The siped sample wiped away the water layer and generated more friction on the ice surface made of saline water. The influence of impurities on the friction process had also been studied by RIPKA et al. [101] with the same result. They compared friction measurements on lake water from Arvidsjaur test track (Sweden) with purified water. Due to the impurities of the lake water the melting point was reduced and the friction level was generally lower [101]. It can be concluded that the level of salinity has a large influence on the rubber-ice friction measurement result as supposed with the fourth hypothesis (cp. Section 3.2) and as it can be found in the literature. This has to be kept in mind when comparing measurements which had been performed on different ice surfaces.

The impact of the grain size on the friction process is much more complex. During the measurements differences between small and large grains could be identified clearly. Small grains deliver a higher friction coefficient compared to large grains. Possible arguments for an existing influence are as follows: The thermal conductivity of the ice can vary between the single grain types. An increasing number of grain boundaries improve the thermal conductivity, and the development of the water layer is harder. The friction coefficient increases. Another reason for the higher friction level of small ice grains is their direct influence on the friction process. They act like the asperities on an asphalt or concrete surface: The front edge of each tread block element sticks on every grain boundary. An increasing amount of grain boundaries results in an increasing resistance, and the friction force increases. An interesting phenomenon can be observed for the mixture of small and large grains: it delivers the smallest friction coefficient. Although the measurements have been done with the same rubber samples and under constant temperature and humidity no explanation can be given for this phenomenon. In opposite to the fifth hypothesis the grain size of the ice has a large influence on the rubber-ice friction process. However, the

grain size is hard to control on the test track but for lab measurements this fact has to be kept in mind for ensuring a better comparability of different measurements.

### 4.5.3 The friction coefficient as a function of the square root of the sliding velocity

The measurement data which was collected for this thesis shall be used to show that the friction coefficient is proportional to the square root of the sliding velocity even for rubber-ice friction. For getting a general overview the decreasing as well as the increasing rubber-ice friction characteristics are investigated in depth (Fig. 4.14). These curves represent the minimum as well as the maximum boundary of the friction process. For this purpose the characteristics of the three siped sample at both pressure states and low humidity and low temperature ( $T = -5^{\circ}\text{C}$ ,  $rF < 50\%$ ) as well as high humidity and the temperature near the melting point ( $T = -1^{\circ}\text{C}$ ,  $rF > 90\%$ ) are chosen. The decreasing characteristic is fitted with

$$\mu = A_D v^{-0,5} + B_D \quad (4.8)$$

and the increasing friction characteristic can be adapted by

$$\mu = A_I v^{0,5} + B_I \quad (4.9)$$

The constants are labeled with the index  $D$  which marks the decreasing characteristic and index  $I$  is used for the increasing part. In this case all four parameters have been chosen in a way that the fit function displays the measurement in a good manner (Table 4.6). It seems that a link can be found between different parameters e.g. both paramters ( $A$  and  $B$ ) decrease if the normal load increases.

**Table 4.6:** Fitting values for measured friction characteristic (Fig. 4.28)

|                              |                            | $A_D$ | $B_D$ |                            | $A_I$ | $B_I$ |
|------------------------------|----------------------------|-------|-------|----------------------------|-------|-------|
| G3 ( $p = 2,5 \text{ bar}$ ) | $T = -5^{\circ}\text{C}$ , | 0,2   | 0,095 | $T = -1^{\circ}\text{C}$ , | 0,03  | 0,075 |
| G3 ( $p = 5 \text{ bar}$ )   | $rF < 50\%$                | 0,125 | 0,05  | $rF > 90\%$                | 0,02  | 0,04  |

The comparison of measurement and fit shows a good correlation (Fig. 4.28). Nearly no difference can be found between the measured values and the fit characteristic for the temperature near the melting point and the high humidity (Fig. 4.28 a). The characteristic of low temperature and humidity differs a little for low sliding velocities which can be caused by fewer supporting points of the measurement (Fig. 4.28 b). However, it is concluded that rubber-ice friction measurements can be fitted with a function containing the square root of the sliding velocity.

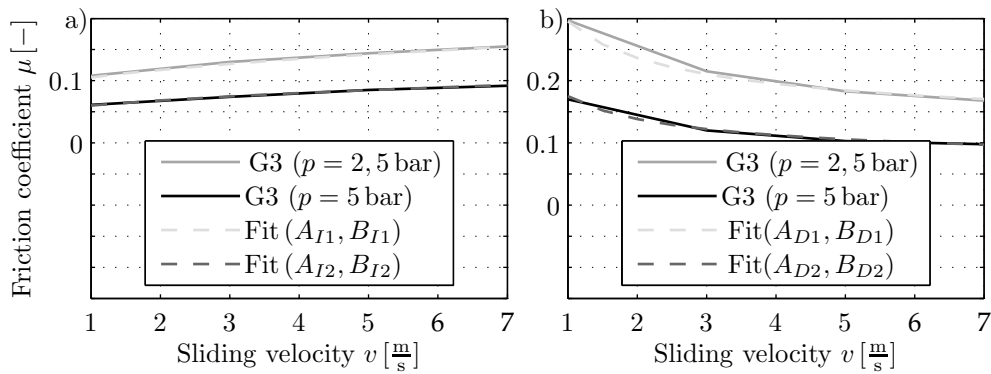


**Figure 4.28:** Correlation of measured friction coefficient and the square of the sliding velocity

## 4.6 Conclusions and consequences for tire development

The following considerations shall primarily point out ideas which can help to optimize future tire performance on ice as well as tire tests. As seen before, the friction characteristic strongly depends on the local contact pressure. Reducing the pressure clearly increases the friction coefficient. This results in the goal of a homogeneous contact pressure distribution within the tire road contact. It can be reached by controlling the surface structure of the tread block (cp. Chapter 2.6.4 and Chapter 2.6.8) and the tread block element deformation. The block bending is influenced, on the one hand by the tread compound and, on the other hand, by the tread geometry. An optimized parameter combination can certainly be found. It has to be kept in mind that a siped block structure delivers higher friction coefficients compared to the non siped block for temperatures near the melting point.

The ice characterization should be improved in the future in order to control the boundary conditions of the tire tests. Until then, the control of ambient temperature and humidity can help to improve the test result quality or to understand differences among the measurement data. An analysis of the water quality over a test season can also help to explain differences in the test results. Anyway, track preparation with new water should be avoided during a test series. This normally causes a change of the ice surface which results in an unpredictable impact on the friction process.

## 5 Development of a simulation model for siped tire tread blocks

Besides outdoor tests and lab experiments, simulations become more and more important. They can be used for studying friction mechanisms of tires or single tire tread blocks but also for developing new tires or new tire components. The simulation is a cost effective alternative compared to tire tests and allows a more flexible acting. No test samples need to be manufactured and no test rig is necessary.

The models which are presented here shall offer the possibility to display the observed rubber-ice friction phenomena. Different measurements performed with HiLiTe are used for validation purposes. Besides the ice performance the snow performance also plays an important role in the winter tire development. For future research, basic snow friction mechanisms are implemented in the analytical models. A difference between ice and snow friction mechanisms is the digging of the tread block elements in the snow and the shearing of snow ridges. The digging of the tire pattern into the snow is very important for snow friction. The loose snow rests in the sipes which influences the friction behaviour of the tread block and therefore should be considered in the simulation. For further details on snow friction mechanisms see BROWNE [17], MUNDL [80], [81] and NAKAJIMA [84].

Different analytical models are introduced and evaluated whether they are suitable for modeling siped tire tread blocks. In the beginning the implementation of the tread block-surface contact in the simulation model is explained with the help of a single mass oscillator. In a second step this model is extended to display the deformation of the siped tread block in more detail. Additionally, the suitability of the EULER-BERNOULLI beam theory as well as the TIMOSHENKO beam theory for simulating siped tire tread blocks is investigated.

There are different needs to be considered in order to model the siped tread block in a realistic way. First of all, it is important to describe the shape of the tread block. Thereby the notation which is commonly used in tire industry for a tire tread block is used although it is unusual for the beam theories: the length of the overall tread block is  $L$  and the tread block width is  $w$ . The size of the single tread block elements is described with the length  $\ell$  and the sipe depth  $d$  (cp. Fig. 4.4 d).

It is also important to take the number of block elements and the distance between them into account if the effect of a variable sipe length should be studied. Furthermore the physical properties like mass, density, stiffness and damping behaviour of the block

elements are required. For getting a realistic model behaviour the friction between the single block elements must also be considered.

The contact problems like tread block on road or ice/snow surface but also the contact of the single block elements with its neighbouring elements is solved with the penalty method. It allows the implementation of an arbitrary friction law which even permits the consideration of rubber snow friction in every single sipe. A universal friction law is implemented in the tread block-surface contact as well. This friction law offers the possibility for considering basic factors like sliding velocity and pressure but also temperature in the contact.

## 5.1 Rigid body model

In a first step a simple rigid body model is introduced. It is used to explain the basic interaction of tread block and surface in friction contact. Afterwards it is extended to increase the accuracy of the simulation results. An extended rigid bar model is used to define the contact law between single elements. Furthermore, a model validation is performed based on basic simulations and measurements with HiLiTe. At the end of the chapter simulation results are discussed which demonstrate the advantages of this analytical model especially for simulating instationary processes.

### 5.1.1 Single degree of freedom model

In a first step a single degree of freedom (SDOF) model is used to represent the motion of a single tread block element (Fig. 5.1). The single degree of freedom system consists of a rigid body which is mounted in point  $A$  and linked to the environment with a torsional spring and damper (spring constant  $c_\varphi$  and damping constant  $d_\varphi$ ). It has a moment of inertia  $J^{(A)}$  with respect to joint  $A$ . The normal contact between tread block and surface is modelled by the deformation  $u_N$  of a penalty spring with constant  $c_N$ . The corresponding contact force  $F_N$  is:

$$F_N = c_N u_N \quad (5.1)$$

Details concerning the penalty spring method can be found e.g. in WRIGGERS [132]. The deformation  $u_N$  of the penalty spring is calculated as follows

$$u_N = y_N + y_a - y_0. \quad (5.2)$$



The distance  $y_0$  is a default parameter which is used to adjust the average normal force (Fig. 5.1). The parameter  $y_N$  represents the undeformed length of the penalty spring. The distance  $y_A$  is related to the rotation of the bar by

$$y_a = \cos \varphi_1 d. \quad (5.3)$$

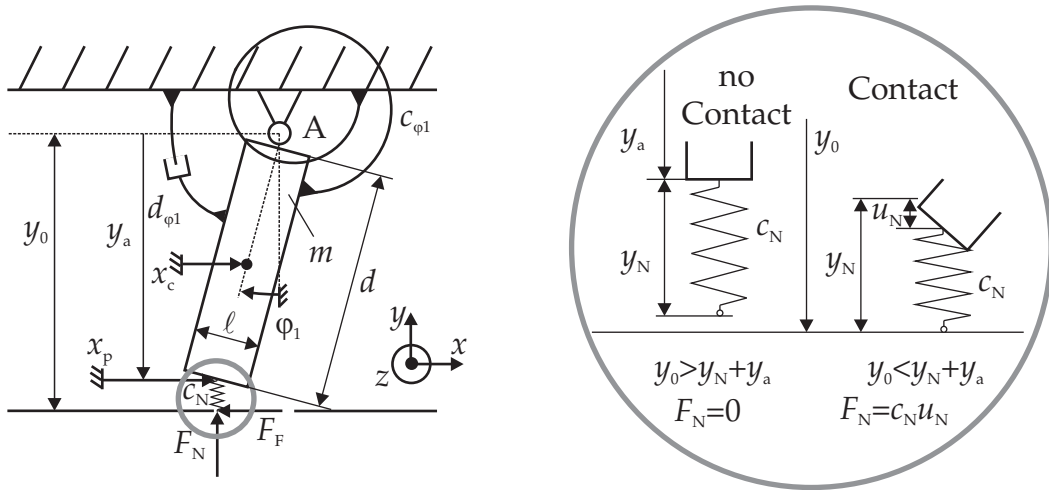


**Figure 5.1:** Single DOF tread block model (According to [97])

For the simulation it is necessary to distinguish two states:

- no contact for:  $y_0 \geq y_N + y_a \Rightarrow F_N = 0$  and
- contact for:  $y_0 < y_N + y_a \Rightarrow F_N$  is calculated according to Equation 5.1.

The friction force  $F_F$  is linked to the normal force  $F_N$  via the friction coefficient  $\mu$ .

$$F_F = \mu F_N. \quad (5.4)$$

Both, normal and friction force are assumed to act at the bottom of the bar at the middle axis (Fig. 5.1). The friction coefficient can be chosen to represent a given friction characteristic. Typical for rubber applications is a velocity depending friction characteristic  $\mu = f(v_{\text{rel}}, \dots)$  [75]. The relative velocity  $v_{\text{rel}}$  in the contact is calculated from the average sliding velocity  $v_0$  (which is equal to the vehicle speed) and the velocity of the tip of the bar  $\dot{x}_p$

$$v_{\text{rel}} = v_0 - \dot{x}_p. \quad (5.5)$$

The average sliding velocity  $v_0$  is a default parameter which has to be defined before the simulation starts. The velocity of the end of the bar is

$$\dot{x}_p = -\cos(\varphi_1)d\dot{\varphi}_1. \quad (5.6)$$

A relative velocity depending friction characteristic was implemented in the simulation which is typical for a winter tire tread block sliding on ice (Fig. 5.2). It is based on measurements performed with HiLiTe.

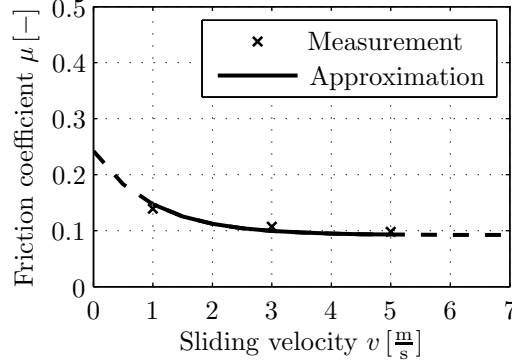


**Figure 5.2:** Relative velocity depending friction characteristic typical for rubber-ice friction

It was fitted as shown by RIPKA et al. [97] by the function

$$\mu(v_{\text{rel}}) = a_1 + a_2 e^{a_3 v_{\text{rel}}}. \quad (5.7)$$

The parameters  $a_1, a_2$  and  $a_3$  are used to fit the measurements. The equation of motion of the system is

$$J^{(A)} \ddot{\varphi}_1 = -d_{\varphi_1} \dot{\varphi}_1 - c_{\varphi_1} \varphi_1 + F_F d \cos \varphi_1 + F_N d \sin \varphi_1. \quad (5.8)$$

with

$$J^{(A)} = \frac{1}{3} m d^2 + \frac{1}{12} m l^2. \quad (5.9)$$

The single DOF model, however, is not sufficient to describe the deformation shape of a tire tread block element. It is, in particular, not capable to model the elastic shear and bending deformation of the tread block elements.

## 5.1.2 Multi degree of freedom model

### 5.1.2.1 Model set-up

The single DOF model (cp. Chapter 5.1.1) is extended with a second DOF to obtain a better modeling of the tire tread block element deformation. This two mass oscillator allows a more detailed description of the block element behaviour. The second bar is attached to the first bar by another rotational spring and damper. Corresponding to the number of tread block elements to be modeled, the system can be set up by an arbitrary number of

two mass oscillators. Fig. 5.3 shows a tread block with four tread block elements and three sipes .

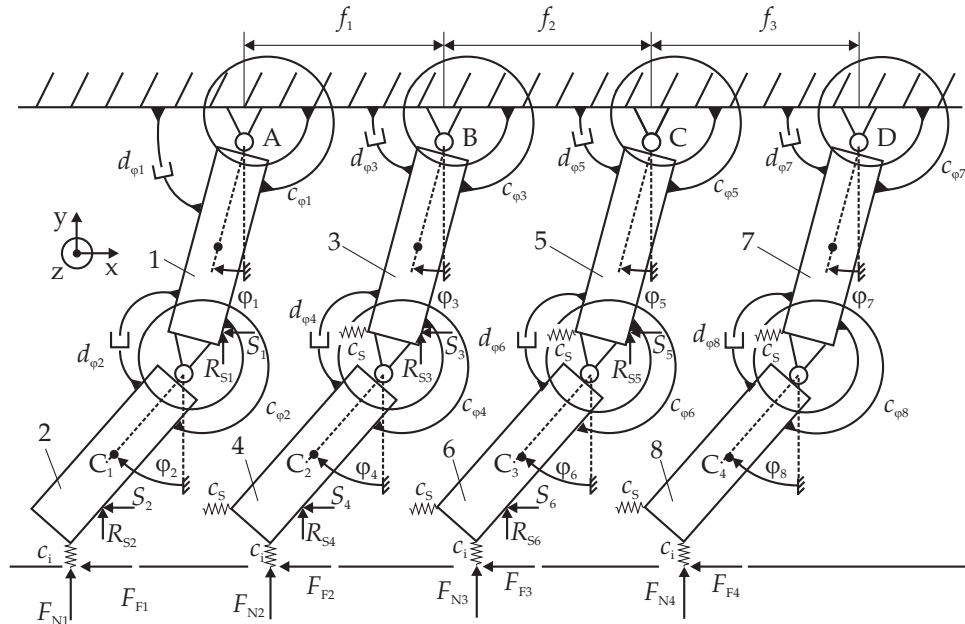


**Figure 5.3:** Four two mass oscillators to model a siped tire tread block (According to [97])

The torsional springs are described by  $c_{\varphi 1}$  to  $c_{\varphi 8}$ . The according dampers are  $d_{\varphi 1}$  to  $d_{\varphi 8}$ . The deformation angle of each bar is marked with  $\varphi_1$  to  $\varphi_8$ . The distance between the single tread block elements is described by  $f_1$  to  $f_3$ . In this way different tread block geometries and mechanical parameters (mass, damping and spring) can be investigated in parameter studies. The contact of each block element with the surface is solved using the penalty method as described in Section 5.1.1. A new feature of the model is the contact between adjacent bar elements which is solved with the penalty method as well. For keeping the model simple and for reducing the computational effort only sliding in one and the same direction is taken into account ( $\varphi > 0$ ). The advantage of this assumption is the need of penalty springs only on one side of the bars (cp. Fig. 5.3) because the deformation of the single block elements occur only in negative x-direction. It is further assumed that the contact forces act only in horizontal direction even if the bar changes its deformation angle. The contact force  $S_i$  is again generated via the deformation of a penalty spring (spring constant  $c_s$ , cp. Fig. 5.3) located at the left edge of each bar. It occurs if a bar penetrates its neighbour due to large deformation. A friction force  $R_{S_i}$  is introduced in order to consider the rubber friction between adjacent tread block elements. It acts orthogonal to the contact force  $S_i$ . Both forces are linked again via the model of COULOMB where the friction characteristic  $\mu$  displays the friction phenomena in the sipe. This method gives the opportunity to consider the influence of an arbitrary material in the sipes on the deformation behaviour of the block elements. Therefore, a friction characteristic which displays this special need has to be implemented in the model. Now the tread block model allows to display the influence of snow in the sipes as it can be observed on a typical siped winter tire. Due to the defined sliding direction and the subsequent deformation of the

two mass oscillators, the force application point of normal force  $F_N$  and friction force  $F_R$  is changed to the bottom right edge of each second bar (cp. Fig. 5.3). The equations of motion for each oscillator were derived similarly to the single DOF model. The equations of motion for bar "3" and "4" are given as an example here:

$$\begin{aligned}
& \left( J^{(B)} + md^2 \right) \ddot{\varphi}_3 + \frac{1}{2} md^2 \cos(\varphi_3 - \varphi_4) \ddot{\varphi}_4 = \\
& - (d_{\varphi_3} + d_{\varphi_4}) \dot{\varphi}_3 + d_{\varphi_4} \dot{\varphi}_4 - (c_{\varphi_3} + c_{\varphi_4}) \varphi_3 + c_{\varphi_4} \varphi_4 + \frac{1}{2} md^2 \sin(\varphi_4 - \varphi_3) \dot{\varphi}_4^2 \\
& - \frac{3}{2} mgd \sin \varphi_3 - \left( d \cos \varphi_3 - \frac{\ell}{2} \sin \varphi_3 \right) S_1 + \left( d \cos \varphi_5 - \frac{\ell}{2} \sin \varphi_5 \right) S_3 \\
& - \left( d \sin \varphi_3 + \frac{\ell}{2} \cos \varphi_3 \right) R_{S1} - \left[ \frac{\ell}{2 \cos \varphi_3} - \left( d \cos \varphi_5 - \frac{\ell}{2} \sin \varphi_5 \right) \tan \varphi_3 \right] R_{S3} \\
& - d \cos \varphi_3 S_2 + d \cos \varphi_3 S_4 - d \sin \varphi_3 R_{S2} \\
& + d \sin \varphi_3 R_{S4} + d \sin \varphi_3 F_{N2} + d \cos \varphi_3 F_{F2}
\end{aligned} \tag{5.10}$$

$$\begin{aligned}
& \left( J^{(C2)} + \frac{1}{4} md^2 \right) \ddot{\varphi}_4 + \frac{1}{2} md^2 \cos(\varphi_3 - \varphi_4) \ddot{\varphi}_3 = \\
& + d_{\varphi_4} \dot{\varphi}_3 - d_{\varphi_4} \dot{\varphi}_4 + c_{\varphi_4} \varphi_3 - c_{\varphi_4} \varphi_4 + \frac{1}{2} md^2 \sin(\varphi_3 - \varphi_4) \dot{\varphi}_3^2 - \frac{1}{2} mgd \sin \varphi_4 \\
& - \left( d \cos \varphi_4 - \frac{\ell}{2} \sin \varphi_4 \right) S_2 + \left( d \cos \varphi_5 + d \cos \varphi_6 - \frac{\ell}{2} \sin \varphi_6 - d \cos \varphi_3 \right) S_4 \\
& - \left( d \sin \varphi_4 + \frac{\ell}{2} \cos \varphi_4 \right) R_{S2} + \left( \frac{d}{2} \sin \varphi_4 - \frac{\ell}{2 \cos \varphi_4} \right) R_{S4} \\
& + \left[ \left( d \cos \varphi_5 + d \cos \varphi_6 - \frac{\ell}{2} \sin \varphi_6 - d \cos \varphi_3 - \frac{d}{2} \cos \varphi_4 \right) \tan \varphi_4 \right] R_{S4} \\
& + \left( d \sin \varphi_4 - \frac{\ell}{2} \cos \varphi_4 \right) F_{N2} + \left( \frac{\ell}{2} \sin \varphi_4 + d \cos \varphi_4 \right) F_{F2}
\end{aligned} \tag{5.11}$$

Details concerning the derivation of the equations of motion of the system as well as the penalty contact algorithm in the model have been explained in detail by RIPKA et al. [97].

### 5.1.2.2 Validation of the siped tread block model

Basic simulations have been done in order to check the correct functionality of the model. Different parameters such as distance  $y_0$  and sliding velocity  $v_0$  have been varied. The first simulation was performed while considering the influence of the displacement  $y_0$  which is related to the normal load. A decreasing distance should result in an increasing deformation of the bars. The simulations were done with two different parameter sets  $y_{0,1} = 4,6 \text{ mm}$  and  $y_{0,2} = 5,1 \text{ mm}$  while the velocity was set to  $v = 5 \frac{\text{m}}{\text{s}}$ . The length of the relaxed tread block element is  $d = 6 \text{ mm}$ . The normal contact between adjacent bars was considered while the friction between the single block elements was neglected ( $R_{Si} = 0$ ) in these simulation. The results clearly show that a decreasing distance  $y_0$  causes

an increasing angle of deformation of the bars (Fig. 5.4). In the top pictures the steady state deformation of the block elements is shown (cp. Fig. 5.4 a). The subjacent plots show the angle of deformation  $\varphi(t)$  of the block elements (cp. Fig. 5.4 b). The negative deflection at the beginning of the simulation (which can be found on every of the following pictures) is caused by the off-centre force application of the normal force (cp. Fig. 5.4, marked with an arrow).

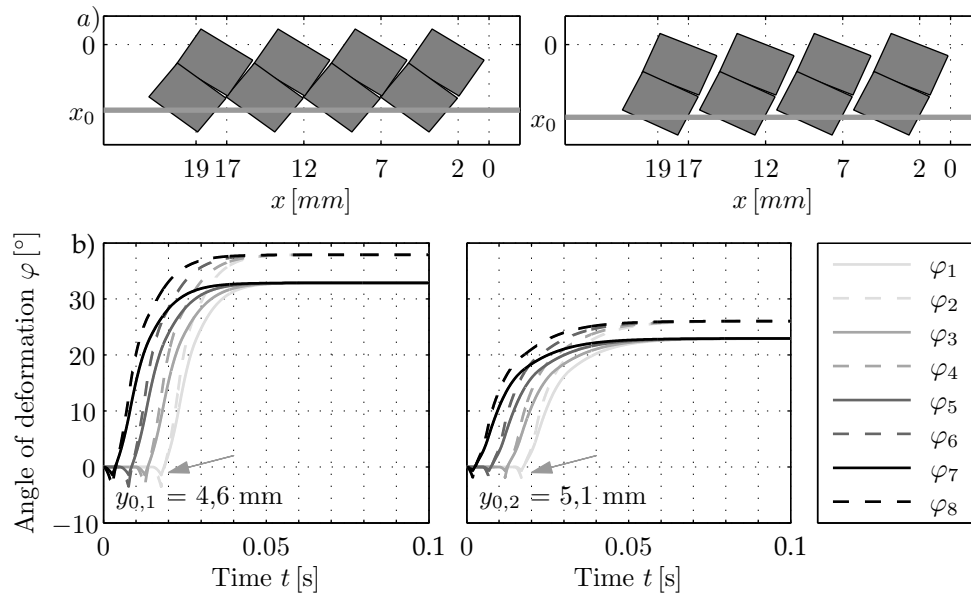


**Figure 5.4:** Variation of preload (Sliding velocity  $v = 5 \frac{\text{m}}{\text{s}}$ ): a) Steady state deformation of the block elements, b) Time depending angle of deformation of the single block elements (According to [97])

A second simulation has been done by the variation of the sliding velocity (Fig. 5.5). The distance was set to  $y_0 = 5,1 \text{ mm}$  and the velocity was set to  $v_{0,1} = 1 \frac{\text{m}}{\text{s}}$  and  $v_{0,2} = 5 \frac{\text{m}}{\text{s}}$ . Comparing both results it can be observed that the angle of deformation depends on the sliding velocity. This behaviour is caused by the friction characteristic (Fig. 5.2) where every sliding velocity is related to another coefficient of friction resulting in different deflection angles after reaching the steady state. Particularly at the lower sliding velocity of  $v_1 = 1 \frac{\text{m}}{\text{s}}$  it can be seen that each block element needs a certain time delay until the deflection starts. Hence, a higher sliding speed  $v_0$  leads to a faster displacement response. However, in this configuration the deformation of the block elements is equal for a certain velocity because the friction between the single elements is neglected ( $R_{S_i} = 0$ ). The normal contact has been considered in the simulation.

### 5.1.2.3 Investigation of instationary sliding motion

Instationary conditions prevail while the tire tread block passes the footprint. Contact pressure, sliding velocity and block deformation change permanently as well as the state of slip. An important advantage of the presented analytical tread block model is the short computing time. Particularly its features with respect to the calculation of transient operations of motion have to be emphasized. The ability of the presented model to perform

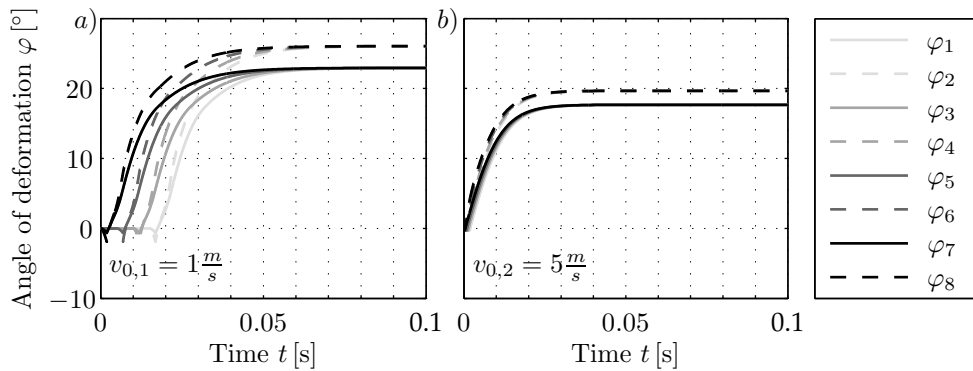


**Figure 5.5:** Variation of sliding velocity  $v$ , distance  $y_0 = 5,1$  mm (According to [97])

simulations in highly dynamical conditions is demonstrated by a simulation of sliding on a rough surface and with a velocity step during the sliding process. In both cases the deflection angles of each block element were calculated. In a first step a rough surface is crossed by the tread block to consider the models behaviour under dynamical conditions. The surface roughness has been transformed into a corresponding distance function  $y_0(t)$ . The surface data [33] was recorded from a concrete surface patch with the band projection method. The single asperities of the concrete surface can clearly be seen (cp. Fig. 5.6, bottom). For the simulation the surface profile has been passed two times. After the simulation starts, the single block elements become deflected one after another by the first bump. The second deflection of the single elements by the same bump is slightly higher due to the system dynamics.

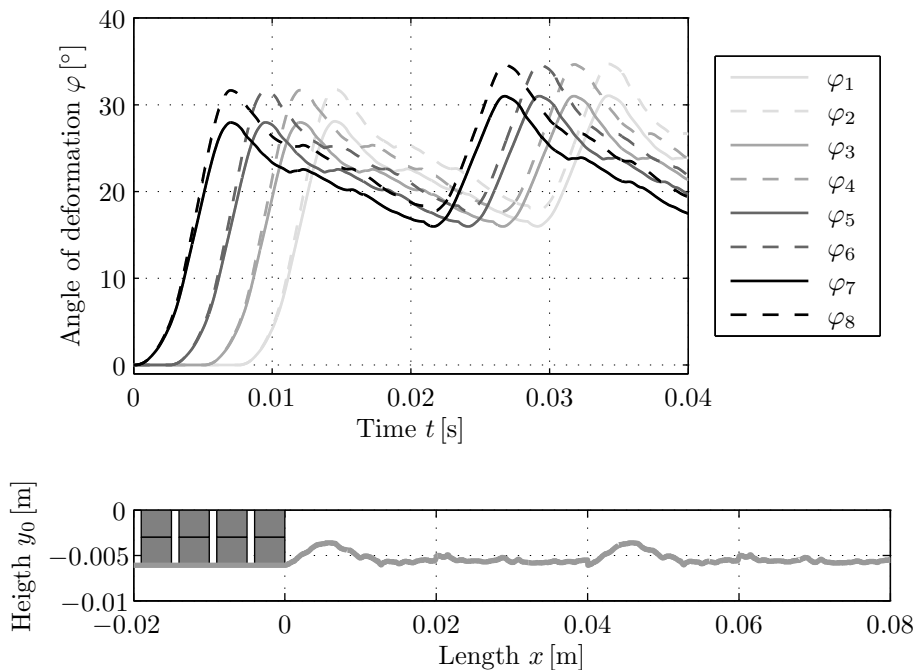


**Figure 5.6:** Siped tread block model crossing a rough surface

In order to demonstrate the flexibility of the presented model concerning the advantages of computing highly dynamical processes, the model's answer to a velocity step during the simulation process was investigated. Therefore, the tread block was accelerated to a

sliding velocity  $v_1$ . After a time of  $t_1 = 0,2$  s the block was then accelerated to a higher velocity  $v_2 > v_1$ . The angle of deflection of the block elements decreased due to the velocity depending friction characteristic (Fig. 5.7, center). In order to experimentally validate the simulation model, the high speed linear test rig "HiLiTe" (cp. Chapter 4.2) was equipped with a high speed camera to observe the deformation of the block elements (Fig. 5.7, top). It was observed that the higher velocity resulted in smaller deflection angles in the experiment. The results of the measurements are marked with "x" (Fig. 5.7, center). Compared to the simulation a very good agreement for the steady state but also for the transient time can be observed. This excellent correlation between measurement and simulation was achieved by the implementation of a time dependence of the friction coefficient as LINDNER did [70]:

$$\tau\mu_R + \dot{\mu}_R = \mu(v_{\text{rel}}). \quad (5.12)$$

The time dependence of the friction coefficient has been implemented in the model due to the large gain of model result accuracy. Without the time dependence of the friction coefficient as shown in Equation 5.12 the simulation result of the tread block deformation at higher sliding velocities was too small. Equation 5.12 results in a time delay of the simulation result as it can be observed in rubber friction. The time constant  $\tau$  (cp. Equation 5.12) is identified with the help of experiments. It strongly depends on the rubber compound. The time dependence of the tread block bending during the velocity step can be explained by considering the contact area in the friction experiment. The time delay of the friction coefficient is caused by the changing contact situation and temperature distribution due to the changing sliding velocity. The stationary level is reached again if the temperature distribution is homogenized again. Concluding the observations of measurement and simulation it can be said that an increasing sliding velocity decreases the steady state deformation angle due to the implemented friction characteristic.

Summarizing both simulation results, it can be said that the presented model was capable to model the instationary behaviour of a siped tire tread block. The introduced model can be used to simulate instationary sliding but the overall deformation shape is still not described sufficiently by the rigid body elements. A more detailed consideration of the deformation shape would require more rigid body elements resulting in a further increase of model complexity. A second even more important drawback is that the shape of the contact area cannot be described and that the transformation of material parameters like modulus of elasticity to the corresponding torsional spring and damper properties of the rigid body system is difficult (cp. Chapter 5.4).

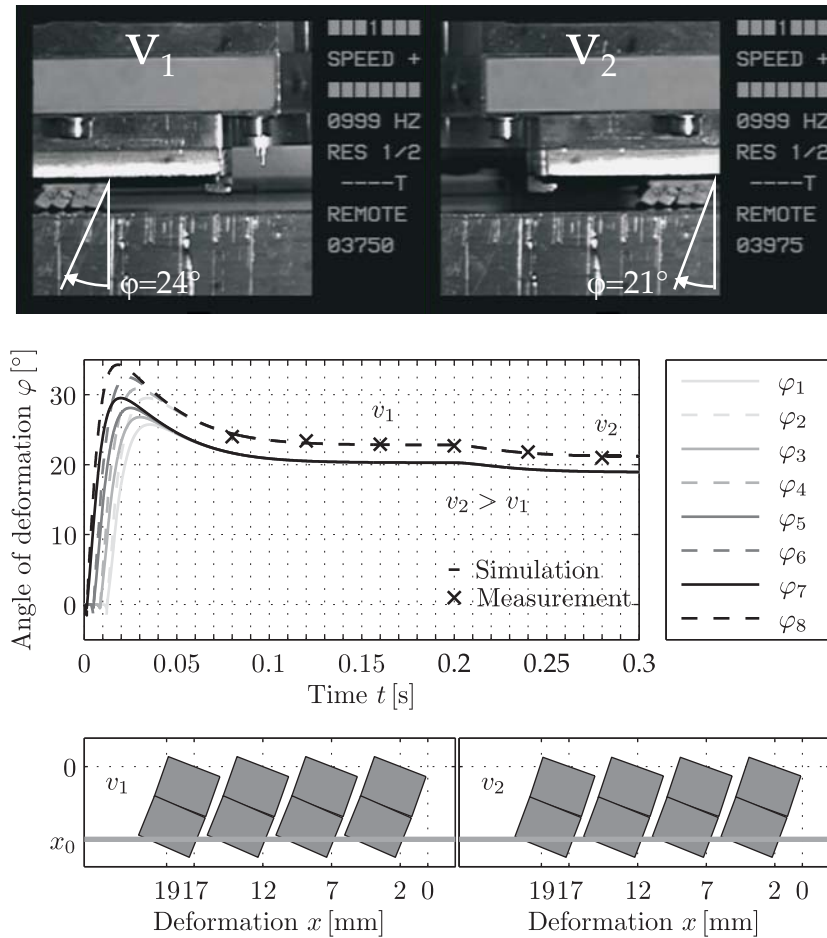


**Figure 5.7:** Measurement and simulation of instationary sliding: A velocity step during the friction process [97]

## 5.2 Approximation of a siped tire tread block with the beam model of EULER and BERNOULLI

The rigid body system delivers satisfying results, but it does not describe the shape of a deformed siped tire tread block element very well. A better approximation can be reached with a continuous approximation, e.g. a beam model. This would also allow to directly use both elasticity and shear modulus in the simulation and thus get rid of the parameter identification for the discrete MDOF system model. The implementation of new material parameters can then be done without complex fitting procedures. Furthermore, the usage of "real material parameters" helps to increase the acceptance of the model and its simulation results. A first approach for approximating the tire tread block elements as a beam can be done with the EULER-BERNOULLI beam theory.

Within the next chapter the EULER-BERNOULLI beam theory is analyzed with regard to its application to a tread block element. Therefore, the potential of the EULER-BERNOULLI beam theory is considered in detail. The differential equation describing the EULER-BERNOULLI beam and the derivation of the equation can be found e.g. in [36] or [43].



This theory considers the deflection which causes a displacement  $w$  at the end of the beam  $w(d)$  (Fig. 5.8 a). It is assumed that the cross section area of the beam is always rectangular to the middle axis. In case of a tread block element, normal and friction forces have to be implemented. The EULER-BERNOULLI beam theory considers forces acting on the neutral axis (Fig. 5.8 b). Observing the deformation shape of a sliding tread block during a friction experiment on HiLiTe (Fig. 5.8 c), it can be seen that predominantly the front edges of the block elements are in contact with the surface. That means that normal and friction force should act at the front edge of the block element in order to model a realistic behaviour (Fig. 5.8 b).

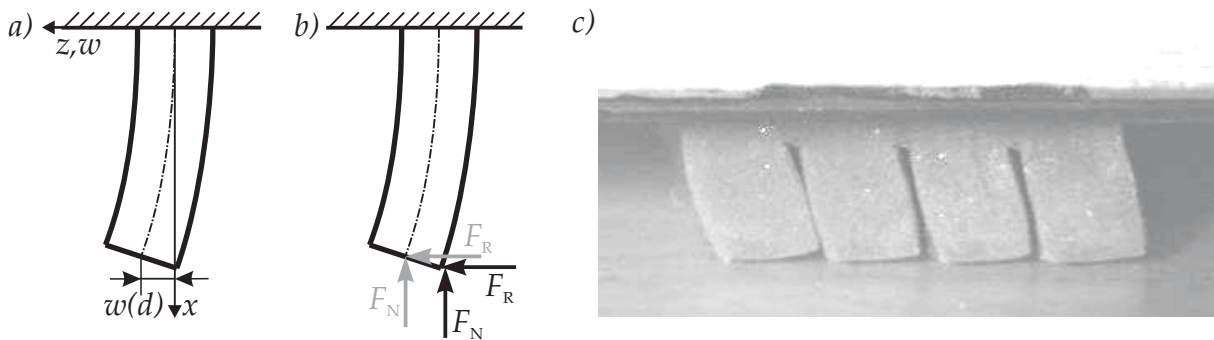


**Figure 5.8:** a) Nomenclature of EULER-BERNOULLI beam, b) Normal and friction force application points at the beam model, c) Side view on the deformation shape of a sliding tire tread block sample on ice during HiLiTe measurement

A serious limitation of the EULER-BERNOULLI beam theory is that the ratio of depth  $d$  to length  $\ell$  of the beam has to be small (For nomenclature cp. Fig. 4.4 d). Depending on the order numbers of natural frequencies  $k$  considered in the simulation, the geometrical parameters should satisfy:

$$\frac{d}{\ell} > 5k \quad [43]. \quad (5.13)$$

Using the first fundamental frequency ( $k = 1$ ) the ratio of depth  $d$  to length  $\ell$  should not be smaller than five. Keeping this fact in mind, the EULER-BERNOULLI beam theory can be used for long block elements with small cross-section area only. The ratio of depth  $d$  to length  $\ell$  calculated with realistic geometrical data of a tire tread block element is in the order of  $\frac{d}{\ell} = \frac{4}{3}$  (cp. Fig 1.2 and Fig. 4.4 b).

First investigations on the behaviour of the EULER-BERNOULLI beam model applied to tire tread blocks have been done by RIPKA and WANGENHEIM [100]. Here, the beam model was introduced and the influence of the number of eigenmodes used on the simulation result was investigated. Summarizing these simulation results and the aforementioned discussion, it can be concluded that the EULER-BERNOULLI beam delivers no advantages compared to the rigid body system due to its geometrical limitations. The deformation shape cannot be displayed in a sufficient way either because it not only comprises bending but also shear (cp. Fig. 5.8 c).

### 5.3 TIMOSHENKO beam model

The following section introduces the TIMOSHENKO beam theory (Fig. 5.9 a) for simulating a siped tire tread block. Its content is based on the publication of RIPKA et al. [102]. The focus is set on the evaluation of the models suitability and not on the detailed derivation of the TIMOSHENKO beam differential equations. Another example for TIMOSHENKO beam theory in tire application is the work of PINNINGTON who used TIMOSHENKO beams to model waves of the tire belt and the sidewalls. He got useable results [94], [93]. The TIMOSHENKO theory used in the following section has been taken from literature and adopted to the depicted tasks. Amongst other things different topics like axial forces on the beam [12], [115], different material laws including damping [57], [115], [128] and non linearity [115] are considered in the literature.

The TIMOSHENKO beam theory extends the EULER-BERNOULLI beam. It was introduced by S.P. TIMOSHENKO in 1921 [120]. HAGEDORN referred in [46] that this beam theory should be named according to BRESSE who declared the differential equations in a book in 1859, see [16]. Its first extension is that the assumption that the cross section area of the beam is always orthogonal to the beams neutral axis is abandoned. So shear deformation  $\gamma$  (Fig. 5.9 b) described by the inclination angle  $\varphi$  (Fig. 5.9 c) and the slope  $w'$  of the rotational inertia of the cross section area is considered. The TIMOSHENKO beam theory allows to investigate depth to length ratios of tread block elements

$$\frac{d}{\ell} > k [43] \quad (5.14)$$

which covers typical geometries of winter tires. Using the coordinates of Fig. 5.9 a-c, the differential equations of motion of the TIMOSHENKO beam are (cp. [43] and [36], Fig. 5.10):

$$\rho A \ddot{r} - A_K G (r'' + \varphi') = q \quad (5.15)$$

$$\rho I \ddot{\varphi} - EI \varphi'' + A_K G (r' + \varphi) = 0. \quad (5.16)$$

Thereby, the dots above variables display the differentiation in time and the dashes mark the differentiation in space coordinate  $x$ . The deflection  $r = r(x, t)$ , the inclination angle  $\varphi = \varphi(x, t)$  and the load  $q = q(x, t)$  depend on the space coordinate  $x$  and the time  $t$  (Fig. 5.10). The density of the beam  $\rho$ , Young's modulus  $E$  and shear modulus  $G = E/3$  (for rubber with Poisson's number  $\nu = 0,5$ , cp. [70]) are material constants. The parameter identification is described later on (cp. Chapter 5.4). The second moment of area  $I$  is

$$I = \frac{w \ell^3}{12} \quad (5.17)$$

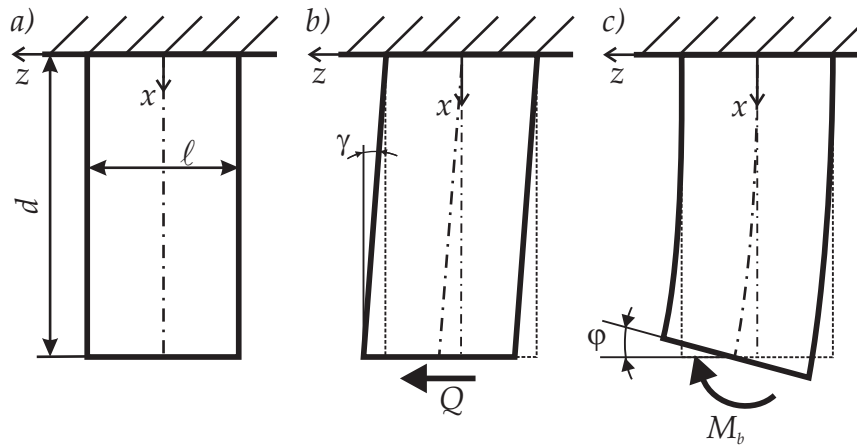


**Figure 5.9:** a) Free TIMOSHENKO beam with geometrical variables, b) Shear deformation of beam, c) Bending deformation of beam

and the equivalent cross-section for shear  $A_K$  is

$$A_K = \kappa A = \kappa w \ell \quad (5.18)$$

which depends on the cross section area  $A$  [42]. According to COWPER [21] shear coefficient  $\kappa$  can be calculated for a rectangular cross section to

$$\kappa = \frac{10(1 - \nu)}{12 + 11\nu} = \frac{6}{7} \quad (5.19)$$

with Poisson's number  $\nu = 0,5$  for rubber. Equation 5.15 and Equation 5.16 are partial differential equations (PDE). PDEs are generally solved numerically, analytical solutions exist for simple problems only. For a numerical solution the Finite Difference Method (FDM) can be used to eliminate the differentiations of space coordinate of the TIMOSHENKO beam equations. Afterwards the time depending differential equations can be solved with MATLAB/Simulink. Of course, other methods exist to solve partial differential equations which are more efficient. The FDM was chosen here because it can be applied to all elasto-mechanical problems [115] and the finite difference quotients can be transferred into code easily [102].

### 5.3.1 TIMOSHENKO beam model setup

A single tread block element will now be approximated with the TIMOSHENKO beam model in order to introduce and verify the new model setup, cp. RIPKA et al. [102].

The TIMOSHENKO beam model delivers new possibilities for the estimation of the contact area size due to the superposition of bending and shear deformation. Tread block elements often show a lift-off of the back part of the contact area during sliding which was observed

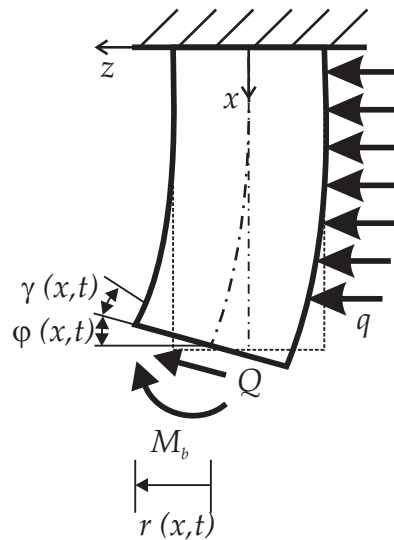


**Figure 5.10:** Overall nomenclature of the beam model

at HiLiTe experiments [99]. Additionally, LINDNER [70] described a pressure peak at the front edge of the sliding tread block element. This peak could be mainly observed on new samples. Transferring this knowledge to the tread block element model, an inhomogeneous pressure distribution over the cross sectional area at the end of the beam ( $x = d$ ) is introduced. Its maximum peak at the front edge of the block element decreases continuously over the contact area  $A_B$  (Fig 5.11 a). Due to friction in the contact the normal pressure distribution  $q_N$  causes frictional stress  $q_R$ .

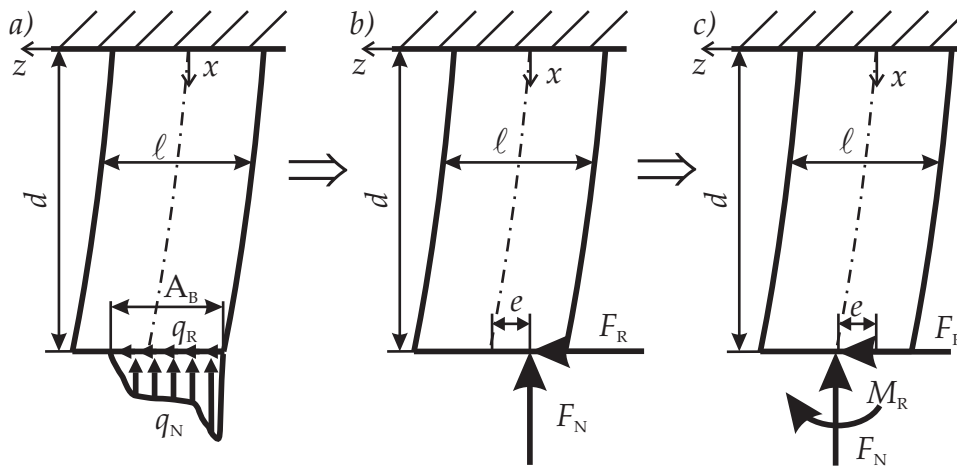


**Figure 5.11:** a) Load distribution under a single tread block element, b) Approximated load in the center of the contact area, c) Implementation of normal and friction force in the beam model (According to [102])

After visualizing the frictional stress in the contact area, this characteristic is implemented in the model. Thereby it has to be kept in mind that the TIMOSHENKO beam theory is one-dimensional. All variables considered in the theory depend on the space coordinate  $x$  and the time  $t$ . The stress distributions  $q_N$  and  $q_R$  are replaced by one representing, concentrated force each, acting in the balance point (Fig. 5.11 b) for a more simple handling

in the model. The distance between the force application point and the neutral axis of the beam is  $e$ . The integration of normal force  $F_N$  and friction force  $F_R$  in the differential equation of the beam is realized by transferring both forces to the neutral axis. According to GERE and TIMOSHENKO this can be done by adding the offset moment  $M_R$  to the middle axis of the beam [37] (Fig 5.11 c).

$$M_R = eN \quad (5.20)$$

Usually the global contact pressure can be calculated from normal load applied to the tread block. A description of the lever arm or excentricity  $e$  based on experiments is still difficult, although a promising approach for identifying contact area details has been presented (cp. Chapter 4.3.6). For giving a reliable description of the excentricity  $e$ , detailed parameter studies have to be done to describe the influencing factors in an adequate way. The lever arm characteristic is dominated by the normal load distribution and the deformation angle  $\varphi$ . Due to this, a first approximation of the lever arm  $e$  is done by a deformation angle  $\varphi$  depending characteristic

$$\varphi \geq 0 : e(t) = \frac{\ell}{4} - e_3 + \frac{1}{\pi} \arctan(-e_1 + e_2 \varphi(d, t)) \left( \frac{\ell}{2} - e_4 \right) \quad (5.21)$$

$$\varphi < 0 : e(t) = - \left[ \frac{\ell}{4} - e_3 + \frac{1}{\pi} \arctan(-e_1 + e_2 (-\varphi(d, t))) \left( \frac{\ell}{2} - e_4 \right) \right] \quad (5.22)$$

The contact point of the normal force cannot be outside the contact area (cp. Figure 5.11 b) which results in the boundary condition  $e_{\max} = \pm \frac{\ell}{2}$ . Based on this limitation the constant parameters  $e_1$ ,  $e_2$ ,  $e_3$  and  $e_4$  can be found. The first characteristic of the lever arm  $e$  was set to  $e \approx 0$  for bending angles up to  $\varphi = \pm 10^\circ$  (cp. Fig. 5.12 a). Angles larger than  $\varphi = \pm 40^\circ$  result in a constant excentricity of  $e \approx 1.9$  mm as depicted in (Fig. 5.12 a).

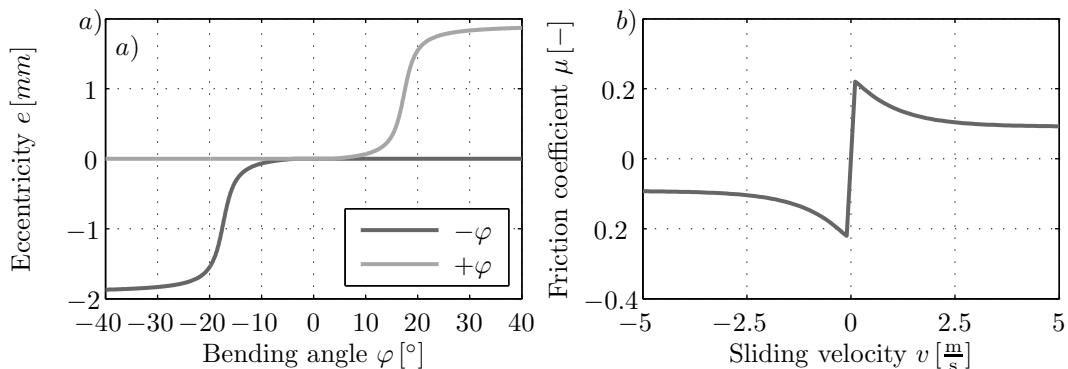


**Figure 5.12:** a) Characteristic of lever arm  $e$ , b) Friction characteristic depending on sliding velocity (According to [102])

In a first step it is assumed that temperature  $T$  and normal pressure  $p$  do not influence the friction coefficient. So the friction characteristic implemented in the model still depends

on the sliding velocity only (cp. Chapter 5.1.1). The friction force is again calculated via the COULOMB model

The relative sliding velocity  $v_{\text{rel}}$  is calculated via the difference of the absolute sliding speed  $v_0(t)$  (which corresponds to the vehicle velocity, sometimes time dependent) and the velocity of the bending deformation at the end of the block element  $\dot{\varphi}(d, t)$

$$v_{\text{rel}} = v_0(t) - \dot{\varphi}(d, t) \quad (5.23)$$

Additionally, the friction characteristic is expanded to negative sliding velocities. They are needed to display stick slip vibrations which are shown for model validation purposes (cp. Chapter 5.3.2). In general, other friction influencing factors like e.g. normal force  $F_N$  and temperature  $T$  can also be implemented in the friction characteristic. It can for example be fitted as follows [74] (Fig. 5.12 b):

$$\mu(v) = \left( k_1 + k_2 e^{(k_3 |v|)} \right) \frac{2}{\pi} \arctan(k_4 v). \quad (5.24)$$

The constants  $k_1, k_2, k_3$  and  $k_4$  are adjusted for different tire tread block surface combinations based on measurements. One limitation of this fitting approach (Equation 5.24) is the zero crossing at sliding velocities equal to zero  $v_{\text{fit}}(0) = 0$  (Fig. 5.12 b). Normally the friction coefficient reaches its maximum at sliding velocities equal to zero due to the static friction  $v_{\text{real}}(0) = \text{max}$ . This limitation is accepted because the change of the direction of the sliding velocity can be computed as it is shown later. The description of the load of the block element, as it can be used by the beam theory, has already been defined (Fig. 5.11 a-c).

In the following step all loads and properties of the block element are implemented in the differential equations of the beam (Equation 5.15 and Equation 5.16). The damping properties of the rubber are modelled as proposed by WAUER [128], and the axial force is implemented as suggested by BISHOP and PRICE [12]. The partial differential equations of motion then are as follows:

$$\varrho A \ddot{r} - A_K G [k_i (\dot{r}'' + \dot{\varphi}') + (r'' + \varphi')] - N \varphi' = q = 0, \quad (5.25)$$

$$\varrho I \ddot{\varphi} - EI [k_i \dot{\varphi}'' + \varphi''] + A_K G [k_i (\dot{r}' + \dot{\varphi}) + (r' + \varphi)] - N (r' + \varphi) = 0. \quad (5.26)$$

The parameter  $k_i$  describes velocity proportional damping of the beam. The surface load  $q$  is set equal to zero. In a later version it can be used to consider the contact between two neighbouring block elements or to simulate the presence of another material in the sipe. The boundary conditions of the beam are as follows:

$$r(0, t) = \varphi(0, t) = 0 \quad (5.27)$$

for the clamped end of the beam and

$$EI(k_i \dot{\varphi}'(d, t) + \varphi'(d, t)) = M_R(t) \quad (5.28)$$

$$A_K G(k_i [\dot{r}'(d, t) + \dot{\varphi}(d, t)] + r'(d, t) + \varphi(d, t)) = R(t) \quad (5.29)$$

at the free end of the beam. For the numerical simulations the initial conditions were chosen as:

$$r(x, t = 0) = \varphi(x, t = 0) = \dot{r}(x, t = 0) = \dot{\varphi}(x, t = 0) = 0 \quad (5.30)$$

They correspond to those of the measuring process during the friction experiments with HiLiTe (cp. Section 4.2). In a first step the sample is loaded with the normal force  $F_N$ . Afterwards it is accelerated to the required sliding velocity.

The space derivatives of  $r$  and  $\varphi$  in Equation 5.25 to Equation 5.30 are approximated using the FDM. The resulting ordinary differential equations are solved with the help of MATLAB/Simulink afterwards. In the beginning the influence of different sliding velocities on the model behaviour are analyzed (Fig. 5.13). The block elements deflection  $r_s(x = \ell)$  has been calculated for three different sliding velocities in order to get a basic impression of the velocity influence (cp. Fig. 5.12 b). From the theoretical point of view it is expected that increasing velocities result in a smaller friction coefficient because of the friction characteristic (cp. Fig. 5.12 b). The result is a smaller deflection of the tread block elements. Considering the simulation results (Fig. 5.13), the theoretical expectations are achieved: A larger sliding velocity corresponds to a smaller deformation of the block element. Additionally, an overshoot is observed in the beginning of each simulation which is caused by the acceleration of the block element until the steady state of the elements deflection is reached. The slower sliding velocities show a higher maximum peak because of the higher friction values. The computational effort for such a simulation is very small. It takes only a few seconds of computation time.

### 5.3.2 Validation of the TIMOSHENKO beam model

The validation of the presented model approach is done again with the help of a HiLiTe measurement (see also Chapter 5.2, Fig. 5.8). Therefore, a sliding tread block was monitored with a high speed camera (cp. Fig. 5.14). A detailed analysis of the image shows that the deflection  $r_m$  of one tread block element (while sliding with constant velocity  $v = 1 \frac{\text{m}}{\text{s}}$ ) is

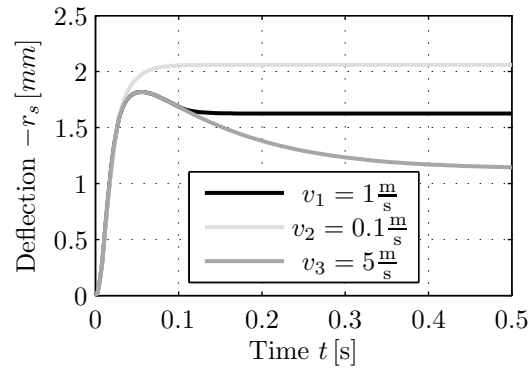


**Figure 5.13:** Influence of different sliding velocities on the simulation result of TIMOSHENKO beam model

$r_m = 1,6$  mm. The angle of deformation of the block element can be determined to approx.  $\alpha_m = 18^\circ$ . Under certain parameter conditions a clear squealing could be heard during the measurements. In these cases the high speed camera film showed a stick slip vibration of the tread block elements. Its frequency was determined to  $f = 1500$  Hz. The occurrence of the stick slip effect strongly depended on the material and test parameters.



**Figure 5.14:** Deformation shape of siped tire tread block sliding on ice, captured with a high speed camera during a friction experiment with HiLiTe

This experimental data has been used for the validation of the simulation model. For a sliding velocity of  $v = 1 \frac{\text{m}}{\text{s}}$  measurement (Fig. 5.14) and simulation (Fig. 5.13) reach the same stationary deflection value  $r_s = r_m = 1.6$  mm at the end of the maneuver. Also the angle of deformation shows good agreement between measurement (Fig. 5.14) and simulation (Fig. 5.15:  $\alpha_s(d = 6 \text{ mm}) = 18.1^\circ$ ). An advantage of the simulation is that bending  $\varphi_s$  and shear deformation  $\gamma_s$  can be separated easily.

It can be observed that the bending part of the deformation clearly increases along the block element length ( $d \rightarrow 6$  mm), while the shear part of the overall deformation sees a slight decrease (cp. Figure 5.15), [102]. The bending angle increases from  $\varphi_s(d = 0) = 0^\circ$  at the fixing of the beam to  $\varphi_s(d = 6 \text{ mm}) \approx 14^\circ$  at the free end. Further simulations show that the influence of bending deformation increases with increasing block element depth as has been expected.

The stationary simulations have been validated in depth and the model can be considered to give a good description of the stationary states of sliding. The measurements already



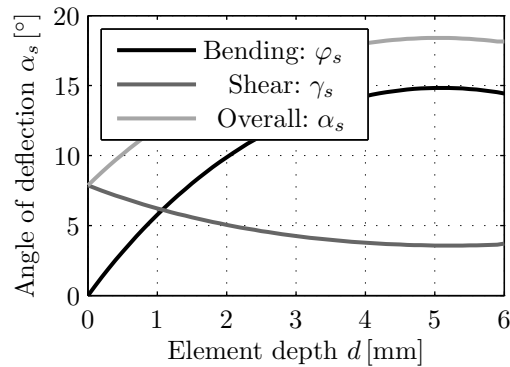


**Figure 5.15:** Shear( $\gamma$ ) and bending ( $\varphi$ ) deformation and slope of beam deflection ( $\alpha$ ) (According to [102])

shown have been done with rubber-like material parameters and similar tread block element geometries but no vibration could be observed for this parameter combination. In order to study the models dynamical behaviour, it was also investigated whether it can be used to describe the experimentally observed instationary friction phenomena like stick-slip vibrations also. Therefore the damping constant  $k_i$  as well as the modulus of elasticity  $E$  have been matched to values such that a stick slip vibration could be observed (Fig 5.16). After reaching a certain deformation level, the model shows a constant stick-slip vibration (Fig. 5.16 a). The deflection is  $r_s = 0,625$  mm and the frequency can be determined to  $f_{\text{sim}} = 1111$  Hz, (Fig. 5.16 b). A difference exists between measurement and simulation which might be due to the fact that the deformation behaviour of the tread block element is inhomogenous. The front edge of the tread block element is curved (cp. Fig. 5.16 d) during the friction measurement. The simulation result is calculated for the middle part (cp. Fig. 5.16 d, "Sim") and the measurement is evaluated at the boundary area (cp. Fig. 5.16 d, "Meas") which influences the result due to boundary effects. Additionally, it is unknown if the whole block element oscillates or if the vibration is limited to the boundary area. There are also serious challenges in the measurement evaluation. The differences between measurement and simulation can be caused from the limited possibilities of evaluating the result of the friction experiment. The observation of the sliding tire tread block with a 3D laser vibrometer can help to improve the accuracy of the measurement result. Additionally, the experimental results spread in a certain range as well because it is difficult to prepare different test tracks with similar properties (cp. Chapter 4.2 and RIPKA et al. [101]). Furthermore, new evaluation methods have to be found for getting the chance to increase the accuracy of model validations with experiments. Due to these differences, the results of experiment and simulation will never be exactly the same because such specific details cannot be considered in a simulation model. Nevertheless, it can be concluded that the TIMOSHENKO theory is suitable for simulating a stick slip vibration of a sliding tire tread block.

The following points of the tread block model still can be improved: 1) It is known that the Young's modulus of rubber is frequency dependent. This has not yet been taken into account in the model. 2) The rubber friction depends on normal load and temperature.

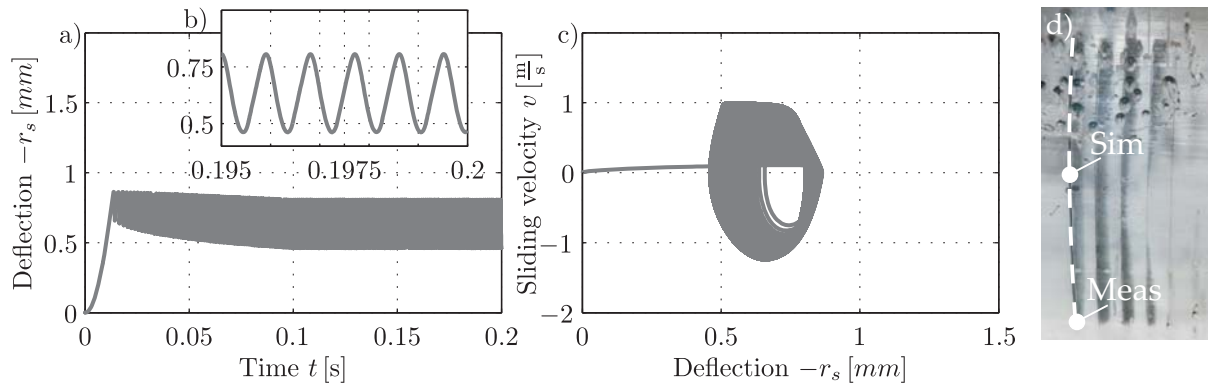


**Figure 5.16:** Stick-slip vibration of the tread block model, a) Time depending beam deflection, b) Stick-slip vibration in detail, c) Limit cycle of stick-slip vibration, d) Contact area of sliding tire tread block with three sipes: Location of measurement evaluation point (Meas) and simulation result (Sim)

These dependencies should be implemented in the friction characteristic in the future. 3) The linearity assumptions in the TIMOSHENKO theory are valid for small deformations while an angle of  $\alpha_s = 18^\circ$  clearly violates these assumptions.

## 5.4 Parameter identification for the tread block models

In general, the initial values for spring and damping constants can be found by evaluating free oscillations. Therefore, the tread block element is deflected and the vibration which occurs after sudden release is measured with a laser vibrometer. The dynamic properties of the tread block element can be determined by exciting the block element with a shaker. The frequency sweep performed with this configuration yields a transfer function. The same frequency sweep is done with the tread block model, and parameters for mass, spring and damping constants are identified. Further methods concerning the identification of mechanical properties of nonlinear multiple DOF systems were investigated by BRUNS [18]. Details of the aforementioned method can be found in [18] as well.

## 6 Conclusion and Outlook

The tire road contact gains more and more attention due to safety reasons. Especially in winterly road conditions the accident probability is very high because of low friction. The usage of winter tires can significantly reduce the risk of accidents due to its optimized performance regarding snow and ice. For an ongoing improvement of winter tires a targeted development is necessary. In this process, friction plays an important role. If the friction phenomena are well known, they can be applied systematically for further improvement of the tire performance. So the research and the understanding of the rubber-ice friction mechanisms are a key for future tire technology. Within the present thesis the rubber-ice friction was investigated in detail. A literature review pointed out the already existing theories and measurements on ice friction phenomena but it has also shown the open gaps. Up to now it is not clearly clarified if pressure melting contributes to the generation of the liquid layer or not. Additionally, it is also unknown if the water layer captures the whole contact or if dry and wet spots prevail. After a discussion of the present state of knowledge the aim of this thesis has been pointed out with the help of five hypotheses. Furthermore additional investigations have been done to explain the tread block friction mechanisms with a phenomenological model. Different approaches have been shown which can be used for simulating sliding siped tire tread blocks.

The high speed linear test rig HiLiTe was built to investigate tire tread block friction on arbitrary surfaces in a wide parameter range. It adopts the sliding movement of the single tread blocks which can also be observed in the tire road contact during the passage of the footprint. HiLiTe is located in a climate chamber. Hence, friction measurements can be done on icy surfaces as well. The test rig was validated against comprehensive vehicle test results. It has been shown that rubber compound effects, but also the influence of the tread block geometry, can be studied with HiLiTe. Additionally, basics on the preparation of icy test tracks has been illustrated. The measurement and the evaluation method have been pointed out.

Due to the varying range of sliding velocities and normal loads which occur in the tire footprint during an ABS braking maneuver the experiments with HiLiTe had also been done in a wide parameter field. In a first step the velocity and normal load dependency of sliding tire tread blocks has been investigated: An increasing sliding velocity or normal load resulted in a decreasing friction characteristic. The same behaviour could be observed for an increasing ambient temperature. A common research hypothesis is that the domi-

nating factor in the rubber-ice friction is the frictional power or frictional heat. The heat caused by the friction process melts the ice. Due to the coefficient of heat conductivity of rubber and ice most of the energy enters the ice. The ice melts (depending on the ambient temperature) and the melt water layer on the ice surface grows, while the overall friction decreases. An increasing humidity and temperature also influences the friction process: More water molecules condensate and evaporate which increases the height of the initial water layer on the ice surface.

The influence of tread block length and tread block inclination angle can be explained by a variation of the local pressure and the amount of friction potential, respectively the maximum available friction force. On the one hand the local contact area is reduced which increases the local pressure. The result is loss of friction due to the strong pressure dependency of the friction coefficient. On the other hand only a certain limit of friction forces can be reached. A further raise of the normal load (at constant friction force) results again in a reduced friction coefficient. The presented friction measurements lead to the hypothesis that the friction coefficient cannot fall below a certain limit at the steady state.

The identification of the real contact area between tire tread block and ice plays an important role. Its size is important for a detailed understanding of the friction mechanisms. Additionally, the footprint size is required for analytical and FE models to calculate the rubber-ice friction. The present thesis introduced an approach which allows the identification of the real contact area of sliding tire tread blocks on ice. The total internal reflection of light beams in the system allows a reliable identification of the footprint area. Based on the contact area measurements of sliding tire tread blocks on ice it is determined that pressure melting has no influence on the rubber-ice friction. The pressure increase on the macroscopic scale is much too small. In the future it is recommended to investigate the rubber-ice contact on the microscopic scale for getting a more detailed impression of the contact phenomena. Note that this method for identifying real contact areas is not limited to tire tread blocks. With some modifications it can also be used to identify the local contact of rolling tires on ice. However, a basic requirement is the existence of clear ice.

The tire tread block ice friction is dominated by the dry run-in area at the leading edge which is followed by a wet contact part. Parameters like sliding velocity, normal load, temperature and humidity influence its length which strongly affects the rubber-ice friction characteristic. The frictional heat melts the ice which results in the reduction of the dry run-in area and therefore in a reduction of the transferrable friction. Additionally, a viscous friction part can sometimes be observed which occurs if a certain ratio between dry and wet contact area size is exceeded. The viscous forces are caused by the shear of the surface water layer which is strongly connected to the ice surface. Depending on the boundary conditions, the viscous friction results in an increasing friction coefficient with increasing sliding velocity or the appearance of a minimum in the friction characteristic.

Besides the rubber the ice also influences the friction process. So the impact of ice impurities on the friction process has been investigated. The impurities shift the melting point of the

ice which results in a change of the water layer properties. Thus, the friction process is affected. Additionally, an influence of the ice grain size on the friction coefficient could be shown as well. An identification of this parameter could be interesting for understanding different test results from outdoor vehicle tests. Probably different ice grain structures exist on the proving grounds depending on their nature. It is expected that test tracks prepared on a lake show larger grains due to the slow freezing process. The ice starts growing as single nucleus which rises until they become integrated in the ice surface. The water freezing process of land tracks starts on many more points due to the cold surface. This results in a structure of small ice grains. The ice grain formation can be visualized with polarized light. Different friction coefficients have been found depending on the single ice grain sizes. However, no clear trend was observed although ambient temperature, humidity and samples have been kept constant. Maybe additional factors exist which influence the rubber-ice friction and which are unknown up to now. It can be concluded that the explanation as well as the proof of the influence of the grain boundaries on the rubber-ice friction process is far away from being completed. More research work has to be done in the future to identify the influence of the ice properties on the friction process.

Different analytical models have been presented for simulating a siped tire tread block. Basic studies have been done on a single mass oscillator. It was expanded to a 2-DOF system to display the tread block deformation in a better way. The model considers the material properties like damping and elasticity as well as the interaction between the single block elements. The surface properties are implemented in the model with the help of a velocity depending friction characteristic. It can be extended with additional dependencies like normal load and ambient temperature. Basic influences like sliding velocity dependency as well as the tread block-surface and the tread block-tread block contact operate very well. The 2-DOF model can display velocity steps during the simulation. Due to the implementation of the time depending friction coefficient, simulation and measurement fit together very well. The tread block model can also slide on a rough surface. It allows the study of the interaction of the single block elements. The EULER-BERNOULLI beam theory has been used to simulate a siped tire tread block, but due to its geometrical limitation it is not suitable for this task. The TIMOSHENKO beam theory considers bending and shear deformation. Both parts could be observed during the friction measurements of sliding tire tread blocks. The model also considers normal and friction force. The contact between single beams was included as well. Additionally, a damping term was implemented in a way that is recommended by literature. The beam equations have been solved with the finite difference method. First simulations which have been done with the TIMOSHENKO beam model show a very good agreement with HiLiTe measurements. Deflection and deformation angle fit very well to the values gained from the experiment. It has been shown that the beam model can also display transient behaviour. A stick slip vibration which has been observed during the measurements with HiLiTe can be modeled. Although the measurement and simulation result of the stick slip vibration do not fit together very well the results achieved with the TIMOSHENKO beam model seems to be promising for studying basic tread block friction mechanisms. It can be concluded that the

presented model gives the possibility to investigate the tread block road interaction with low computational effort and sufficient accuracy for stationary simulations. Judging the accuracy of the instationary simulation results requires a more detailed evaluation of the measurements.

For future tire development and tire tests it is recommended that ambient temperature and humidity should be controlled due to their high impact on the friction process. A large gain on rubber-ice friction could be realized by activating the shear of the water layer in the tire road contact. Therefore, further investigations on the tire footprint are necessary especially on the microscopic scale. Additionally, the evaluation of the contact area shall be improved to ensure a correct analysis of its size. The ice-tread block contact should be investigated in more depth to verify the friction model. What happens to the contact area size in case of an increasing friction coefficient? Besides this, the influence of other factors on the rubber-ice friction shall be checked. What is the influence of the sipe length? Does the water layer refreeze within the sipe? Is it possible to find a parameter combination which characterizes the ice to allow the comparison of friction measurements from different ice surfaces without the need of a reference sample? The model activity shall be focused on the expansion of the TIMOSHENKO beam model to investigate siped tire tread blocks. The friction characteristic can be extended by a pressure and temperature dependency. The interaction between block element and surface can be displayed in a more detailed way by implementing a thermodynamical model into the contact by calculating the frictional heat. Additionally, a temperature dependency of the friction characteristic has to be implemented to consider the different states of frictional heat in the friction coefficient. The model accuracy can be raised by considering a frequency depending Young's modulus. This is important with regard to the simulation of unsteady motions like stick slip phenomena.

In spite of all ice research its results and the friction theories, it has to be kept in mind that a tire needs to be optimized for every surface condition. The target conflicts cannot be neglected as they significantly change the tire development focus. The mechanisms which yield to good snow traction, confident wet braking, excellent dry handling and the environmental friendliness also have to be kept in mind.

## Bibliography

- [1] § 2 Abs. 3 a StVO (*Strassenverkehrsordnung*), in German
- [2] ACKERMANN, S. A. ; KNOX, J. A.: *Meteorology: Understanding the Atmosphere*. Thomson Brooks/Cole, 2007
- [3] ALBRACHT, F. ; REICHEL, S. ; WINKLER, V. ; KERN, H.: Untersuchung von Einflussfaktoren auf das tribologische Verhalten von Werkstoffen gegen Eis. In: *Materialwissenschaft und Werkstofftechnik* (2004, in German), S. 620–625
- [4] ANDRLE, S. J. ; KROEGER, D. ; GIESEMANN, D. ; BURDINE, N.: Highway Maintenance Concept Vehicle / Final Report Phase Four, Centre for Transportation Research and Education, Iowa State University. 2002
- [5] AUSTRELL, P. E.: *Modeling of Elasticity and Damping for filled Elastomers*, Lund University, Sweden, Lund Institute of Technology, Diss., 1997
- [6] BACHMANN, T.: *Literaturrecherche zum Reibwert zwischen Reifen und Fahrbahn*. VDI Fortschritt-Berichte, Reihe 12, Verkehrstechnik/Fahrzeugtechnik, Nr. 286, 1996, in German
- [7] BACHMANN, T.: *Wechselwirkungen im Prozess der Reibung zwischen Reifen und Fahrbahn*. Dissertation, in VDI Fortschritt-Berichte, Reihe 12, Verkehrstechnik/Fahrzeugtechnik, Nr. 360, 1998, in German
- [8] BÄURLE, L.: *Sliding Friction of Polyethylene on Snow and Ice*. L. Bäurle, Swiss Federal Institute of Technology Zurich, Diss., 2006
- [9] BÄURLE, L. ; KAEMPFER, U. ; SZABO, D. ; SPENCER, N.D.: Sliding Friction of Polyethylene on Snow and Ice: Contact Area and Modeling. In: *Cold Regions Science and Technology* 47 (2007), S. 276–289
- [10] BÄURLE, L. ; SZABO, D. ; FAUVRE, M. ; RHYMER, H. ; SPENCER, N.D.: Sliding Friction of Polyethylene on Ice: Tribometer Measurements. In: *Tribology Letters* Vol. 24 (2006), Nr. 1, S. 77–84
- [11] BECKER, R.: *Verfahren und Vorrichtung zum Erfassen eines Druckes*. Patent DE 10 2004 055 701 A1, 2006, in German
- [12] BISHOP, R.E.D. ; PRICE, W.G.: The Vibration Characteristics of a Beam with an Axial Force. In: *Journal of Sound and Vibration* Vol. 59, No. 2 (1978), S. 237–244

- [13] BLOK, H.: Theoretical Study of Temperature Rise at Surface of Actual Contact under Oiliness Lubricating Conditions. In: *Proc. Gen. Disc. Lubricationa and Lubricants 2*, Inst. Mech. Eng., London (1937), S. 222–235
- [14] BOLZ, G.: *Entwicklung eines Prüfverfahrens für Reifenmessungen auf Schnee im Labor*. PhD thesis, Shaker Verlag, Aachen, 2006, in German
- [15] BOWDEN, F.P. ; HUGHES, T.P.: The Mechanism of Sliding on Ice and Snow. In: *Proceedings of the Royal Society of London* Vol. 172, No. 949 (1939), S. 280–298
- [16] BRESSE, M.: *Cours de Mécanique Appliquée*. Imprimerie de Mallet-Bachelier, 1859
- [17] BROWNE, A.L. ; HAYS, D.F. (Hrsg.): *Tire Traction on Snow-Covered Pavements*. Plenum Press, New York - London, The physics of tire traction - Theory and Experiment 1974. – 99–139 S
- [18] BRUNS, J.-U.: *Detektion und Identifikation von Nichtlinearitäten in mechanischen Schwingungssystemen*. Dissertation, in VDI Fortschritt-Berichte, Reihe 11, Schwingungstechnik, Nr. 324, 2004, in German
- [19] CLARK, S. K.: *Mechanics of Pneumatic Tires*. U.S. Department of Transportation, National Highway Traffic Safety Administration, Washington, D.C. 20590, 1981
- [20] COMMITTEE, Highway Tire Forum S.: Passenger car and light truck tire dynamic driving traction in snow / Society of Automotive Engineers, SAE J 1466. 1985
- [21] COWPER, G.R.: The Shear Coefficient in Timoshenko's Beam Theory. In: *Journal of Applied Mechanics* (1966), S. 335–340
- [22] DAVIS, J. B. ; WILD, J. R. ; JOHN, N. W. S.: Winter Tire Testing / Society of Automotive Engineers (SAE). 1980 ( 820344).
- [23] DO, M.-T. ; ROE, P. G.: D04: Report on State-of-the-Art of Test Methods / Tyre and Road Surface Optimisation for Skid Resistance and Further Effects (TYROSAFE), FP7-217920. 2008
- [24] DOMBECK, D. C.: Winter Tire Testing as Seen by the Independent Tester / Society of Automotive Engineers (SAE). 1982 ( 820838).
- [25] DOPORTO, M. ; MUNDL, R. ; WIES, B.: Zusammenwirken von Profil und Laufflächenmischung zur Erzielung eines optimalen Reifenverhaltens. In: *Automobiltechnische Zeitschrift ATZ* 3/2003 (2003, in German), S. 238–249
- [26] DÖPPENSCHMIDT, Astrid: *Die Eisoberfläche*, University Mainz, Diss., 2000, in German
- [27] ENGEMANN, S.C.: *Premelting at the ice-SiO<sub>2</sub> interface. A high-energy x-ray microbeam diffraction study*, Fakultät für Mathematik und Physik der Universität Stuttgart, Diss., 2005
- [28] EVANS, D.C.B. ; NYE, J.F. ; CHEESEMAN, K.J.: The Kinetic Friction of Ice. In: *Proceedings of the Royal Society of London* (1975), S. 493–512



- [29] FINK, J.: *Beitrag zur Untersuchung des Kraftschlusses von Gummi auf vereisten Oberflächen*, Technische Universität München, Diss., 1982
- [30] FISCHLEIN, H.: *Untersuchung des Fahrbahnoberflächeneinflusses auf das Kraftschlussverhalten von PKW-Reifen*. VDI Fortschritt-Berichte, Reihe 12, Verkehrstechnik/Fahrzeugtechnik, Nr. 414, 2000, in German
- [31] FISCHLEIN, H. ; GNADLER, R. ; UNRAU, H.-J.: Der Einfluss der Fahrbahnoberflächenstruktur auf das Kraftschlussverhalten von PKW-Reifen. In: *Automobiltechnische Zeitschrift ATZ* 10/2001 (2001, in German), S. 950–962
- [32] FRANKS, C.I.: *Foot Pressure Measurement System*. United States Patent 4,858,621, 1989
- [33] GÄBEL, G. ; WALLASCHEK, J. (Hrsg.): *Wechselwirkungen zwischen Reifen und Fahrbahn: Ursachen, Wirkungen und Erklärungen lokaler Kontaktphänomene*. Report of the Institute of Dynamics and Vibration Research, 5/2009
- [34] GABL, K. ; LACKINGER, B. ; TIROL, Land (Hrsg.): *Lawinenhandbuch*. Tyrolia Verlaganstalt, 1988, in German
- [35] GAL, A. L.: *Investigation and Modelling of Ruber Stationary Friction on Rough Surfaces*, Gottfried Wilhelm Leibniz University Hannover, Germany, Diss., 2007
- [36] GASCH, R. ; KNOTHE, K.: *Strukturdynamik, Band 2: Kontinua und ihre Diskretisierung*. Springer Verlag, 1989, in German
- [37] GERE, J. ; TIMOSHENKO, S.: *Mechanics of Materials*. Stanley Thornes, 1999
- [38] GIESSLER, M. ; GAUTERIN, F. ; WIESE, K. ; WIES, B.: Influence of Friction Heat on Tire Traction on Ice and Snow. In: *Tire, Science and Technology* (2010), Nr. TSTCA, Vol. 38, No. 1, S. 4–23
- [39] GIESSLER, Martin: *Mechanismen der Kraftübertragung des Reifens auf Schnee und Eis*. Dissertation, KIT Scientific Publishing, 2012, in German
- [40] GNADLER, R. ; HUININK, H. ; FREY, M. ; MUNDL, R. ; SOMMER, J. ; UNRAU, H.-J. ; WIES, B.: Kraftschlussmessungen auf Schnee mit dem Reifen-Innentrommel-Prüfstand. In: *Automobiltechnische Zeitschrift ATZ* 3/2005 (2005, in German), S. 198–207
- [41] GROSCH, K.A. ; SCHALLAMACH, A. ; SOUTHERN, E. ; SWIFT, P.McL.: Natural Rubber in Winter Tyres and Industrial Tyres. In: *Rubber Dev., Natural Rubber Technol. Suppl.* 9 (1970), S. 1–12
- [42] GROSS, D. ; HAUGER, W. ; SCHRÖDER, J. ; WALL, W.A.: *Technische Mechanik - Band 2: Elastostatik*. Springer Verlag, 2009, in German
- [43] GROSS, D. ; HAUGER, W. ; WRIGGERS, P.: *Technische Mechanik - Band 4: Hydromechanik, Elemente der höheren Mechanik, Numerische Methoden*. Springer Verlag, 2007, in German

- [44] GUTZEIT, F.: *Experimentelle und Theoretische Untersuchungen zum dynamischen Rollkontakt von Elastomeren*. PhD Thesis, in VDI Fortschritt-Berichte, Reihe 11, Schwingungstechnik, Nr. 338, 2009, in German
- [45] HÄCKEL, H.: *Meteorologie*. Eugen Ulmer Stuttgart, 2005, in German
- [46] HAGEDORN, P.: *Technische Schwingungslehre, Bd. 2: Lineare Schwingungen kontinuierlicher mechanischer Systeme*. Springer Verlag, 1989
- [47] HAYS, D.F. ; BROWNE, A.L.: *The Physics of Tire Traction: Theory and Experiment*. Plenum Press, 1974
- [48] HEISSING, B. ; ERSOY, M.: *Fahrwerkhandbuch*. Vieweg+Teubner, 2008, 2. verbesserte und aktualisierte Auflage, in German
- [49] HERING, E. ; MARTIN, R. ; STOHRER, M.: *Physik für Ingenieure*. Springer Verlag, 2002, in German
- [50] HERING, E. ; MARTIN, R. ; STOHRER, M.: *Physik für Ingenieure*. Springer Verlag, 2007, in German
- [51] HOBBS, P.V.: *Ice Physics*. Clarendon Press, Oxford, 1974
- [52] HOFSTETTER, K.: *Thermo-Mechanical Simulation of Rubber Tread Blocks during Frictional Sliding*, TU Wien, Institut für Festigkeitslehre, Diss., 2004
- [53] HUEMER, T. ; EBERHARDSTEINER, J. ; LIU, W.N. ; H.A.MANG: Experimental and numerical investigation of the friction behaviour of rubber blocks on concrete and ice surfaces. In: *Constitutive Models for Rubber*, 1999, S. 139–144
- [54] HUEMER, T. ; LIU, W. N. ; EBERHARDSTEINER, J. ; MANG, H. A. ; MESCHKE, G.: Sliding Behaviour of Rubber on Snow and Concrete Surfaces. In: *KGK Kautschuk Gummi Kunststoffe* (9/2001), S. 458–462
- [55] HUPFER, P.: *Witterung und Klima: Eine Einführung in die Meteorologie und Klimatologie*. B. G. Teubner Verlag, 2006, in German
- [56] IHLEMANN, J.: *Kontinuumsmechanische Nachbildung hochbelasteter technischer Gummiwerkstoffe*. PhD Thesis, in VDI Fortschritt-Berichte, Reihe 18, Mechanik/Bruchmechanik, Nr. 288, 2003, in German
- [57] IRIE, T. ; YAMADA, G. ; TAKAHASHI, I.: The Steady State In-Plane Response of a Curved Timoshenko Beam with Internal Damping. In: *Ingenieur Archiv* (1980), S. 41–49
- [58] IVANOVI, V. ; DEUR, J. ; KOSTELAC, M. ; HEROLD, Z. ; TROULIS, M. ; MIANO, C. ; HROVAT, D. ; ASGARI, J. ; HIGGINS, D. ; BLACKFORD, J. ; KOUTSOS, V.: Experimental Identification of Dynamic Tire Friction Potential on Ice Surfaces. In: *Vehicle System Dynamics* Vol. 44, No.1 (2006), S. 93–103
- [59] JANOWSKI, W. R.: Tire Traction Testing in the Winter Environment / Society of Automotive Engineers (SAE). 1980 ( 800839).

- [60] JELLINEK, H. H. G.: Liquid-Like (Transition) Layer on Ice. In: *Journal of Colloid and Interface Science* (1967), Nr. 25, S. 192–205
- [61] KENDZIORRA, N. ; MOLDENHAUER, P. ; WIES, B.: Verschiedene Aspekte der Reibdynamik am Fahrzeugreifen. In: *Nichtlineare Schwingungen, Reibung und Kontaktmechanik* (2007, in German), VDI-Berichte 2022,, S. 1–19
- [62] KING, T.R.: Tire Traction Testing Devices and Procedures - An Overview / Society of Automotive Engineers (SAE). 1984 ( 840064).
- [63] KISHIMOTO, Hiroyuki: Dynamic Observation of Contact Behavior Between Rubber for Tires and Ice by Refraction Contact Imaging. In: *Spring-8 Res Front 2003* (2004), S. 102–103
- [64] KÖNE, S.: *Vorrichtung und Verfahren zur Demonstration und/oder zur Ermittlung der Bewegung von mit farblichen Markierungen versehenen Profilelementen eines Reifens mit profilierter Lauffläche*. Patent DE 199 21 650 A1, 2000, in German
- [65] KRÖGER, M. ; POPP, K. ; KENDZIORRA, N.: Experimental and Analytical Investigation of Rubber Adhesion. In: *Machine Dynamics Problems* Vol. 28, No. 1 (2004), S. 79–89
- [66] KUMMER, H. W.: *Unified Theory of Rubber and Tire Friction*. The Pennsylvania State University, Engineering Research Bulletin B-94, 1966
- [67] KUROIWA, D.: The Kinetic Friction on Snow and Ice. In: *Journal of Glaciology* Vol. 19, No. 81 (1977), S. 141–152
- [68] LAHAYNE, O.: *Experimentelle Reibungsuntersuchungen und Modellrechnungen zum Verhalten von Reifenmaterialien*, TU Wien, Institut für Mechanik der Werkstoffe und Strukturen, Diss., 2007, in German
- [69] LEISTER, G. ; RUNTSCH, G.: Ermittlung objektiver Reifeneigenschaften im Entwicklungsprozess mit einem Reifenmessbus. In: *Tagungsband 2. Darmstädter Reifenkolloquium* (1998, in German), VDI-Berichte, Nr. VDI Fortschrittberichte Reihe 12, No. 362, S. 40–55
- [70] LINDNER, M.: *Experimentelle und Theoretische Untersuchungen zur Gummireibung an Profilklötzen und Dichtungen*. PhD Thesis, in VDI Fortschritt-Berichte, Reihe 11, Schwingungstechnik, Nr. 331, 2006, in German
- [71] MAYER, G. ; SLUIS, S. van d. ; STEINAUER, B.: *Forschung, Strassenbau und Verkehrstechnik: Griffigkeit von Fahrbahnoberflächen*. Bundesministerium für Verkehr, Bau und Wohnungswesen, Heft 841, 2002, in German
- [72] MEYER, W. E. ; KUMMER, H. W.: Die Kraftübertragung zwischen Reifen und Fahrbahn. In: *Automobiltechnische Zeitschrift ATZ* Vol. 66, No. 9 (1964, in German), S. 245–250

- [73] MITSUHASHI, K. ; HIROKI, E. ; MIDORIKAWA, S. ; SHINODA, S.: Study on the Friction Property of Studless Tires on Icy Road. In: *Journal of the Society of Rubber Industry, Japan* (1997), Nr. Vol. 70, No. 3, S. 140–146
- [74] MOLDENHAUER, P.: *Modellierung und Simulation der Dynamik des Kontakts von Reifenprofilbl.* PhD Thesis, in VDI Fortschritt-Berichte, Reihe 12, Verkehrstechnik/Fahrzeugtechnik, Nr. 720, 2010, in German
- [75] MOLDENHAUER, P. ; GÄBEL, G. ; KRÖGER, M.: Modellierung reibungsselbsterregter Systeme am Beispiel eines Profilklotzes. In: *Proceedings of the 7th Rubber Fall Colloquium (KHK 2006)* (2006, in German), S. 371–381
- [76] MOLDENHAUER, P. ; RIPKA, S. ; GÄBEL, G. ; KRÖGER, M.: Tire Tread Block Dynamics: Investigating Sliding Friction. In: *Tire Technology International 2008, The Annual Review of Tire Materials and Tire Manufacturing Technology* (2008), S. 96–100
- [77] MOORE, D. F.: *The friction of Pneumatic Tyres.* Elsevier Scientific Publishing Company, 1975
- [78] MULLER, H.K. ; NAU, B. ; MULLER, A.: *Fluid Sealing Technology: Principles and Applications.* Marcel Dekker Inc., 1998
- [79] MULLINS, L.: Softening of Rubber by Deformation. In: *Rubber Chemistry and Technology* Vol. 42 (1969), S. 339–362
- [80] MUNDL, R.: Traktionsmechanismen von Fahrzeugreifen auf flexiblem Untergrund. In: *3. Symposium Geländefahrzeuge in Theorie und Praxis*, 1992, in German
- [81] MUNDL, R. ; MESCHKE, G. ; LIEDERER, W.: Kraftübertragung von Profilstollen auf Schneefahrbahnen. In: *5. Int. Congress on Tire, Chassis and Road* (1995), VDI-Berichte 1224,, S. 79–99
- [82] MUNDL, R. ; MESCHKE, G. ; LIEDERER, W.: Kraftübertragung von Profilstollen auf Schneefahrbahnen. In: *4.Int. Congress on Tire, Chassis and Road* (1995, in German), VDI-Berichte, Nr. 1224, S. 79–99
- [83] MUNDL, R. ; MESCHKE, G. ; LIEDERER, W.: Friction Mechanism of Tread Blocks on Snow Surfaces. In: *Tire, Science and Technology TSTCA*, Vol.25 (1997), Nr. 4, S. 245–264
- [84] NAKAJIMA, Y.: Analytical Model of Longitudinal Tire Traction in Snow. In: *Journal of Terramechanics* (2003), S. 63–82
- [85] NESBITT, T.R. ; BARRON, D.J.: *Prediction of Driving Traction Performance on Snow.* Society of Automotive Engineers, SAE Technical Paper Series 800836, 1980
- [86] OHOYAMA, K. ; NISHINA, S.: Tire Snow Traction Performance. In: *JSAE Review* Vol. 11, No. 1 (1990), S. 86–88
- [87] OKSANEN, P. ; KEINONEN, J.: The Mechanism of Friction of Ice. In: *Wear* (1982), Nr. 78, S. 315–324

- [88] OKSANEN, Pekka: *Friction and Adhesion of Ice*, Technical Research Centre Finland, Diss., 1983
- [89] PAYNE, A. R.: The Dynamic Properties of Carbon Black-Loaded Natural Rubber Vulcanizates. Part I. In: *Journal of Applied Polymer Science* Vol. 6, No. 19 (1962), S. 57–63
- [90] PENMAN, H.L.: Natural evaporation from open water, bare soil and grass. In: *Proc. Soc. London A(194)* (1948), S. 120–145
- [91] PETRENKO, V. F. ; WHITWORTH, R. W.: *Physics of Ice*. Oxford University Press, 2006
- [92] PETRENKO, V.F.: *The Surface of Ice* / US Army Corps of Engineers, Cold Regions Research & Engineering Laboratory. 1994
- [93] PINNINGTON, R.J.: Radial Force Transmission to the Hub from Unloaded Stationary Tyre. In: *Journal of Sound and Vibration* Vol. 253, Nr. 5 (2002), S. 961–983
- [94] PINNINGTON, R.J. ; BRISCOE, A.R.: A Wave Model for a Pneumatic Tyre Belt. In: *Journal of Sound and Vibration* Vol. 235, No. 5 (2002), S. 941–959
- [95] RANTONEN, M. ; TUONONEN, A.J. ; SAINIO, P.: Measuring stud and rubber friction on ice under laboratory conditions. In: *Int. J. Vehicle Systems Modelling and Testing* Vol. 7 (2012), Nr. 2, S. 194–207
- [96] RIEDEL, E.: *Allgemeine und Anorganische Chemie*. Walter de Gruyter, 1999
- [97] RIPKA, S. ; GÄBEL, G. ; WANGENHEIM, M.: Dynamics of a Siped Tire Tread Block-Experiment and Simulation. In: *Tire, Science and Technology TSTCA*, Vol.37 (2009), Nr. 4, S. 323–339
- [98] RIPKA, S. ; LIND, H. ; WANGENHEIM, M. ; WALLASCHEK, J. ; WIESE, K. ; WIES, B.: Investigation of Friction Mechanisms of Siped Tire Tread Blocks on Snowy and Icy Surfaces. In: *Tire, Science and Technology TSTCA*, Vol. 40 (2012), Nr. 1, S. 1–24
- [99] RIPKA, S. ; MIHAJLOVIC, M. ; WANGENHEIM, M. ; WALLASCHEK, J. ; WIESE, K. ; WIES, B.: Tread Block Mechanics on Ice and Snow Surfaces studied with a new High Speed Linear Friction Test Rig. In: *12. Int. Congress on Tire, Chassis and Road* (2009), VDI-Berichte 2086, S. 239–254
- [100] RIPKA, S. ; WANGENHEIM, M.: Simulation of a Siped Tire Tread Block by Euler-Bernoulli Beams. In: *PAMM-Proc 9, Applied Analysis* (2009), S. 531–532
- [101] RIPKA, S. ; WANGENHEIM, M. ; WIESE, K. ; WIES, B.: Laboratory observation of the influence of snow and ice tracks on tire tread block friction. In: *Physics and Chemistry of Ice 2010*, 2011, S. 29–36
- [102] RIPKA, S. ; ZIMMERMANN, M. ; WALLASCHEK, J.: Modeling Tire Tread Block Dynamics by a Timoshenko Beam Model. In: *Proceedings of the ASME 2009 International Mechanical Engineering & Exposition* (2011), IMECE 2011-63367 (Noise, Vibration & Reliability in Vehicle Systems), S. 1–10

- [103] ROBERTS, A. D. ; RICHARDSON, J. C.: Interface Study of Rubber-Ice Friction. In: *Wear* 67 (1981), S. 55–69
- [104] ROBERTS, A.D.: Rubber-Ice Adhesion and Friction. In: *Journal of Adhesion* Vol. 13 (1981), S. 77–86
- [105] ROBERTS, A.D. ; LANE, J.D.: Friction of Rubber on Ice in the Presence of Salt. In: *Journal of Physics D: Applied Physics* (1983), S. 275–285
- [106] SCHRAMM, J. ; MUNDL, R. ; WIES, B. ; BECKER, A. ; EBERHARDSTEINER, J. ; LAHAYNE, O.: Reibtests von Gummi auf Schnee und Eis zum Studium des Einflusses von Profil und Mischung im Reifen-Strasse-Kontakt. In: *Nichtlineare Schwingungen, Reibung und Kontaktmechanik* (2007, in German), VDI-Berichte 2022,, S. 225–239
- [107] SHOOP, S. ; YOUNG, B. ; ALGER, R. ; DAVIS, J.: Effect of Test Method on Winter Traction Measurements. In: *Journal of Terramechanics* (1994), Nr. Vol 31, No. 3, S. 153–161
- [108] SHOOP, S. ; YOUNG, B. ; ALGER, R. ; DAVIS, J.: Three Approaches to Winter Traction Testing using Instrumented Vehicles / Society of Automotive Engineers (SAE). 1994 ( 940110).
- [109] SKOUVAKLIS, G. ; BLACKFORD, J.R. ; KOUTSOS, V.: Friction of rubber on ice: a new machine, influence of rubber properties and sliding parameters. In: *Tribology International* doi: 10.1016/j.triboint.2011.12.015 (2012)
- [110] SONNTAG, D. ; HEINZE, D.: *Sättigungsdampfdruck- und Sättigungsdampfdichtetafeln für Wasser und Eis*. Deutscher Verlag für Grundstoffindustrie, 1982, in German
- [111] SOUTHERN, E. ; WALKER, R:W:: Friction of Rubber on Ice. In: *Nature Physical Science* Vol. 237 (1972), S. 142–144
- [112] SPERLING, L. H.: *Introduction to Physical Polymer Science*. John Wiley & Sons, Inc., Hoboken, New York, USA, fourth edition, 2005
- [113] SPRING, E. ; PIHKALA, P. ; LEINO, M. A. H.: An Apparatus for the Measurement of Friction on Ice and Snow. In: *Applied Physics No. 148* (1985), S. 3–12
- [114] STEEN, R. van d.: *Enhanced Friction Modeling for Steady-State rolling Tires*, Eindhoven University of Technology, Eindhoven, the Netherlands, Diss., 2010
- [115] STEPHAN, W. ; POSTL, R.: *Schwingungen elastischer Kontinua*. B.G. Teubner, Stuttgart, 1995, in German
- [116] STRIBECK, R.: Die wesentlichen Eigenschaften der Gleit- und Rollenlager. In: *Zeitschrift des Vereines Deutscher Ingenieure* Vol. 46, Nr. 36 (1902, in German), S. 1341–1348
- [117] TAKIMI, A. ; IWAI, T. ; SHOUKAKU, Y.: Measurement of Water Film Thickness due to Sipe Edges of Studless Tire / Presentation held at the 30th annual conference on tire, science and technology, Akron, Ohio. 2011

- [118] TESTING, American S. ; MATERIALS: Standard Test Methods for Tire Performance Testing on Snow and Ice Surfaces / ASTM International, F1572-99. 1999
- [119] TESTING, American S. ; MATERIALS: Standard Test Method for Single Wheel Driving Traction in a Straight Line on Snow- and Ice-Covered Surfaces / ASTM International, F1805-00. 2001
- [120] TIMOSHENKO, S.P.: On the Correction for Shear of the Differential Equation for Transverse Vibrations of Prismatic Bars. In: *Philosophical Magazine* Vol. 6, No. 41 (1921), S. 744–746
- [121] TOPP, A. ; KENDZIORRA, N. ; WIES, B. ; LANGE, H.: *Braking Force Transfer Capabilities of Tires on wet Roads*. 17th EVU Conference, Nice, 2008
- [122] TRELOAR, L. R. G.: *The Physics of Rubber Elasticity*. Clarendon Press, Oxford, 1949
- [123] VAINIKKA, J. ; PIRJOLA, H.: ARTTU Final Report / Laboratory of Automotive Engineering, Helsinki University of Technology. 2003
- [124] VAINIKKA, J. ; PIRJOLA, H.: Mini-mu-Road and Lontra-Arctic Friction Measuring Devices in Laboratory and on Field and their Correlation. In: *Proc. Fista World Automotive Congress, Barcelona, Spain* (2004)
- [125] VENKATESH, S.: Laboratory Studies of the Friction of Rubber on Ice. In: *Tribology international* (1975), Nr. 4, S. 51–55
- [126] WADA, Y. ; KAJIKAWA, A.: *Apparatus for determining Shape of Contact Patch and Contact Pressure of Tires*. United States Patent 5,092,166, 1992
- [127] WANGENHEIM, M. ; RIPKA, S.: Temperature Investigations in Tire/Road Contact. In: *Proceedings of the ASME 2009 International Mechanical Engineering & Exposition* (2009), IMECE2009-11165 (Transportation Systems), S. 1–10
- [128] WAUER, J.: *Kontinuumsschwingungen*. Vieweg+Teubner, 2008, in German
- [129] WEBER, R.: *Der Kraftschluss von Fahrzeugreifen und Gummiprüfungen auf vereister Oberfläche*, Universität Karlsruhe, Diss., 1970, in German
- [130] WIES, B.: *Business, Technology & Development of Vehicle Tires*. Lecture notes, Leibniz University Hannover, Institute of Dynamics and Vibration Research, 2011
- [131] WIESE, K. ; KESSEL, T. ; MUNDL, R. ; WIES, B.: An Analytical Thermodynamical Approach to Friction of Rubber on Ice. In: *Tire, Science and Technology TSTCA*, Vol. (2012), Nr. 1, S. 1–10
- [132] WRIGGERS, P.: *Computational Contact Mechanics*. Springer Verlag, 2006
- [133] YAMAZAKI, S. ; YAMAGUCHI, M. ; HIROKI, E. ; SUZUKI, T.: Effects of the Number of Siping Edges in a Tire Tread Block on Friction Property and Contact with an Icy Road. In: *Tire, Science and Technology* (2000), Nr. TSTCA, Vol. 28, No. 1, S. 58–69

- [134] ZAZZARA, R. ; MUNDL, R. ; HAGN, N.: Bewertung des Blockierbremsvermögens von Fahrzeugreifen mittels thermografischer Bildanalyse. In: *2. Int. Congress Tire-Chassis-Road* (1989, in German), VDI-Berichte, Nr. 778, S. 217 ff.

### **Supervised collegiate theses (unpublished)**

- [135] AHLWEDE, Matthias: *Charakterisierung der Eigenschaften von im Labor hergestelltem Eis und Untersuchung der Einflüsse auf den Reibwert*. Projektarbeit, 2009
- [136] AHLWEDE, Matthias: *Untersuchung der Wiederholbarkeit beim Einstellen bestimmter Oberflächeneigenschaften von im Labor hergestellten Schneefahrbahnen*. Laborarbeit, 2009
- [137] ALBRECHT, Alexander: *Experimentelle Untersuchung von Einflussparametern auf die Reibung von Reifenprofilklötzen auf Eis*. Laborarbeit, 2010
- [138] BAUMEISTER, Jan: *Simulation des Materialverhaltens von Schnee*. Projektarbeit, 2009
- [139] HAASE, Jürgen: *Untersuchung der dynamischen Kontaktfläche von Reifenprofilklötzen beim Gleiten auf Eis*. Masterarbeit, 2010
- [140] HARTMANN, Werner: *Messung der Kontaktfläche eines gleitenden, lamellierten Reifenprofilklotzes und Untersuchung der Einflüsse auf die Eisreibung*. Diplomarbeit, 2010
- [141] HEITZMANN, Patrick: *Experimentelle Untersuchungen zum Einfluss verschiedener Parameter auf die Gleitreibung von Gummi auf Eis*. Laborarbeit, 2009
- [142] KLEINGROTHER, Lukas: *Beobachtung und Analyse der dynamischen Kontaktfläche von Reifenprofilklötzen beim Gleiten auf Eis*. Bachelorarbeit, 2011
- [143] KRÄMER, Carsten: *Untersuchung von Reibungsmechanismen lamellierter Reifenprofilblöcke auf Eis und Schnee*. Diplomarbeit, 2008
- [144] KRIEGER, Sebastian: *Untersuchung der Eigenschaften von im Labor hergestelltem Schnee*. Projektarbeit, 2011
- [145] KÜHBACH, Nico: *Simulation eines lamellierten Reifenprofilblocks mit dem Ansatz der Timoshenko Balkentheorie*. Projektarbeit, 2011
- [146] LIND, Hagen: *Untersuchung von Einflüssen auf den adhäsiven Effekt bei Elastomeren*. Laborarbeit, 2009
- [147] LIND, Hagen: *Entwicklung und Validierung eines numerischen Modells zur Analyse der Reibverhältnisse eines gleitenden Reifenprofilklotzes auf Eis*. Diplomarbeit, 2010
- [148] LIND, Hagen: *Experimentelle Untersuchung von Mechanismen und Einflussgrößen der Reibung von Reifenprofilklötzen auf Schnee und Eis*. Projektarbeit, 2010
- [149] LINKE, Tim: *Validierung und Optimierung von Spikebettungen mit Hilfe einer auf der Finite-Elemente-Methode basierenden Simulation*. Diplomarbeit, 2011
- [150] MEYER, Björn: *Untersuchung des Einflusses der Luftfeuchtigkeit auf die Gummi-Eis Reibung in Abhängigkeit der Umgebungstemperatur*. Projektarbeit, 2012



- [151] SCHURZIG, Daniel: *Simulation eines lamellierten Reifenprofilklotzes über den Ansatz einer nichtlinearen Balkentheorie*. Diplomarbeit, 2008
- [152] STÖPPELKAMP, Carsten: *Untersuchung des Einflusses des Herstellungsverfahrens einer Eisfahrbahn auf die Wiederholbarkeit der Reibeigenschaften der Eisfahrbahnoberfläche*. Projektarbeit, 2010
- [153] TOBER, Patrick: *Konstruktion und Erprobung eines Universalprobenhalters für den Hochgeschwindigkeitslinearprüfstand "HiLiTe"*. Projektarbeit, 2009
- [154] WOLF, Alexander: *Untersuchung von Mechanismen der Eisreibung um den Gefrierpunkt*. Projektarbeit, 2009
- [155] WULF, Felix: *Herstellung und Präparation von Schneefahrbahnen im Labor zur Untersuchung von Elastomerreibung*. Projektarbeit, 2008
- [156] YANG, Lei: *Simulation eines lamellierten Profilklotzes*. Projektarbeit, 2008
- [157] ZIMMERMANN, Martin: *Balkentheorien zur Modellierung eines lamellierten Reifenprofilklotzes -Bewertung und Simulation-*. Diplomarbeit, 2010



# Curriculum Vitae

## Persönliche Daten

Stefan Ripka  
geboren am 21. April 1980 in Hannover

## Schulbildung

1986-1990 Astrid Lindgren Grundschule Wennigsen  
1990-1992 Orientierungsstufe Wennigsen  
1992-1997 Matthias Claudius Gymnasium Gehrden  
1997-2000 Fachgymnasium Technik der Berufsbildenden Schule 5 Hannover

## Grundwehrdienst

2000-2001 2./ Sanitätsregiment 1, Hildesheim

## Studium

2001-2007 Studium des Maschinenbaus  
an der Gottfried Wilhelm Leibniz Universität Hannover

## Berufliche Tätigkeit

2007-2012 Wissenschaftlicher Mitarbeiter  
am Institut für Dynamik und Schwingungen  
der Leibniz Universität Hannover  
seit 06/2012 Mitarbeiter der Continental Reifen Deutschland GmbH